Vacuum Assisted Resin Transfer Molding of Foam Sandwich Composite Materials: Process Development and Model Verification

Rebecca Ann McGrane

Thesis submitted to the Faculty of the
Virginia Polytechnic Institute and State University
in partial fulfillment of the requirements for the degree of

Master of Science
in
Engineering Mechanics

Alfred C. Loos, Chair
Romesh C. Batra
Zafer Gurdal

October 12, 2001
Blacksburg, VA

Keywords: vacuum assisted resin transfer molding, VARTM, sandwich structures, polymer composite processing

Vacuum Assisted Resin Transfer Molding of Foam Sandwich Composite Materials: Process Development and Model Verification

Rebecca Ann McGrane

(ABSTRACT)

Vacuum assisted resin transfer molding (VARTM) is a low cost resin infusion process being developed for the manufacture of composite structures. VARTM is being evaluated for the manufacture of primary aircraft structures, including foam sandwich composite materials. One of the benefits of VARTM is the ability to resin infiltrate large or complex shaped components. However, trial and error process development of these types of composite structures can prove costly and ineffective. Therefore, process modeling of the associated flow details and infiltration times can aide in manufacturing design and optimization.

The purpose of this research was to develop a process using VARTM to resin infiltrate stitched and unstitched dry carbon fiber preforms with polymethacrylimide foam cores to produce composite sandwich structures. The infiltration process was then used to experimentally verify a three-dimensional finite element model for VARTM injection of stitched sandwich structures.

Using the processes developed for the resin infiltration of stitched foam core preforms, visualization experiments were performed to verify the finite element model. The flow front progression as a function of time and the total infiltration time were recorded and compared with model predictions. Four preform configurations were examined in which foam thickness and stitch row spacing were varied. For the preform with 12.7 mm thick foam core and 12.7 mm stitch row spacing, model prediction and experimental data agreed within 5%. The 12.7 mm thick foam core preform with 6.35 mm row spacing

experimental and model predicted data agreed within 8%. However, for the 12.7 mm thick foam core preform with 25.4 mm row spacing, the model overpredicted infiltration times by more 20%. The final case was the 25.4 mm thick foam core preform with 12.7 mm row spacing. In this case, the model overpredicted infiltration times by more than 50%. This indicates that the model did not accurately describe flow through the needle perforations in the foam core and could be addressed by changing the mesh elements connecting the two face sheets.

Acknowledgements

I would first like to thank NASA Langley Research Center for funding the research presented.

I would also like to thank several people who have offered assistance throughout my research. I would like to thank the members of my advisory committee for their time and guidance: Dr. Alfred C. Loos, Dr. Romesh C. Batra, and Dr. Zafer Gurdal. I would also like to thank Jay Sayre and Todd Bullions for their help in training and advice, Xioalan Song and Aziz Dursan for providing the analytical model, and Alex Cardinali for capturing the flow front images.

Lastly, I would like to thank my family and friends, who offered support and encouragement and without whom none of this would have been possible.

Table of Contents

List of Figures

List of Tables

Chapter 1. Introduction

Resin transfer molding (RTM) has been the subject of interest for the manufacture of polymer composites since the late 1970s. Used in industries such as aerospace, sporting goods, and automotive, the process relies on inserting dry fiber preforms into a closed matched mold and injecting with a liquid resin under pressure to infiltrate the part. The short production times make RTM a relatively inexpensive process which can create near-net shape parts with good tolerance control. However, tooling design is a critical factor in the success of RTM. Resin must completely infiltrate the preform prior to gelation of the resin, and all sections of the preform must be uniformly wet out. Improper mold design can lead to resin rich or resin poor areas, and injection pressures can cause movement of the reinforcing materials. Thus tooling design can be a limitation in creating large and complex shaped parts, and molding costs can be high.

To address some of the problems inherent in RTM, several variants of the process have been developed. Among the processes are resin film infusion, vacuum assisted resin injection, and vacuum assisted resin transfer molding (VARTM). All of the processes rely on the basic concepts of RTM with some minor variations. In the VARTM process, a dry fiber preform is placed on a tool surface and covered with a flexible bagging material. Resin is introduced into the system and infiltrates the preform under negative or vacuum pressure. VARTM has many advantages over traditional RTM, the most important being the low tooling cost. Unlike RTM, the vacuum bag acts as flexible tooling and does not require that a matched mold be made. This reduces capital investments and makes VARTM attractive for the manufacture of large-scale components. Used in combination with room temperature cure resin systems, VARTM can also eliminate the need for large oven or autoclave cure cycles. VARTM is effective in controlling volatile organic compounds associated with many of the room temperature processing resins, such as styrene. This is critical in many industries where stringent health and safety regulations govern manufacturing practices. In addition, the vacuum assist provides a favorable pressure gradient for pulling the resin through the preform,

which enables large parts to be manufactured with low void content, while the low injection pressures reduces movement of the fibers during injection.

VARTM has been successfully used to manufacture a wide variety of structures, and is being evaluated for use in aerospace applications due to the low cost. Sandwich structures are also being considered for use in primary aircraft structures due to their light weight and good resistance to shearing. Common sandwich materials include lightweight honeycomb and foam cores. Recent studies have shown transverse stitching can improve damage tolerance of these structures, making them better suited for service in structural applications. Though many manufacturing methods are used to fabricate sandwich structures, VARTM is an attractive procedure for sandwich panel manufacture.

One of the drawbacks of large-scale composite production of components using RTM or VARTM is that trial and error development can prove costly and ineffective. Thus, the focus of many researchers has been to develop three-dimensional modeling packages to analyze flow details and infiltration times of the manufacturing processes. Accurate modeling software can aide in process design and optimization.

To this end, the objectives of this research were to use VARTM to resin infiltrate stitched and unstitched dry carbon fiber preforms with polymethacrylimide foam cores to produce composite sandwich structures. Process parameters varied included the effects of stitch density and foam core thickness on the processing of sandwich structures.

A three-dimensional finite element model for VARTM injection of stitched sandwich structures was experimentally verified. Comparisons of flow front location versus time and total infiltration time were made between experimental observation and finite element model predictions.

A review of recent research in the areas of vacuum assisted resin transfer molding, composite sandwich structures, and process modeling is presented in Chapter 2. Chapter 3 details some of the kinetic and viscosity behavior of the resin used in this study, Dow

Derakane 510A-40 vinyl ester. Results of differential scanning calorimetry (DSC) analysis and viscosity studies for two different batches of resin are presented. The manufacturing procedures for both stitched and unstitched panels are discussed in Chapter 4. Finally, a description of the finite element model and the results of the visual experiments are presented in Chapter 5, and concluding remarks and recommendations for future work in Chapter 6.

Chapter 2. Literature Review

2.1 Vacuum assisted resin transfer molding (VARTM) and Seemann Composites Resin Infusion Molding Process (SCRIMP)

2.1.1 Applications

Resin transfer molding (RTM) has been the subject of interest for the manufacture of polymer composites since the late 1970s. RTM is based on liquid molding techniques for non-reinforced plastics. It is a relatively inexpensive process and can create near-net shape parts with good tolerance control. However, there are some limitations to RTM, such as mold and tooling design, which have led to process modifications [1]. The tooling design in RTM is critical, due to the fact that the part must be injected prior to gelation of the resin, and all sections of the preform must be uniformly wet out.

More recently, new technologies have been developed which are based on resin transfer molding. One notable technique is called vacuum assisted resin transfer molding (VARTM). VARTM has many advantages over traditional RTM, the most important being the low tooling cost. In the VARTM process, a dry fibrous mat or preform is injected with liquid resin using only vacuum pressure to draw the resin through. A single tool surface is used, and the other surface is covered with a flexible bagging material. Unlike RTM, the vacuum bag acts as flexible tooling and does not require that a matched-metal mold be made. VARTM is also good for controlling volatiles associated with many of the room temperature processing resins, such as styrene. In addition, the vacuum assist provides a favorable pressure gradient for pulling the resin through the preform, which enables large parts to be manufactured with low void content.

To date, VARTM has been used primarily in marine applications. Seemann Composites Resin Infusion Molding Process (SCRIMP) is a patented, but well known VARTM technique which was developed for boatbuilding. Developed in part to combat the stringent environmental regulations facing the marine industry with regards to volatile

organic compound emissions, SCRIMP has proven to be an effective method for injecting large scale and complex shape components. This reduces the need for joining and has in many cases reduced the manufacturing costs of large composite structures. When coupled with a near-net shape preform, the process can be completed relatively quickly without the labor intensive wet hand-layup traditionally seen with FRP boatbuilding. Additionally, when using room temperature cure resins, the entire procedure can take place at room temperatures without the need for elevated temperature postcure or autoclave processing.

The SCRIMP process has been successfully demonstrated in a number of large-scale marine applications. North End Marine has used a variant of the SCRIMP process, called progressive gelation, to inject a sandwich hull of a 90 foot motor yacht in a single shot [2]. The Hinkley Company has licensed the SCRIMP process to manufacture sail and powerboats ranging in size from 36 to over 70 feet, and Martin Tooling & Laminates manufactures canoes and kayaks with a non-patented VARTM process [3].

The successful commercial applications of VARTM in the marine industry has led to development in the military sector. The Navy has evaluated the use of resin infusion techniques through the Naval Surface Warfare Center, Carderock Division (NSWCCD). Recognizing the advantages which composites hold over metal constructions, including improved fatigue and corrosion resistance, lighter weight, higher stiffness, and the ability to tailor material properties, NSWCCD evaluated four processes to manufacture one-half scale midship sections of a naval combatant ship. These processes include VARTM and UV-VARTM, which is a variant of the VARTM process which uses ultraviolet light curing resins. The sections had dimensions of 26 feet in length, 20 feet in beam, and 9 feet in height. The section included a stiffened single skin hull, main deck, sandwich platform deck, two water-tight sandwich bulkheads, and a sandwich keel tank, with the total construction weighing over 10 tons. Though the UV-VARTM process was limited both by the relative inexperience in using the manufacturing method and laminate thickness which can be cured by UV, the VARTM process proved to be an effective manufacturing method. Using the SCRIMP progressive gelation process, the

manufactured structure was deemed highly successful and cost competitive with metal constructions [4].

There have been several other successful technology demonstrations of the VARTM process in the military. The Composite Armored Vehicle Advanced Technology Demonstrator Program (CAV ATD) began in 1994 to address the need for a lightweight ground combat vehicle that could be rapidly deployed and air transportable. The goals of the CAV project were to reduce weight by 33% over the metal construction while costing no more than 1.4 times the cost of the equivalent metallic vehicle. The initial CAV design included manufacturing lower hull and crew capsule components by VARTM, and using Automated Fiber Placement (AFP) for the upper hull. Mechanical tests of VARTM manufactured components were deemed successful [5], and development of the CAV is presently in its second stage.

Later research by the CAV team showed that VARTM offered a 21% total cost savings over AFP for manufacturing the structural laminates with integrated armor used in the upper hull. VARTM had distinct advantages over AFP, including a lower raw material cost due to the room temperature cure resin system. Also, because of the tooling required for VARTM, there was a lower capital investment required to implement the process. Pike, et. al. [6] determined the mechanical behavior of components fabricated with VARTM using open hole compression and short beam shear tests. They found that the mechanical properties of laminates fabricated by VARTM were comparable to those fabricated with AFP, and met all of the performance requirements specified by CAV-ATD program. This was the first demonstration of a fully integrated armor and structure composite hull fabricated with VARTM. A second group of researchers led by Hosur [7] measured the static compression strength of composite panels fabricated by VARTM to determine that thick S2-glass/vinyl ester composites could be used in integral armor applications.

VARTM applications have also been seen in the automotive industry. Weinhold and Wozniak [8] successfully developed an Integrated Storage System (ISS) for use in

compressed natural gas vehicles. The project, developed through The Johns Hopkins University Applied Physics Laboratory, used a SCRIMP/VARTM process to develop a high-pressure natural gas storage unit. The ISS consisted of three filament wound pressure cells protected with an impact-absorbing foam inside of a fiberglass shell. Mechanical test data were measured for E-glass/vinyl ester panels which included tensile, flexural, and impact strength, and the fiber volume fraction was measured. The finished parts were subjected to stringent Department of Transportation certification testing for impact damage tolerance. VARTM was determined to be a cost-effective method for prototype design based on its limited tooling costs and reduced lay-up time. The final part met all design requirements and testing limits.

A second automotive application was the development of a composite body for an electric bus. Using VARTM to manufacture the five body panels, a total weight savings of 30% over the metal body was achieved while reducing the manufacturing time by 25% [9]. VARTM was selected because of its low cost and ability to inject very large shapes quickly.

VARTM also has applications in civil and military infrastructure. The U.S. Army has launched an extensive program to create lightweight short-span mobile assault bridging systems [10]. The Composite Assault Bridge (CAB) project is a full technology demonstration that spans from materials evaluation, bridge design analysis, and manufacturing analysis to component and full-scale mechanical testing. After evaluating many different material combinations, graphite fibers with an elevated temperature epoxy were selected. Eight different manufacturing methods were evaluated, and a VARTM method was selected to complete full-scale development. The compression strength, shear strength, and adhesive properties were measured. Full scale roadway deck and composite treadway testing were also conducted. These tests showed the VARTM injected graphite/epoxy bridges equaled the performance of the commercially available aluminum bridges while offering a weight savings of 25% and a cost savings of 20%. The second phase of development looks to bring further cost and weight savings to the program.

2.1.2 Process improvements

Because VARTM is still a relatively new and rapidly evolving process, process characterization and development work has been concurrent with the development of new applications. One major focus of the processing has been coupling VARTM with rapid-cure techniques to further reduce the time required to manufacture large components and thus the associated costs, making VARTM attractive and cost-competitive in more industries.

Livesay [11] and Shepherd [3] are developing the use of ultraviolet light curing resin systems with VARTM manufacturing. The driving factor in UV-VARTM development is the high production rates possible with this combination of techniques. Many light curing systems can be cured in under seven minutes, leading to an increase in the number of times the molds can be used in one day.

Electron beam curing in conjunction with VARTM [12] is also being considered for aircraft applications. E-beam has the advantage of reducing costs due to the lower processing temperatures, decreasing cycle times, and co-curing varying resin systems.

Another area of interest is process monitoring. Heider [13-15], in three separate studies, has examined several areas for process monitoring and feedback control during VARTM manufacturing, with the ultimate goal of developing an intelligent VARTM workcell. One study [13] attempts to develop an understanding of the material response during cure through the use of Bragg grating, extrinsic Fabry-Perot interferometers, thermocouples, and a resin flow sensor (SMARTweave). These sensing devices measure the flow, cure behavior, and induced stresses during cure. This type of information can be used to predict residual stresses caused by processing and can be used for health-monitoring of components during their service lives.

A second study [14] developed a feedback control system for the vacuum gradients during processing. Using in-situ vacuum sensors coupled with computer controlled

pressure regulators and venturi pumps, the vacuum levels at various injection ports were able to be quickly controlled. This has the potential to affect flow front geometry during injection, and thus the overall quality and reliability of the finished part. Ultimately, a fuzzy logic controller incorporated into the loop could provide real-time process control for VARTM manufacturing.

The third study [15] combined flow monitoring techniques (SMARTweave) with computer actuated valves to control the sequential injection of a thick-section composite part manufactured by VARTM. Through computer controlled automation, the opening and closing of injection ports was done without the aide of engineering supervision, thus fully automating the injection process. This can decrease cycle times by as much as 66%.

2.1.3 Aerospace applications

All of these successful applications and process developments of VARTM techniques have led to investigations in the suitability of VARTM for aerospace applications. Though composites have been used extensively in the aerospace industry due to their light weight, the applications have generally been secondary structures. The performance and tolerance requirements of aircraft-grade composites dictate a high-cost, labor-intensive, autoclave cure system. Autoclave size has limited the size and geometry of structures which can be manufactured with composites. However, the ability of VARTM to successfully infiltrate large components at low cost and without autoclave cure has made it attractive for the manufacture of primary wing structures.

NASA Langley started an advanced composites technology program in 1989 to develop composite primary structures for commercial aircraft [16]. The research focus was on the analytical side: developing models to predict resin flow and strength and elastic properties, creating a database of damage tolerance and mechanical properties of materials, and developing test methods for evaluative purposes. Stitched/resin film infusion (RFI) processes were considered as the manufacturing method, but proved to be a costly process due to the materials, tooling, and associated autoclave costs. VARTM

was considered for injecting these same stitched/RFI components with varying degrees of success [2]. Some of the major limitations to adopting VARTM are the available resins, which do not meet the performance requirements necessary for the aerospace industry, and the low fiber volume fraction and high void content due to the absence of autoclave pressure.

2.2 Sandwich structures

Honeycomb materials have been used by the aerospace industry for decades [17]. Like structural members such as the I-beam, the face sheets of a sandwich structure support applied bending loads, while the core material resists shear and increases rigidity. While honeycomb materials provide high torsional rigidity, foam cores offer continuous load transfer and thus increases the torsional rigidity further [18]. Foam cores are also resistant to fatigue and exhibit good damage tolerance, making them suited for marine and aircraft applications.

Because the suitability of sandwich structures for many applications is still being determined, much of the current literature focuses on the design and mechanical properties of sandwich structures with manufacturing methods being secondary. One area which must be proven for composite sandwich structures to be considered competitive or superior to metallic structures is impact resistance and damage tolerance. Many studies have focused on this issue, and only a summary of the literature is presented here.

McGowan [19] studied the effect of impact and compression-after-impact (CAI) properties for panels subjected to barely visible impact damage (BVID). This is a critical issue for such low-velocity impacts as dropping tools during manufacturing or runway debris and hailstones during service. Also studied was the effect of compressive preloading sandwich panels prior to impact. Results of the study showed that for low energy impacts, the resulting damage was similar for dropped-weight and airgun impact collisions. As the impact energy was increased to levels which cause BVID, airgun

impacts caused greater damage than dropped-weight impacts for the same level of impact energy. Also for low impact energies, CAI response was not affected. However, for higher impact energy specimens, the residual strength decreased. For the panels which were subjected to a compressive preload prior to impact, the order in which the panel is impacted and loaded did not seem to affect damage. However, it was determined that a threshold value of strain existed after which point impact energies which would normally cause BVID could cause failure.

Other variables studied with respect to impact and CAI properties include the hygrothermal effects on damage tolerance. Ishai [20] determined that for sandwich structures, moisture absorption affects both the failure mode and mechanical properties of sandwich panels. Hybrid glass/carbon fiber skins were bonded to a syntactic foam core and were subjected to immersion in water and impact loaded, then tested for CAI. Results of the testing showed that hygrothermal aging has only a slight affect on damage size, while having a severe affect on damage depth. Additionally, immersed specimens failed from core shear during the CAI testing due to the strength degradation caused by moisture sorption of the syntactic foam core.

Ishai [21] later showed that using an interleaved foam core, that is, one which was toughened by interleaving with glass/epoxy interlayers, could improve the damage tolerance of sandwich structures. The interleaved layers acted to arrest crack propagation through the specimen. This caused higher residual strength and stiffness in the damaged specimens.

Fatigue properties have also been examined at length [22, 23]. King used VARTM to manufacture tapered sandwich structures. Two tapering conditions were evaluated, one which considered a filleted transition from the sandwich region to the solid laminate, and one which considered a square drop-off from one region to the next. Results showed that the filleted drop-off caused a stress concentration between the sandwich and solid laminate that decreased fatigue life. The square drop-off contained a resin rich area in

between the core and laminate which transitioned the load more gradually and concurrently absorbed some of the bending energy thus increasing fatigue life.

Compressive failure of sandwich structures has been treated extensively in the literature, often coupled with compression after impact testing. Hodge et. al. [24] used VARTM to resin infiltrate a graphite preform with a syntactic foam core. Room temperature and elevated temperature (177 °C) mechanical testing included edgewise compression, open-hole compression, compression after impact, and edgewise, open-hole, and flatwise tension tests. Mechanical tests of sandwich panels were compared to samples taken from a prototype of a solid rocket booster nose cap manufactured with the same materials. Compressive properties showed no sensitivity to aerothermal testing or moisture conditioning in a water bath for 10 days at 82 °C. Compression after impact showed a residual strength plateau after an impact energy of 27 Joules.

In a second study of VARTM manufactured sandwich panels, a glass/vinyl ester structure with a PVC foam core was evaluated [25]. Sandwich beam testing included three and four-point bending to determine the bending stiffness and shear stiffness of the beams. The three-point bend tests did not agree well with theoretical predictions for the behavior of the material. However, the four-point bending data agreed within 5% of the predicted deflection.

To date, relatively little work has been done to evaluate the effect of transverse stitching on the properties of sandwich structures. Standardized test methods have not been developed, and several issues regarding failure mechanisms must be considered. Stanley et. al. [26] have used VARTM to manufacture sandwich structures from carbon fiber facings and closed cell polyurethane foam. The panel was stitched through the thickness with Kevlar thread and infiltrated with an epoxy resin. Two types of tests were used to evaluate the mechanical properties of the stitched sandwich structure. Sandwich flexure testing was used to determine the flexural rigidity and flexural toughness of both stitched and unstitched panels, showing that energy absorption can be increased significantly due

to stitching. Flatwise tensile testing was performed which showed an increase in out-of-plane tensile strength which is dependent upon the size of the bobbin thread.

2.3 Polymethacylimide foam

Polymethacrylimide (PMI) closed-cell structural foams have been used for the manufacture of sandwich structures. PMI is thermoformable and can produced in a variety of shapes. PMI has service temperatures of up to 375 °F, and can be cured in autoclaves at pressures of up to 100 psi. PMI has very good chemical resistance and fatigue properties. Applications for the foam include marine, aerospace, electronics, and radiation equipment. The closed-cell nature makes it appropriate for sandwich structures because it will not soak up resin during infiltration.

PMI foam cores can be bonded to both thermoplastic and thermosetting systems. McGarva [27] examined the compression molding of closed cell PMI cores to thermoplastic glass/polyamide 12 face sheets. Results of testing the glass/PA12 were compared to a glass/vinyl ester system to determine the effects of temperature of the face sheets and molding pressure on the mechanical properties of the structure. Using double cantilever beam tests to determine the fracture toughness of the PMI sandwich structures, the results showed that increasing molding pressure increases the fracture toughness of the material. The combination of heat and molding pressure results in densification, which is caused by the walls of the cells near the interface partially or totally collapsing. Increasing the molding pressure increases the core density in the interfacial region. This densification was shown to increase the fracture toughness of the material. An initiated crack propagates in a stable manner along the skin-core interface. Increasing face temperature shows a similar trend up to 240 °C, at which point the foam experiences heat degradation and the fracture toughness decreases.

Kwon et. al. [28] examined the compressive failure of graphite/epoxy skins bonded to a PMI core. Varying core thickness was considered, as well as the effects of holes or partial delaminations in the beams. Experimental results were compared to finite element

predictions of the behavior. Several test cases were considered: no delamination and no hole, partial delamination, hole, hole and delamination. For the samples with no delamination or holes, failure was dominated by buckling followed by core shear. For the samples with a partial delamination, a threshold value for the delamination crack size of 1.27 cm was determined. Above this threshold, the failure mode and failure load changed, however for a crack size below 1.27 cm, there was no effect of the crack on the failure. For the samples with holes, two types of failures occurred. For diameters below a critical value, failure occurred as foam core shear around the quarter-point. For diameters above this value, failure occurred as bending stress in the face sheets at the hole. For samples with holes and delaminations, failure was dominated by the crack tip if the crack was large and the hole was small. Otherwise, failure occurred in the skin at the hole.

2.4 Vinyl ester resin

Vinyl ester resin systems have very low viscosities and frequently can be cured at room temperature, making them ideally suited for VARTM. Several groups have developed both mechanistic and phenomenological models for low temperature cure of vinyl ester resins. These types of relations are potentially important in the modeling of resin transfer molding processes using vinyl ester resins, because flow mechanics and heat transfer during infiltration will depend on cure kinetics of the resin. This is especially true if long processing times are encountered. Additionally, degree of cure of the finished composite affects the mechanical properties.

The most common phenomenological model used to describe the kinetic behavior of vinyl ester systems is the autocatalytic rate expression [29]:

$$\frac{d\alpha(t)}{dt} = k\alpha(t)^m (1-\alpha(t))^n \qquad (1)$$

where m and n are the kinetic exponents and (m + n = 2) is the overall reaction order, k is the reaction rate constant, and α is the degree of cure. Data are obtained from isothermal and dynamic scans using differential scanning calorimetry (DSC). For elevated temperature cure systems, this technique is adequate to determine the associated constants. However, systems which use low temperature promoters, such as cobalt napthenate, and low temperature initiators, such as organic peroxides (methyl ethyl ketone peroxide among them), are highly reactive at room temperature. This makes it very difficult to accurately measure the total heat of reaction using DSC because the resin begins to cure immediately upon mixing.

Um [30] states that low temperature, rapidly curing resin systems cannot be accurately measured using isothermal DSC data. An approach is presented to use dynamic temperature scanning to develop a kinetic model. A function of the form

$$\alpha = f_1 + f_2 = \frac{1}{1+\exp[-m_1(T-m_2)]} + m_3 \exp[-m_4(T-m_5)^2] \qquad (2)$$

is proposed to describe the rate of conversion, where f_1 is the primary reaction part, f_2 is the secondary reaction part, α is the conversion, T is the temperature, and m_1 through m_5 are coefficients that depend on the accelerator concentration and temperature ramp. A three part resin system was tested. Comparison of predicted and measured results showed good agreement.

DSC data only describes the heat generation that accompanies cure, and not the actual reaction chemistry of the resin. For this reason, several research teams [29, 31-34] have used Fourier transform infrared spectroscopy (FTIR) to determine the conversion rates of the styrene and vinyl ester monomers in the resin. This data can be used to determine more mechanistic models of the cure reaction. Vinyl ester (VE) resins are usually a reaction product of methacrylated epoxy compounds which are frequently diluted in styrene (ST) monomers. Three competing reactions take place: the homopolymerization of the VE monomer, homopolymerization of the ST monomer, and copolymerization of

the two components. FTIR allows for measurement of these reactions by detecting the concentration of the chemical groups. These studies proposed new kinetic models based on testing various vinyl ester formulations with different initiator and promoter contents.

2.5 Process modeling

One of the most notable features of VARTM processing is also what makes accurate analytical models of the process a necessity: the ability to infiltrate large structures. As VARTM is still a relatively new manufacturing technique, many of the associated process variables are being studied in greater depth to understand the process. Much of the manufacturing developments have been made by trail and error. For large-scale components, such as marine or aerospace structures, trial and error development can be cost-prohibitive due to the large quantity and cost of raw materials required. Thus, it is necessary to develop infiltration and flow models of the VARTM process. By accurately modeling the process, more time can be spent on design and optimization of parts fabricated by VARTM.

A variety of researchers have attempted to model the VARTM process. Like many resin infusion processes, several factors affect the success of manufacturing. Integral to the modeling of any resin transfer method is an understanding of the fluid mechanics and infiltration times associated with manufacturing. This relies on two factors: resin behavior and preform characteristics. Resin behavior includes the cure kinetics, heat transfer mechanisms, and viscosity profile, while the preform characteristics include such factors as compaction, permeability, distribution medium, and injection source.

Hammami and Gebart [35] developed a 1-D analytical model to simulate VARTM injection of glass laminates with unsaturated polyester resin and vinyl ester resin. Initial studies were conducted to determine the effect of various processing parameters on the system. Existing data from RTM could not be directly applied due to the presence of the vacuum bag and distribution media in VARTM, which changes the behavior of such parameters as compaction, permeability, and response to different resin infusion sources.

Reinforcement compaction tests were performed, isolating such variables as number of layers, stacking sequence, and compaction rates. Results showed that for dry stacking and low compaction pressures (≤ 1 bar), neither the stacking sequence nor the number of layers affect the compaction behavior. However, for wet stacking, stacking sequence does influence the compaction. It is possible to achieve higher fiber volume fractions by alternating the stacking sequence of the laminae of the composite. For the saturated reinforcement, a fiber volume fraction of 49% could be achieved at a pressure of 0.08 MPa for a $[(0°)_5/(90°)_5]$ lay-up, compared to a 55% fiber volume fraction for a $[(0°/90°)_5]$ lay-up. At higher compaction rates, there appears to be a resin relaxation phenomenon which affects compaction pressure. For low rates, the resin is able to bleed out of stack and higher fiber volume fractions are attainable. However, at higher speeds, the resin is unable to flow fast enough to relax the pressure build-up, resulting in lower fiber volume fractions. Two possible solutions are to subject the stack to repeated loading or to hold the pressure longer, allowing the resin to 'relax'.

Permeability was also recognized as a critical factor in fill time. The influence of the vacuum bag and distribution medium is not treated in many of the existing permeability models. Other models do not account for transverse permeability, which is critical in VARTM because resin flow occurs in two regions, in-plane flow across the distribution medium and transverse flow through the thickness of the preform [35].

Different resin sources were also considered as part of the study. Point injection versus line injection can greatly affect infiltration time, by some accounts, line injection can be up to 10 times faster than a point source.

The final factor considered was the distribution medium, or flow enhancement layers. Three materials, Rovicore, Multimat, and a continuous strand mat (CSM), were used as distribution media and tested to determine the affect on total infiltration time of a glass laminate. Results showed that the Rovicore and CSM decreased infiltration time of the laminate, while the Multimat actually increased infiltration time over injection without an enhancement layer.

A one-dimensional model was developed to take into account the factors described above: compaction, permeability, resin injection source, and distribution medium. Darcy's law and the continuity equation were used to derive a flow model for the process. An equation of transverse equilibrium was introduced to take into account the fact that the thickness changes due to the flexible vacuum bag. Assumptions for the model included constant resin viscosity, constant pressure injection, and quasi-stationary flow, meaning the cavity height will have time to approach its static equilibrium value at every instant in time during the infusion process.

As the thickness of the mold cavity is pressure dependent, combining Darcy's law and the continuity equation yields,

$$\frac{\partial}{\partial x}\left(-\frac{K \cdot h(p)}{\mu}\frac{\partial p}{\partial x}\right) = -\frac{\partial h}{\partial t} \tag{3}$$

where, K is the permeability of the preform, p is the pressure, h is the cavity thickness, and μ is the resin viscosity.

Two boundary conditions were applied:

- pressure is constant at the inlet, ($x = 0$, $p = p_0$)
- pressure is equal to the vacuum pressure at the flow front, ($x = x_f$, $p = p_{vac}$)

The geometry was then discretized using a finite volume scheme. Initial results showed reasonable agreement with experimental injections. However, the model showed great sensitivity to compaction behavior and permeability. Generalized forms of permeability, such as the Kozeny-Carman equation did not seem adequate to describe the behavior of the preforms given the influence of the distribution medium and vacuum bag.

As recognized by the previous study, one very important variable in the VARTM process is the high-permeable distribution medium. This is because the flow mechanism for infiltration of the fibers consists of the resin first being pulled across the distribution medium and then leaking through the transverse direction to wet out the part. Therefore, the purpose of the high permeable distribution medium is to supply a low-resistance pathway for resin flow.

Sun et. al. [36], have characterized the effect of the distribution medium on the processing of polymer composites. A three-dimensional control volume/finite element method was developed to model the SCRIMP mold filling based on the use of a high-permeable distribution medium, and was experimentally verified.

The permeability of the distribution medium was determined using an unsteady state method. Flow front locations versus time were measured, and an analytical solution for the permeability was calculated using the following solution for unidirectional flow:

$$t = \frac{\mu \phi s^2}{2KP_0} \tag{4}$$

where, t is the time, K is the permeability, s is the distance from the inlet to the flow front, μ is the viscosity of the measurement fluid, ϕ is the porosity of the high permeable medium, and P_o is the pressure at the inlet. The permeability is calculated from the slope of the t vs. s^2 plot.

Two cases were considered: one in which only the high permeable medium was injected, and another in which the high-permeable medium was stacked on top of a peel ply and fiber mat. The permeability was determined to be much lower in the stacked configuration. This can be attributed the nestling effect, which reduces the porosity of the material by increasing the packing density of the fibers.

Experimental visualization was performed by resin injecting a dry fiber preform with a peel ply and high permeable distribution medium placed on top. Experimental results showed that infiltration time with the high permeable medium was less than one-seventh of the time to infiltrate a preform without the distribution medium. Experiments were also run to determine the effect of the peel ply on infiltration time. The presence of the peel ply in the system increases flow resistance in the transverse direction. However, the peel ply also reduces the nestling effect between the distribution medium and preform, thus increasing permeability. Experiments confirmed that the latter effect dominates the behavior, and thus decreases the mold filling time.

A control volume/finite element method approach was taken for modeling the system. Using Darcy's law with the measured permeability data as an input, the model was used to calculate infiltration times. The model predictions showed good agreement with experimental measurements. Changing process parameters, the model results were used to determine that infiltration is highly dependent on the permeability of the distribution medium, and not very sensitive to the permeability of the fiber preform.

A model was developed by Ni et. al. [37] to determine the behavior of the SCRIMP process based on grooves rather than a high permeable distribution medium. In this case, a low-density core is prepared with cut grooves or channels to carry the resin. The preform is placed on top of the core and resin infuses the entire structure. The idea behind SCRIMP based on grooves is two-fold. First, the core becomes an integral part of the structure, thereby reducing the need for both a distribution medium and a peel ply. Secondly, the permeability of the grooves is much higher than that of the distribution medium, thus the part can be infiltrated more quickly.

Several experimental injections were performed to determine the effect of such parameters as groove size, spacing, and number of layers which could be infiltrated with this process. One experimental observation was the basis of the modeling: the resin fills the grooves before infiltrating the fiber mat.

Because the size of the grooves and the structures manufactured with VARTM can be large, it was viewed as impractical to create the meshes necessary for analysis by a control volume/finite element method scheme. Therefore, a leakage flow model was created to describe infiltration by grooves. The leakage flow assumed one-dimensional line flow in the grooves, followed by infiltration into the preform. The preform was considered to be a sink, and an iterative procedure was used to calculate the pressure distribution in the groove and the leakage flow into the fibers.

The leakage flow model was compared to the CV/FEM model for a simple case and showed good agreement while taking substantially less computational time to run. The leakage flow model was then compared to experimental results, showing good agreement.

Sayre [38] modified a three-dimensional RTM/RFI model [44 – 47] to simulate preform infiltration by VARTM. Specifically, the model was modified to include the effects of capillary pressure and gravity. Rather than assuming pressure the flow front to equal the vacuum pressure, capillary pressure was incorporated:

$$P_{flowfront} = \frac{2}{r_h} \gamma_{lv} \cos\theta \qquad (5)$$

where r_h is the hydraulic radius of the fiber bundle, γ_{lv} is the surface tension, and θ is the contact angle.

A second modification was made to incorporate gravity into the governing equations:

$$\frac{\partial}{\partial x_i}\left(\frac{S_{ij}}{\eta}\frac{\partial P}{\partial x_j} - \frac{S_{ij}}{\eta}\rho g_j\right) = 0 \qquad (6)$$

where ρg_j is the pressure due to gravity.

Experimental verification of the model including capillary pressure and gravity terms showed very good agreement. Accounting for capillary pressure reduced error associated with the zero pressure at the flow front boundary condition. Experimental and predicted response agreed within 2%. Gravity was found to be negligible in all cases.

Permeability studies were performed on a variety of distribution mediums. After the isotropy of the mediums was confirmed, the permeability was measured using a one-dimensional advancing front technique. Model results were verified experimentally by injecting E-glass and carbon multiaxial warp knit preforms with an vinyl ester resin. The model results showed limited affects of changing the permeability of the distribution medium (from 2.92 E-09 m^2 to 3.45 E-09 m^2) on the total infiltration time. However, when the placement of the distribution medium on the preform was changed, there were marked effects on the total time required to infiltrate the preform.

Several studies have addressed the modeling of sandwich structures. Two studies have modeled the behavior of sandwich structures which have some sort of transverse reinforcement. McNamara and McNamara [39] studied a foam core composite sandwich structure reinforced with single and multiple braided glass fiber composite tubes or ties, 0.5 mm in diameter. The structures were developed as energy dissipating composites, to increase the energy absorption of sandwich structures. Using an ABAQUS software package, classical laminate theory was used to model the behavior of the skin materials. The foam was modeled with a crushable foam plasticity model included in the software package, and the ties were mapped with two-noded cubic beam elements.

Mechanical testing was performed on test plaques for both a single-tie plaque and a multi-tie plaque. Four-point bend flexure tests and shear tests were conducted. Experimental results matched model predictions well. The model predicted plasticity of the foam core, which was seen experimentally. The full failure behavior of the ties was not modeled, but the response in the elastic region corresponded well with experimental behavior.

van Vuure et. al. [40] modeled the core properties of woven-sandwich fabric preforms. These fabrics are produced by velvet weaving, and are interwoven with pile fibers through the core. These fabrics can then be injected with resin and cured, or the core can be filled with a thermoformed core, such as polyurethane, phenolic, or syntactic polyester foam. In the case of the foam-filled structures, the finished structure would resemble a foam core composite sandwich structure reinforced with transverse stitching.

Only resin injected panels have been modeled to date. Foam filled panels have not been considered. Using a finite element program to analyze a unit cell of the material, pile shape and resin distribution has been modeled. This is input into a more comprehensive model which simulates the deformations and stresses in the structure.

A third study examined the development of a mold filling simulation for the manufacture of sandwich structures by liquid molding [41]. Using the continuity equation and Darcy's law to describe resin flow, a control volume/finite element model was developed. Model outputs include flow front geometry and position, total infiltration time, pressure and flow rates, and pressure distribution along the walls. Three case studies were conducted to evaluate the effect of different parameters on processing. Results show that the permeability of the face sheets has a great effect on infiltration time and flow front geometry. A second study showed the influence of the injection edge position on infiltration. In all cases tested, the flow fronts merged and progressed towards the vacuum vent. The third study illustrated a "sink effect" of fiber tows. Individual strands were placed on the core material rather than a fibrous mat, and were found to absorb resin even after the flow front had passed. This has implications as to the quality of the finished structure.

2.6 Conclusions

Manufacturing costs have become a critical issue as composite applications move into newer industries. VARTM is a low-cost manufacturing method capable of resin injecting large structures without the use of an autoclave. This is especially attractive to the

aerospace industry, where autoclave size limits the size of the composite structures that can be manufactured. Much of the manufacturing development for VARTM has been done on a trial and error basis. However, trial and error methods are not suited for large-scale production, as the raw material costs can be high. A three-dimensional process model could aide in design and optimization of composites manufactured by VARTM.

Several researchers have attempted to model the flow behavior of the resin during VARTM. These models are based on Darcy's law and the continuity equation as the governing equations. Critical parameters include the resin behavior (i.e., cure kinetics, heat transfer, and viscosity) and the preform characteristics (i.e., permeability, compaction, distribution medium, and injection source).

Sandwich structures have a wide variety of applications, including aerospace, marine, and sporting goods. Transverse stitching has been shown to increase the damage tolerance of the structures, previously a drawback of using sandwich structures. Though some research has been conducted into the mechanical behavior of sandwich structures with transverse reinforcement, a flow model for the resin infiltration of sandwich structures has not yet been developed and verified.

The objectives of this research were to use VARTM to resin infiltrate stitched and unstitched dry carbon fiber preforms with polymethacrylimide foam cores to produce composite sandwich structures. Process parameters considered were the effect of stitch density and foam core thickness on the processing of sandwich structures.

A three-dimensional finite element model for VARTM injection of stitched sandwich structures was experimentally verified. Comparisons of flow front location versus time and total infiltration time were made between experimental observation and finite element model predictions.

Chapter 3. Material Characterization

This chapter details the materials used for fabricating the composite panels. The stitched foam core composite panels consisted of Saertex carbon fiber multiaxial warp knit face sheets secured to a Rohacell 31 IG polymethacrylimide core. Core materials of two different thicknesses, 12.7 mm and 25.4 mm, were used. The density of all core materials used was 32 kg/m^3. The face sheets and core were stitched together in the transverse direction using a 1600 denier Kevlar/PVA thread (four 400 denier strands wrapped together). The unstitched panels were manufactured using the same materials, but were not reinforced in the transverse direction with the Kevlar stitching. The resin used in all experiments was a room temperature cure Dow Derakane 510A-40 vinyl ester. Two different resin mixtures were evaluated. The first used a cobalt napthenate catalyst at 0.3 weight % and a methyl ethyl ketone peroxide (MEKP) promoter at 1.25 weight %. A second mixture was evaluated with decreased amounts of catalyst and promoter added. This mixture consisted of 0.2 weight % cobalt napthenate and 1.0 weight % MEKP.

3.1 Resin viscosity

The time to gelation for the 0.3 weight % cobalt napthenate and 1.25 weight % MEKP was less than one hour. This was insufficient for complete processing of the composite panels and thus the quantities of each were decreased to increase the working time of the resin. Though the Derakane 510A-40 was used in all model verification studies, four different batches of the vinyl ester were used over the course of experimentation. Each had subtle differences in resin viscosity, and thus the viscosity of each was evaluated.

All viscosity measurements were taken with a Brookfield Model DV-III Concentric Cylinder Digital Rheometer. The rheometer measures the resin viscosity by rotating a spindle immersed in test fluid. The viscous drag caused by the fluid is measured using the deflection of a calibratred spring. All tests were run with a constant spindle speed of 10 revolutions per minute.

Because all panels were manufactured at room temperature, only isothermal measurements at room temperature were conducted. The results of Batch 1 are shown in Figures 3.1 and 3.2. Figure 3.1 shows the 0.3 weight % cobalt napthenate and 1.25 weight % MEKP mixture. Figure 3.2 shows the 0.2 weight % cobalt napthenate and 1.0 weight % MEKP mixture. Based on data presented by Sayre [38], the expected gel time of this mixture should have approached one hour. However, the Batch 1 resin gelled in approximately 25 minutes. As this was insufficient time to process a of 30.5 cm x 64.5 cm panel, the resin formulation was changed. Using the second formulation of 0.2 weight % cobalt napthenate and 1.0 weight % MEKP, the time to gel increased to greater than 50 minutes. However, the initial viscosity of the resin was 0.55 Pa·s. This was substantially higher than the viscosity measured in the other samples of vinyl ester, and thus no panels were injected using Batch 1.

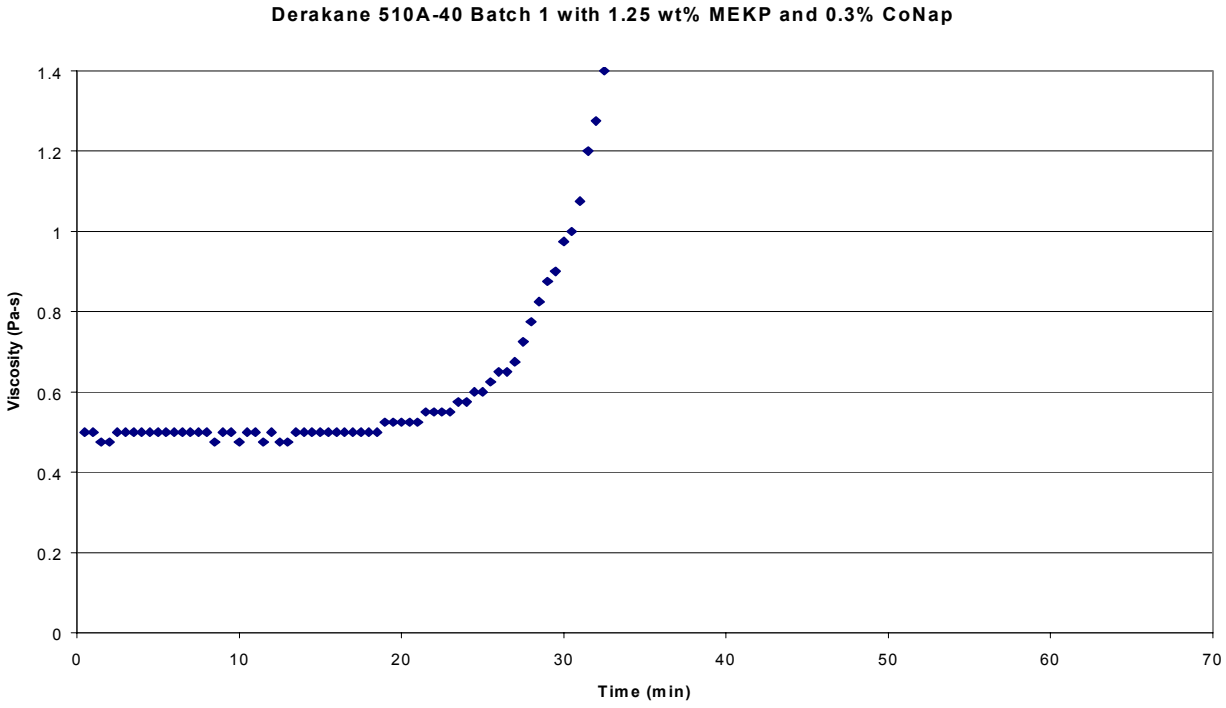

Figure 3.1 – Viscosity trace of Derakane 510A-40 vinyl ester resin with 0.3% CoNap and 1.25% MEKP.

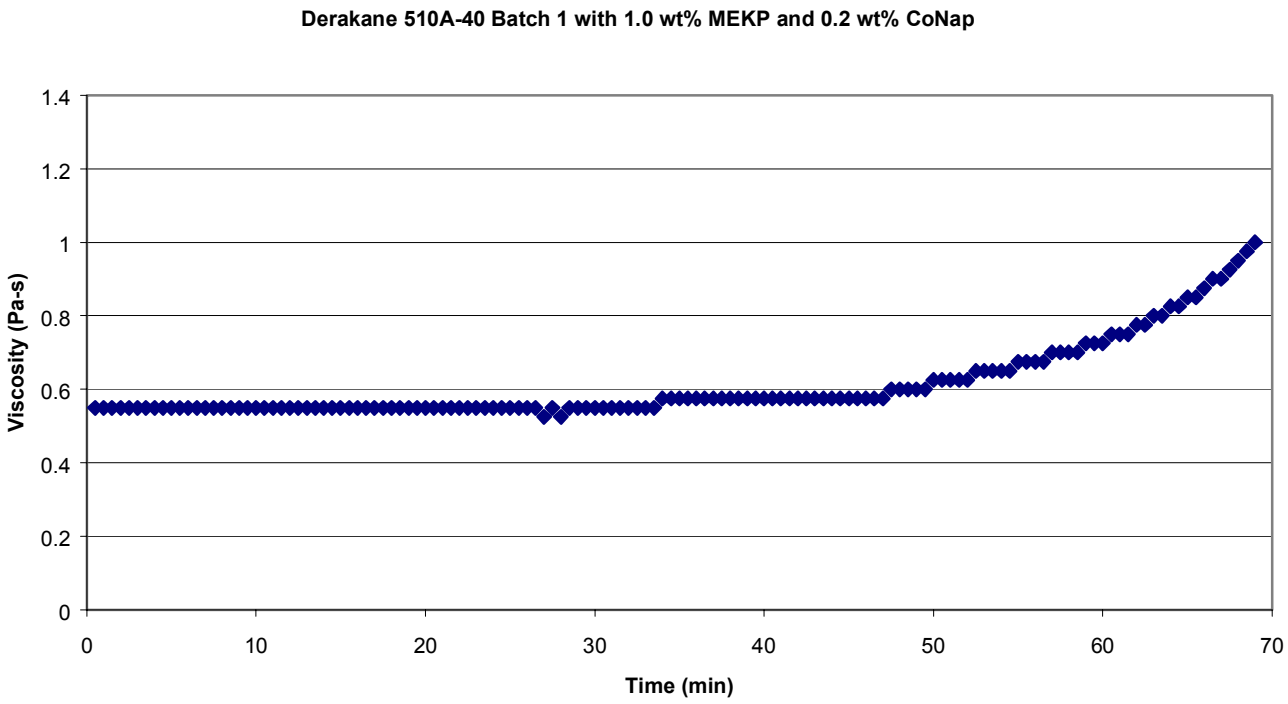

Figure 3.2 – Viscosity trace of Derakane 510A-40 Batch 1 with 0.2% CoNap and 1.0% MEKP.

Batch 2 results are shown in Figure 3.3 and 3.4. Using the first formulation, the resin gelled in approximately 40 minutes with an initial viscosity of 0.45 Pa·s. The second formulation increased the t_{gel} to approximately 50 minutes with an initial viscosity of 0.475 Pa·s.

Results of the rheology study were used to determine that the second formulation (0.2% CoNap and 1.0% MEKP) would be used for all of the experiments. Batch 3 resin was evaluated using the second formulation, the results of which can be found in Figure 3.5. Batch 3 had a t_{gel} of approximately 50 minutes and an initial viscosity of 0.425 Pa·s.

Batch 4 was evaluated using the second formulation and the results are shown in Figure 3.6. Batch 4 had a t_{gel} of approximately 50 minutes and an initial viscosity of 0.4 Pa·s. The rheology of the system indicates that the resin is a reactive system, with a dynamic viscosity profile during cure.

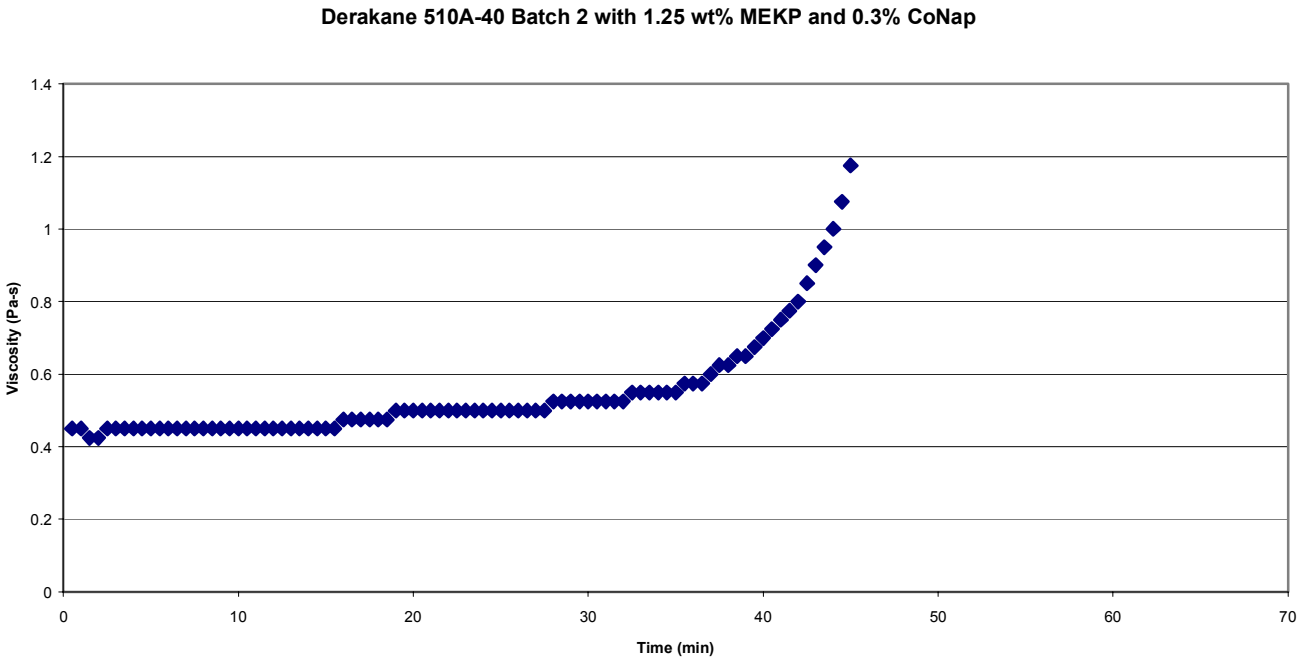

Figure 3.3 – Viscosity trace of Derakane 510A-40 Batch 2 resin with 0.3% CoNap and 1.25% MEKP.

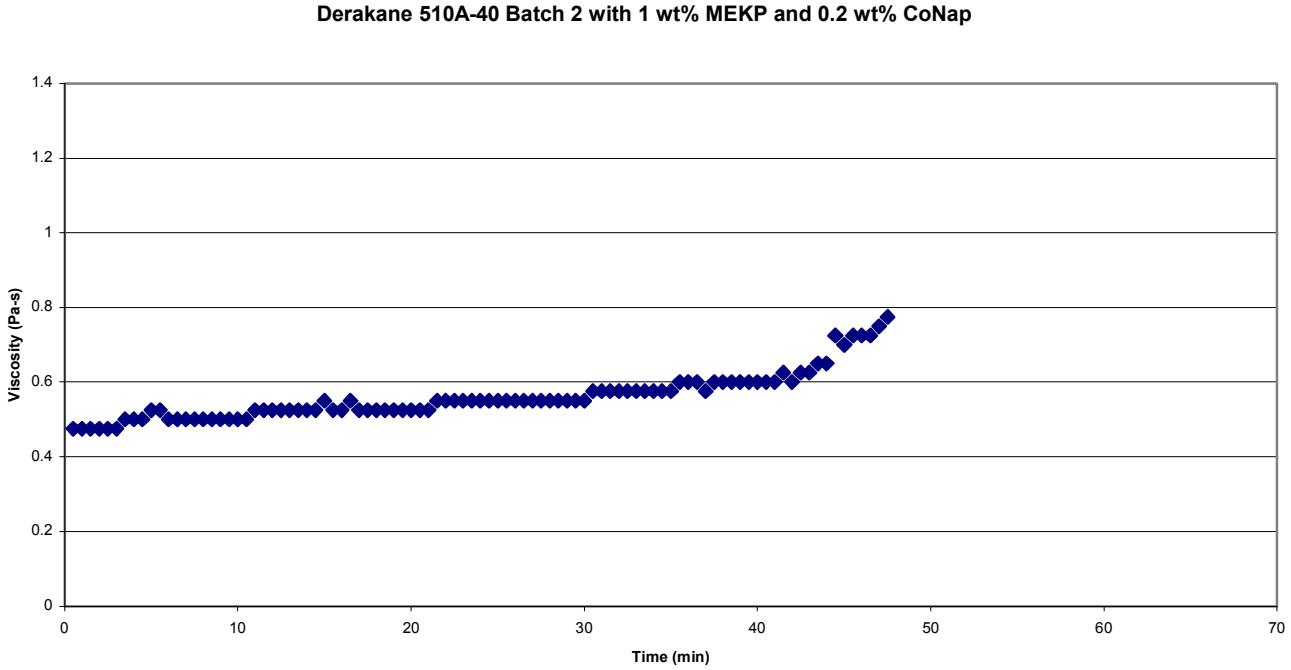

Figure 3.4 – Viscosity trace of Derakane 510A-40 Batch 2 resin with 0.2% CoNap and 1.0% MEKP.

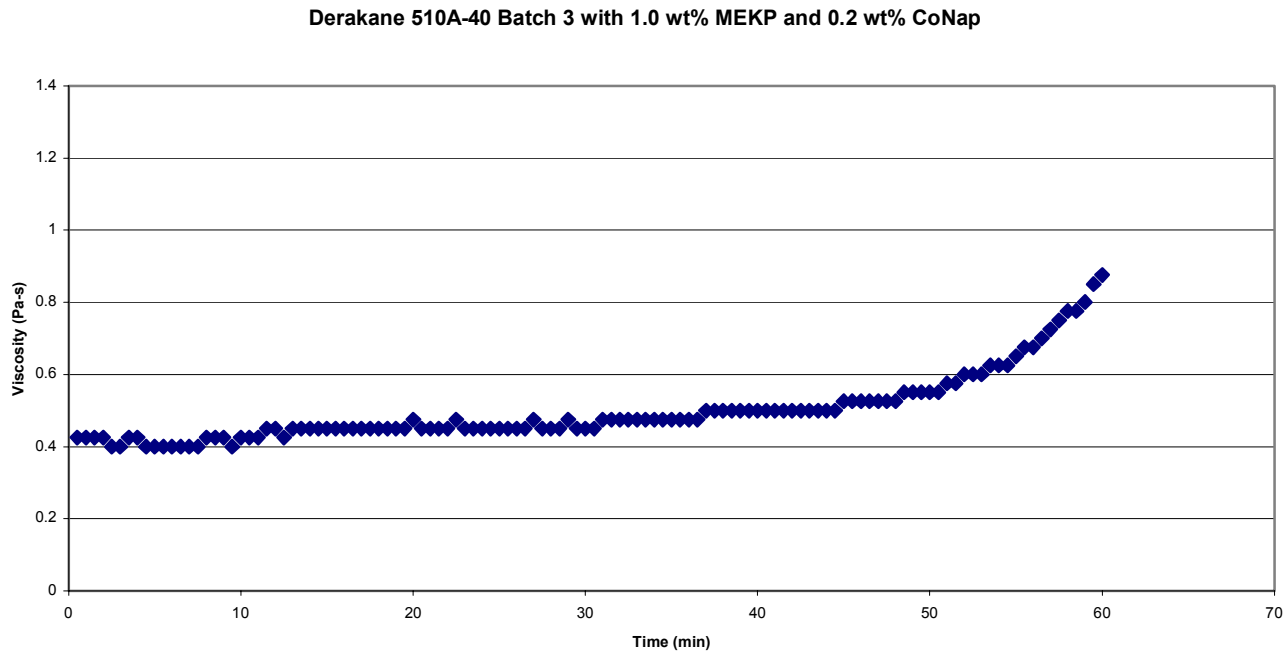

Figure 3.5 – Viscosity trace of Derakane 510A-40 Batch 3 with 0.2% CoNap and 1.0% MEKP.

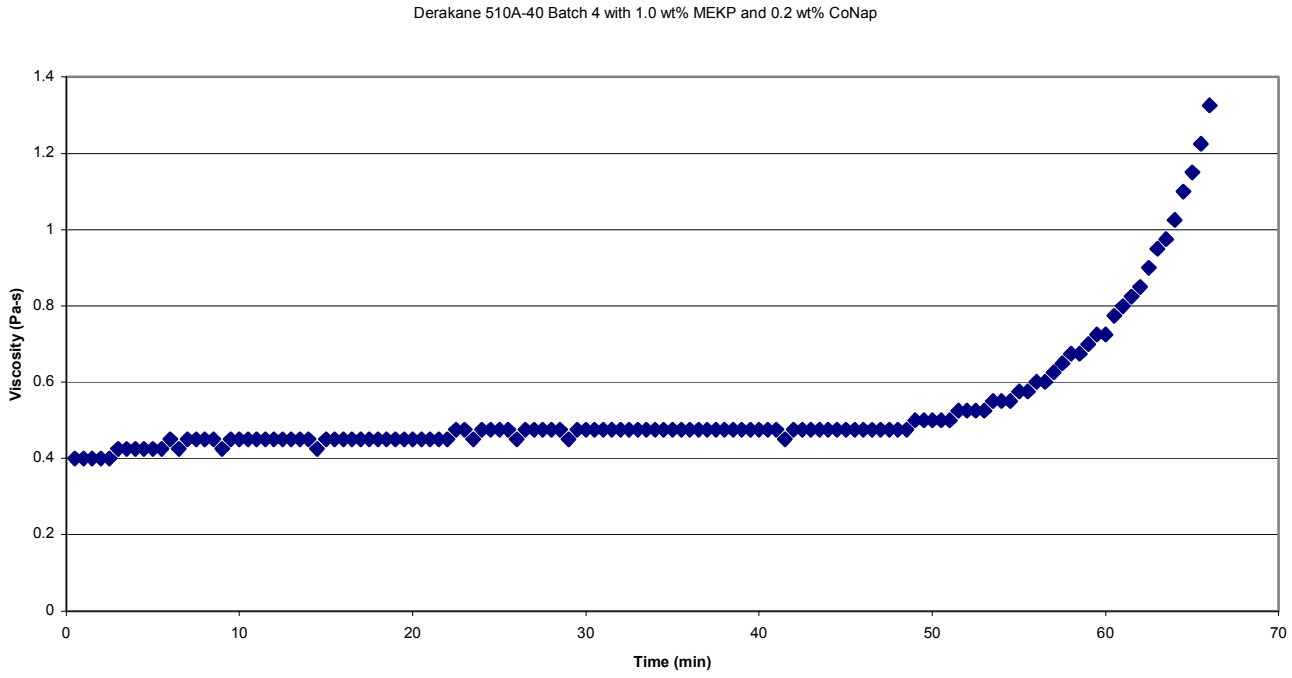

Figure 3.6 – Viscosity trace of Derakane 510A-40 Batch 4 with 0.2% CoNap and 1.0% MEKP.

3.2 Differential scanning calorimetry

Differential scanning calorimetry (DSC) is a thermal analysis method used to evaluate the kinetic behavior of the resin systems and to estimate the degree of cure of the cured resin. In all DSC experiments, the basic assumption is that the rate of heat generation is proportional to the rate of the cure reaction. The degree of cure, $\alpha(t)$, can be defined as:

$$\alpha(t) = \frac{H(t)}{H_R} \tag{1}$$

where *H(t)* is the heat evolved from the beginning of the reaction to some intermediate time, *t*, and H_R is the total heat of reaction during cure. The value of α ranges from 0 for an uncured resin to 1 for a fully cured resin. The heat terms are defined as:

$$H(t) = \int_0^t \left(\frac{dH}{dt} \right) dt \tag{2}$$

$$H_R = \int_0^{t_c} \left(\frac{dH}{dt} \right) dt \tag{3}$$

where t_c is the total time for the resin to cure. These integrals represent the area under the curve of the $\frac{dH}{dt}$ vs. *t* graphs.

There are some inherent flaws in using DSC to measure heat generation. Isothermal scans have limitations when measuring room temperature cure resins, or resins with a fast reaction rate. Some studies have shown the initial 10% of the data from isothermal scans to be inaccurate [30, 42]. Because of the highly reactive nature of the resin system used in this study, dynamic scans were used to evaluate the thermal properties of the resin.

DSC experiments were performed on a TA Instruments DCS Model 2920 with a 35 ml/min nitrogen purge. The equipment was calibrated using standard indium and lead samples. All samples ranged from 5.0 mg – 9.0 mg and were encapsulated in hermetically sealed aluminum pans.

Dynamic scans of the resin were performed at a rate of 10 °C/min from room temperature to 220 °C. Only Batch 3 and Batch 4 resins were examined as a part of this study. For each batch of resin, duplicate samples were run for both virgin samples and samples after 24 hours of cure at room temperature.

The virgin samples were used to determine the total heat of reaction. However, because the vinyl ester cures at room temperature, it is extremely difficult to accurately determine the total heat of reaction. Figure 3.7 shows the results of a dynamic scan of the virgin sample of Batch 3 resin. The total heat of reaction was measured as 248 J/g. Figure 3.8 shows the results of the dynamic scan of the sample which was cured for 24 hours prior to testing. This shows a residual heat of reaction of 79.8 J/g. The sample had an approximate degree of cure of 0.68. Figure 3.9 shows the results of a dynamic scan of the virgin sample of Batch 4 resin. The total heat of reaction was measured as 255 J/g. Figure 3.10 shows the results of the dynamic scan of the sample which was cured for 24 hours prior to testing. This shows a residual heat of 93.7 J/g. The sample had an approximate degree of cure of 0.63. Both samples indicate that an elevated temperature post cure may be helpful in increasing the degree of cure for the resin.

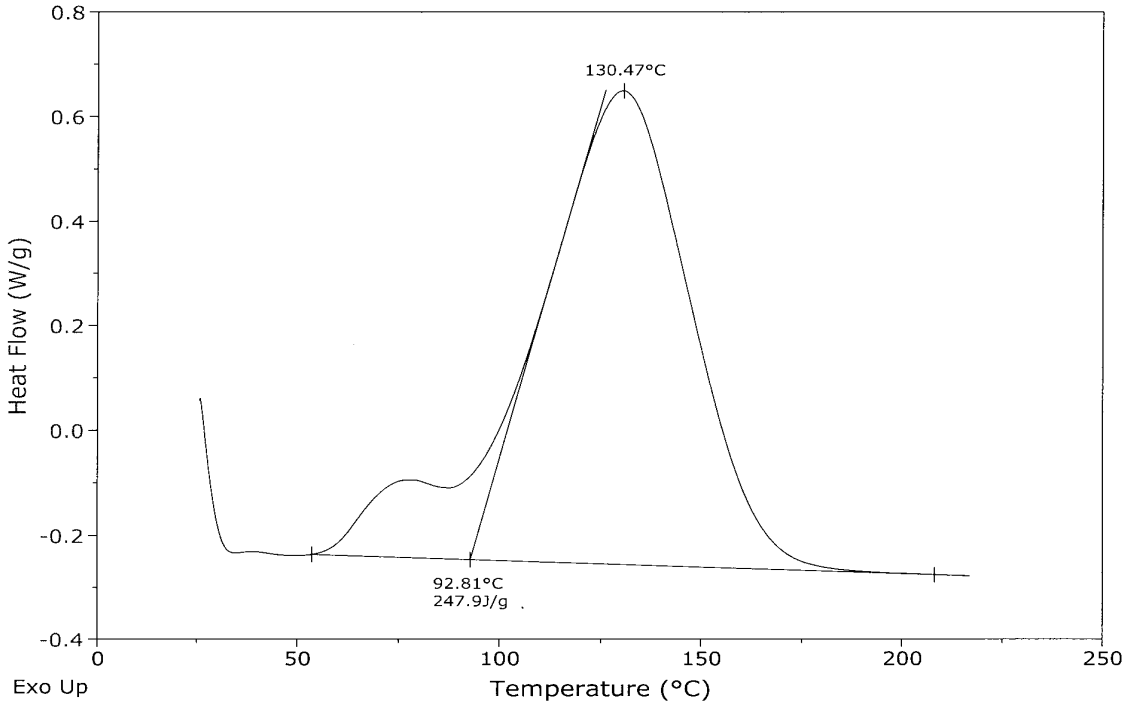

Figure 3.7 – Dynamic DSC scan of virgin Derakane 510A-40 Batch 3 resin at 10°C/min from 25°C to 220°C. The total heat of reaction was 247.9 J/g.

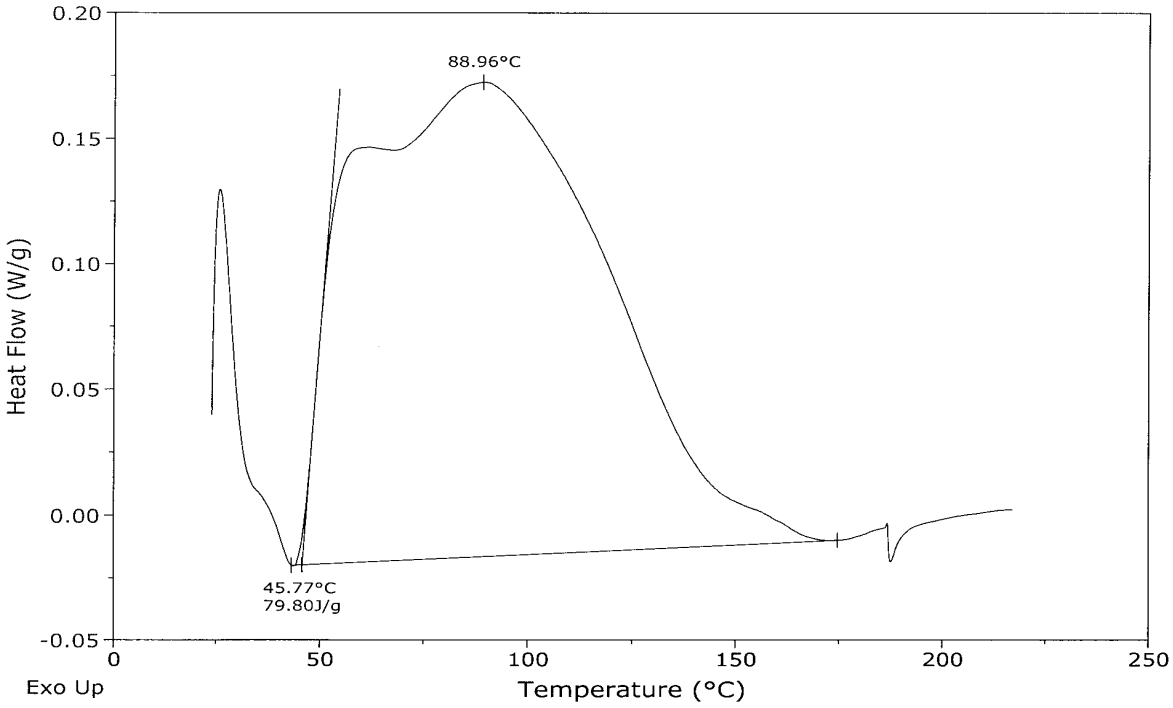

Figure 3.8 – Residual DSC scan of Derakane 510A-40 Batch 3 at 10°C/min from 25°C to 220°C. The residual heat of reaction was 79.80 J/g.

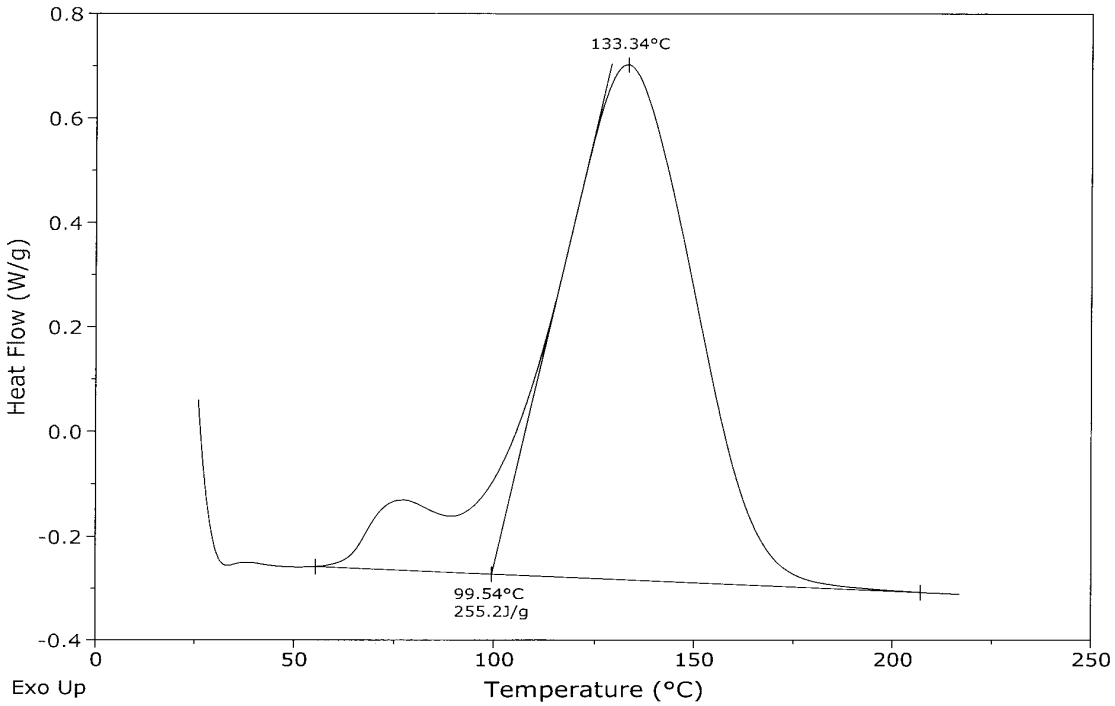

Figure 3.9 – Dynamic DSC scan of virgin Derakane 510A-40 Batch 4 resin at 10°C/min from 25°C to 220°C. The total heat of reaction was 255.2 J/g.

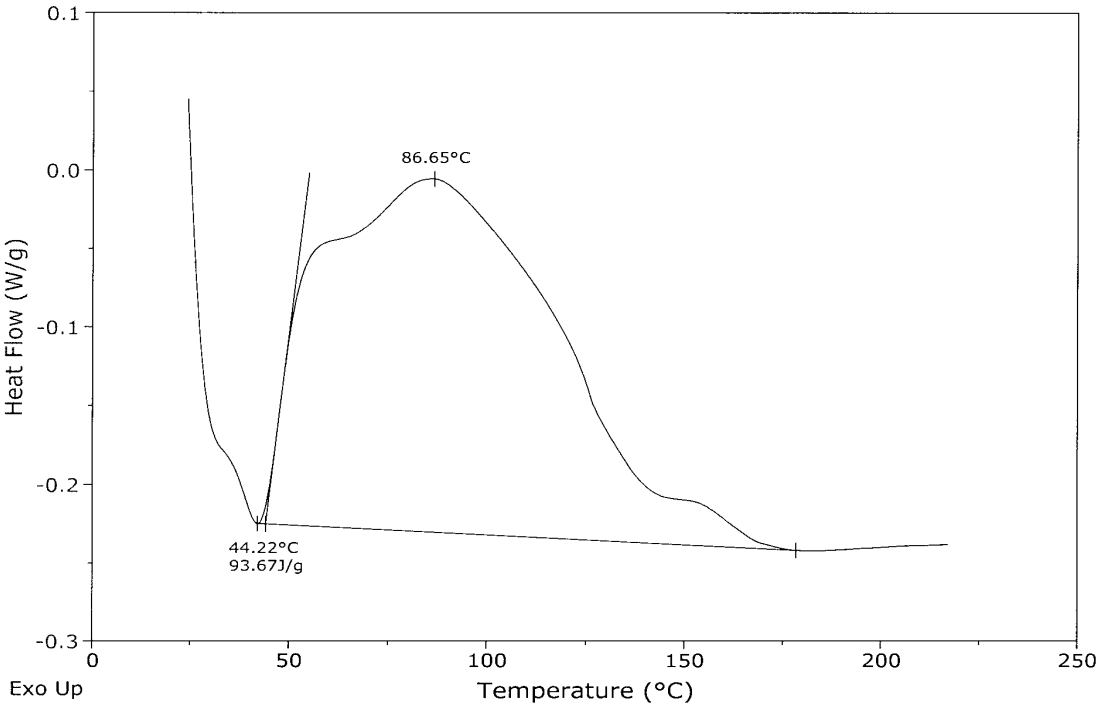

Figure 3.10 – Residual DSC scan of Derakane 510A-40 Batch 4 resin at 10°C/min from 25°C to 220°C. The residual heat of reaction was 93.67 J/g.

3.3 Foam Core Properties

Rohacell 31 IG polymethacrylimide foam with 32 kg/m^3 density was used as the core material for both the stitched an unstitched panels. Thicknesses of 12.7 mm and 25.4 mm were used. The mechanical property data for the Rohacell foam was provided by Northern Fiber Glass Sales, Inc. [43], a supplier of Rohacell products. Table 3.1 lists the mechanical properties of the foam.

Table 3.1 – Selected mechanical properties of Rohacell 31 IG polymethacrylimide closed cell foam

Property	Value
Density	32 kg/m^3
Compressive Strength	0.4 MPa
Tensile Strength	1.0 MPa
Flexural Strength	0.8 MPa
Shear Strength	0.4 MPa
Elastic Modulus	36 MPa
Shear Modulus	13 MPa
Elongation at Break	3.5%
Heat Distortion Resistance	180 °C

Chapter 4. Manufacturing

Two manufacturing procedures were developed as part of this study. First, manufacturing of an unstitched foam core composite panel was explored. The unstitched panels consist of two Saertex carbon fiber multiaxial warp knit face sheets bonded to a Rohacell polymethacylimide foam core using a room temperature cure Derakane 510A-40 vinyl ester resin.

Next, the manufacturing procedure for a stitched preform was developed. The stitched preform consists of two 3-mm thick Saertex carbon fiber multiaxial warp knit face sheets and a Rohacell 31 IG PMI foam core. The sandwich preform was stitched through the thickness with a 1600 denier Kevlar/PVA thread. A 12.7 mm thick foam core and a 25.4 mm thick foam core were examined. For the 12.7 mm foam core, stitch row spacings of 6.35, 12.7, and 25.4 mm were fabricated. For the 25.4 mm thick foam core, only the 12.7 mm row spacing was injected. All panels had a pitch of 4 stitches per 25.4 mm. The resin used for processing all panels was the Derakane 510A-40 vinyl ester.

4.1 VARTM processing of unstitched foam core composite panels

A typical layup of an unstitched foam core composite panel is shown in Figure 4.1. The panel is comprised of carbon face sheets and a polymethacrylimide foam core. Two different unstitched preform configurations were resin injected. During the initial phase of manufacturing development, an arbitrary panel size of 20.3 cm x 30.5 cm was selected. A single 1.5 mm thick layer of the Saertex multiaxial warp knit (MAWK) material was cut for each skin. These skins were bonded to a 19 mm thick Rohacell 71 IG PMI foam core with a density of 75 kg/m^3. Once appropriate manufacturing practices were developed, they were used to resin infuse a second panel configuration which more closely resembled the makeup of the stitched panels. For the second configuration, the panel size was 30.5 cm x 64.5 cm. The skins consisted of two layers of the Saertex carbon MAWK material, with approximate thickness of 3 mm, bonded to a 12.7 mm thick Rohacell 31 IG PMI foam core with a density of 32 kg/m^3. For both panel types, the manufacturing process was the same.

The desired number of face sheets and the foam core were cut to the same selected dimensions. Two sheets of porous peel-ply material were cut to the same size as the core and facing sheets. Two pieces of nylon high permeable distribution medium were cut to be approximately 25.4 mm smaller than the preform in both width and length dimensions. The distribution medium has smaller dimensions than the preform to prevent the development of high-permeable flow pathways around the perimeter of the preform. These flow paths could cause race tracking around the panel or a separated flow front, resulting in entrapped air voids in the finished part.

After all materials were prepared, the panel was laid up. The unstitched panel is vacuum bagged on both the top and bottom surfaces. A layer of vacuum bag was first placed on an aluminum tool plate. The nylon screen, followed by the peel ply, carbon fabric and foam core were laid onto the vacuum bag. The peel ply, carbon fabric and foam core were aligned on all sides. The nylon distribution medium was aligned with the injection edge of the panel and centered. Another layer of carbon fabric was placed on top of the core material, the peel ply was placed on top of the fabric, and the nylon distribution medium was positioned on top of the peel ply and aligned with the injection edge of the panel. Next, the resin distribution tube was prepared by drilling 3.18 mm diameter holes 25.4 mm apart along the length. One end of the tube is plugged with a brass fitting.

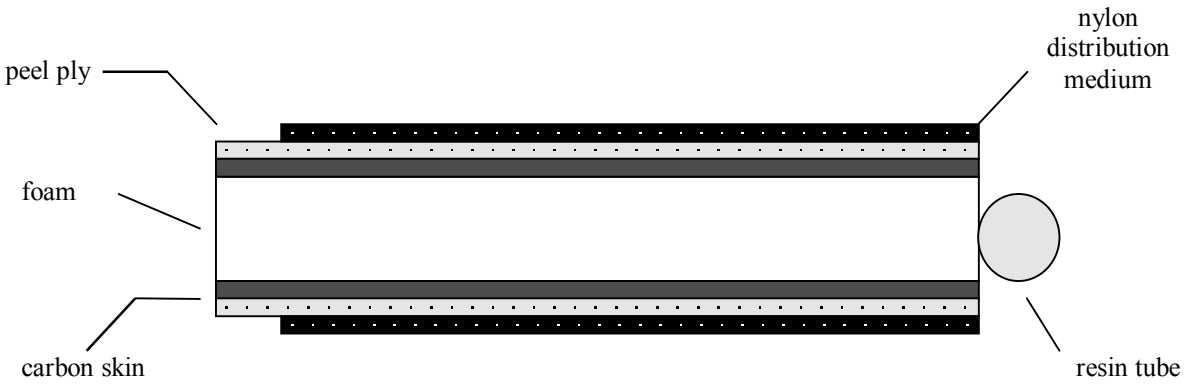

Figure 4.1 – Side schematic diagram of VARTM lay-up for an unstitched sandwich panel.

Vacuum bag sealant was placed around the entire assembly, building up to half the thickness of the panel at the injection edge. The resin tube was secured on top of the sealant, centered along the injection edge of the panel. Bleeder/breather material was cut

to the same width as the preform and positioned at the end opposite the resin tube. A vacuum port was placed in the center of the bleeder/breather material. Finally, another layer of vacuum bag is sealed over the entire assembly, and the other end of the resin tube is plugged. A top view of the lay-up is shown in Figure 4.2.

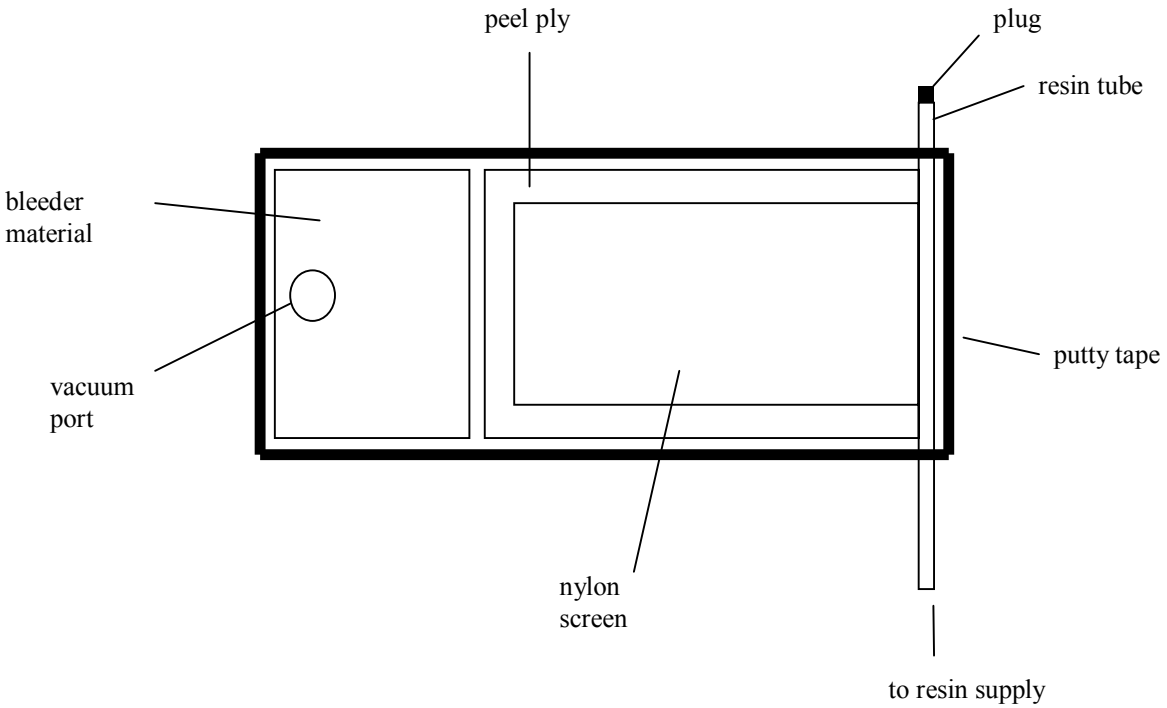

Figure 4.2 – Top view of VARTM lay-up for injection of an unstitched sandwich structure.

Once the lay-up was completed, vacuum was applied to the assembly to expel any air and check for leaks. When using the Derakane 510A-40 vinyl ester resin, approximately 1300 g resin was used to inject the 30.5 cm x 64.5 cm panels. The vinyl ester resin with 1.0 weight % MEKP and 0.2 weight % cobalt napthanate has a processing time of approximately 45 minutes at room temperature, though the exact time varies and should be verified prior to injection. After mixing, the resin was allowed to degas prior to injection. When the system equilibrated and all air leaks were contained, the seal was removed from one end of the resin tube and the tube was placed in the resin source. Resin was allowed to flow into the preform until both face sheets were infiltrated and then the resin distribution tube was clamped off.

The vacuum source was left on until the resin had completely gelled. The panel was then cured at room temperature for 24 hours before disassembling the lay-up.

4.2 VARTM processing of stitched foam core composite panels

A dry, stitched foam core preform consists of two carbon face sheets of approximately 3 mm thickness attached to a polymethacrylimide foam core by stitching through the thickness of the preform with a 1600 denier Kevlar/PVA thread. A 12.7 mm thick foam core and a 25.4 mm thick foam core were examined. 12.7 mm thick foam core panels were fabricated with stitch row spacings of 6.25, 12.7, and 25.4 mm. The 25.4 mm thick foam core panel was fabricated with a stitch row spacing of 12.7 mm. For all stitched panels, the pitch was 4 stitches per 25.4 mm. All panels had the approximate dimensions of 30.5 cm x 64.5 cm.

The needle penetrations caused by the stitching act as resin paths from the top surface to the bottom surface of the preform. Therefore, resin need only be infused along the top face sheet. A schematic diagram of the lay-up for the stitched preforms is shown in Figure 4.3.

An aluminum tool plate was treated with a release agent over the area on which manufacturing took place. A porous peel ply material was cut with dimensions of 30.5 cm x 64.5 cm to fit the area of the preform, and was placed directly on top of the preform. Then, a nylon high-permeable distribution medium was cut to be approximately 25.4 mm smaller than the preform in both width and length for reasons as described in the previous section. The nylon was placed on top of the peel ply, aligned with the injection edge of the panel and centered. A resin distribution tube was prepared by drilling 3.18 mm diameter holes 25.4 mm apart along the length. The number of holes is determined by the width of the panel. One end of the tube was plugged with a brass fitting. Finally, glass bleeder/breather material was cut to the same width as the preform and placed on the tool plate at the end opposite the resin tube.

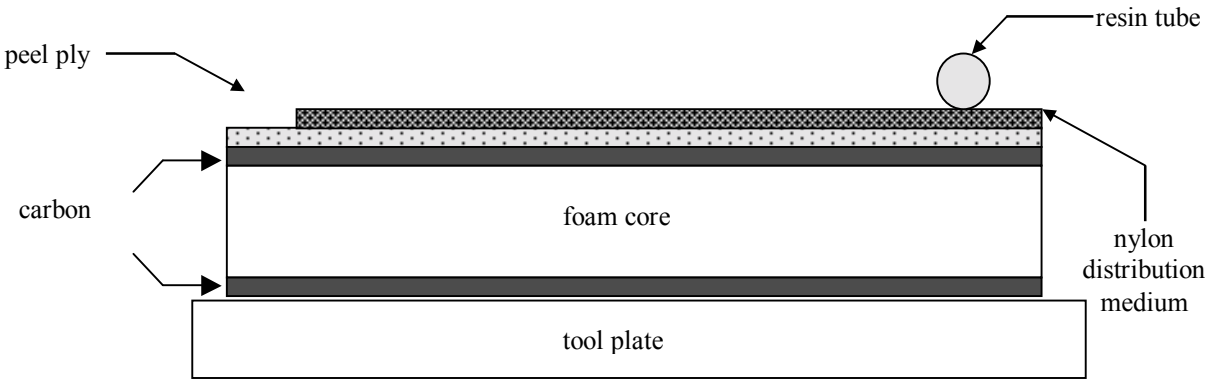

Figure 4.3 – Side schematic diagram of VARTM lay-up for stitched sandwich structures.

After the materials were prepared and assembled, vacuum bag sealant was placed around the entire assembly, building up to the thickness of the panel at a distance of 25.4 mm from the injection edge. The resin tube was placed on top of the distribution medium at a distance of 25.4 mm from the edge and secured using the sealant. A vacuum port was centered on the bleeder/breather material. Finally, the vacuum bag was sealed over the entire assembly. The other end of the resin tube was plugged, and a vacuum was applied to expel any air. Figure 4.4 shows the entire assembly lay-up.

Figure 4.4 – VARTM processing set-up for a stitched foam core composite panel.

Once the lay-up was completed, processing was begun. When using the Derakane 510A-40 vinyl ester resin, approximately 1300 g resin was used to inject the 30.5 cm x 64.5 cm panels. The vinyl ester resin with 1.0 weight % MEKP and 0.2 weight % cobalt napthanate has a processing time of approximately 45 minutes at room temperature, though the exact time varies and should be verified prior to injection. After mixing, the resin was allowed to degas prior to injection. When the system equilibrated and all air leaks were contained, one end of the resin tube was cut and placed in the resin source.

The resin infiltrates the preform in two ways. First, the resin moves across the high permeable distribution medium, and then the resin 'leaks' through the stitch paths to infiltrate in the transverse direction. When both face sheets were completely infiltrated, the resin distribution tube was clamped off.

The vacuum source was left on until the resin in the panel gelled. The panel was then left to cure at room temperature for 24 hours before removing from the tool plate.

Chapter 5. Experimental Model Verification

5.1 Model development

A three-dimensional finite element model has been developed to simulate resin flow through a dry fiber preform. Originally developed as a two-dimensional model to simulate resin transfer molding (RTM) processes and resin film infusion (RFI) processes [44], the program was expanded to consider three-dimensional RTM processes [45], and three-dimensional RTM/RFI processes [46]. Most recently the model, 3DINFIL, has been modified to include vacuum assisted resin transfer molding processes by considering capillary effects and gravitational forces [38].

3DINFIL is a three-dimensional finite element model which consists of submodels to analyze heat transfer, cure kinetics, preform compaction, residual stresses and resin flow during processing. Using PATRAN, a three dimensional mesh of the preform is developed using eight noded brick elements. Along with the mesh, temperature and pressure cycles and boundary conditions are input to the code. A database exists of material properties for both the resin and fiber systems. The code then uses the given inputs to numerically solve the governing equations.

For analyzing resin infiltration of stitched sandwich structures, only the resin flow submodel was used. This submodel allows for the calculation of pressure and velocity fields in the resin. From these quantities, flow front location versus time and total time required to infiltrate the preform can be determined and output from the code.

The governing equation for flow through a porous medium is Darcy's Law:

$$q_i = -\frac{1}{\eta} S_{ij} \frac{\partial P}{\partial x_j} \qquad (1)$$

where, q_i is the superficial velocity vector, η is the resin viscosity, S_{ij} is the three-dimensional permeability tensor, and $\frac{\partial P}{\partial x_j}$ are the pressure gradients within the preform. Darcy's Law assumes the following:

- flow is laminar
- preform is a heterogeneous, anisotropic porous medium
- fluid is incompressible

The boundary conditions used to solve this equation include:

- inlet pressure is known, i.e. $P_{inlet} = P$
- pressure at the flow front is equal to zero
- there is no flow through the mold walls, i.e. the velocity normal to the wall at the boundary is zero

5.1.1 *Strip model for stitched sandwich structures*

A finite element model was created to evaluate resin infiltration of stitched sandwich structures. Flow occurs in the preform in two ways. First, the resin flows across the region of high permeability, infiltrates the top face sheet, flows through the non-porous foam by 'leaking' through the holes created by the needle penetrations of the stitching, and finally infiltrates the bottom face sheet. Therefore, for the stitched preform, the finite element mesh includes a high permeable distribution medium and two porous multiaxial warp knit face sheets separated by a foam core. The compaction and permeability of the face sheets has been measured [47] and is included in the 3DINFIL material database as a multiaxial warp knit Tenax material. The permeability of the high permeable distribution medium has been determined and incorporated into the material database [38]. The core is modeled as having porous regions or 'strips' encompassing the transverse stitching. These strips allow resin flow in the transverse direction of the foam core while flow in the in-plane directions of the foam is zero.

For the 12.7 mm thick foam core preform, each strip has the dimensions of 3.18 mm x 619 mm x 12.7 mm which represents one row of stitching. Therefore, the panel with the 6.35 mm stitch spacing has a total of 44 strips, the panel with the 12.7 mm stitch spacing has a total of 23 strips, and the panel with the 25.4 mm stitch spacing has a total of 12 strips. Due to variations in the dimensions of the preforms, the 25.4 mm thick foam core preform has strips with dimensions of 3.18 mm x 603 mm x 25.4 mm.

The porosity of each strip is determined by considering the ratio of the pore area to the total area of the strip as follows:

$$\varphi = \frac{A_{pores}}{A_{strips}} \tag{2}$$

where, ϕ is the porosity, A_{pores} is the total area of all the pores through which resin can flow, and A_{strips} is the total area of the strips.

The area of the pores is calculated by considering the area of the hole made by the needle and subtracting the area of the stitching threads filling the holes,

$$A_{pores} = n \times (A_{hole} - 2A_{thread}) \tag{3}$$

where, n is the number of stitches per inch, A_{hole} is the area of the needle penetration in the foam core and A_{thread} is the area of the reinforcing Kevlar thread, determined from the denier of the thread.

5.2 Experimental setup

Visualization experiments were performed to verify the finite element model. Using the manufacturing procedures described in Chapter 4, panels were resin injected to measure the flow front location as a function of time, as well as, the total infiltration time.

The model verification experiments were performed by placing the stitched foam core preform on a tempered glass tool plate. The glass plate was placed on a polycarbonate infiltration table so that resin infiltration of the bottom preform surface could be observed. The preform was prepared for injection using the manufacturing procedures described in Chapter 4. In order to measure the flow front position in the upper and lower carbon face sheets, straight lines were drawn at measured intervals on the surface of the vacuum bag and on the bottom surface of the glass tool plate, respectively. The complete preform layup with grid markings shown can be seen in Figure 5.1.

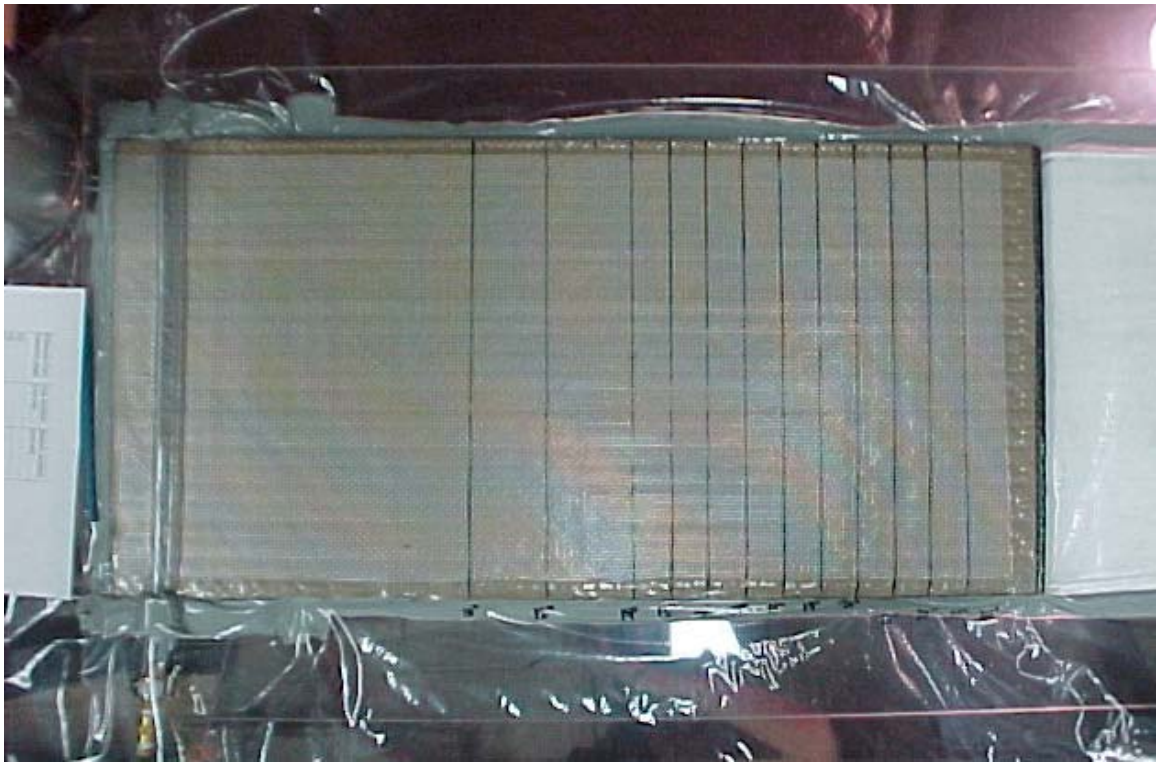

Figure 5.1 – Experimental setup of a stitched preform. The grid marks are used to determine the flow front location as a function of time.

Visual observations were made in two ways. On the top surface, a digital camera was used to capture images of the flow front as a function of time. A minute/second timer was used to record the infiltration time. The timer is started when the resin filled the resin tube. Then, as the flow reaches a grid mark, the time is recorded and a digital image is captured. Using an angled mirror, the images from the bottom surface are

reflected and recorded using a video camera. Subsequent flow front position versus time readings are determined from review of the video tape. A schematic diagram of the experimental verification setup is shown in Figure 5.2.

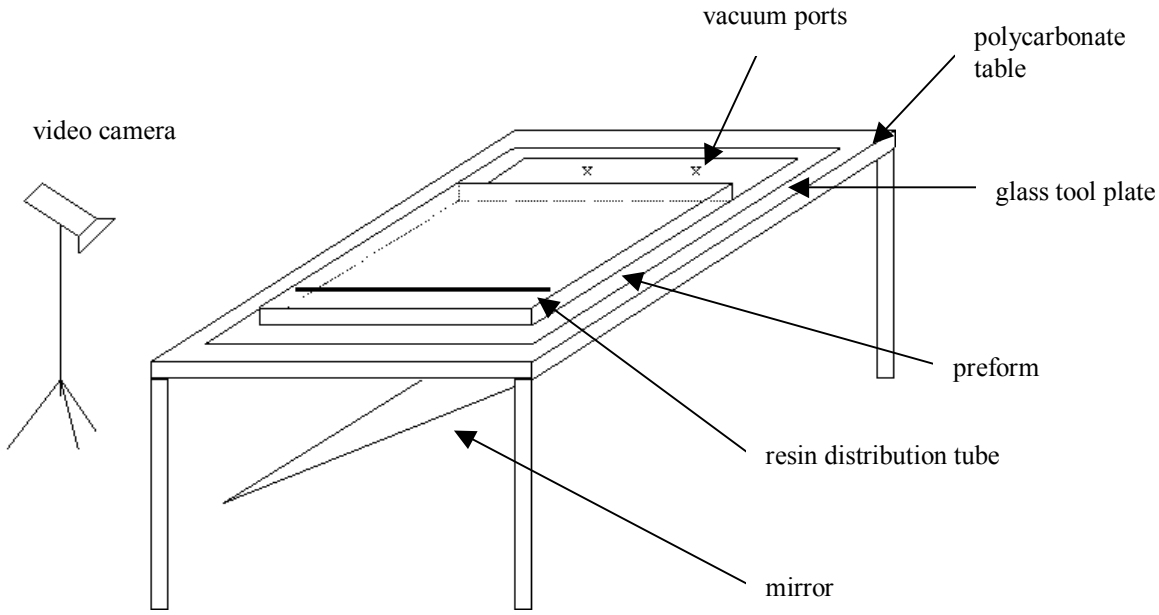

Figure 5.2 – Schematic diagram of setup for experimental model verification.

There was some error associated with determining the infiltration time on the bottom surface of the preform due to the fact that the flow front is non-uniform. The time was recorded when the bulk of the flow front reached the demarcation, and the same procedure was used throughout when analyzing the data.

5.3 Flow front location and total infiltration time

Three stitched preforms with 3 mm thick carbon face sheets and 12.7 mm thick foam cores were resin injected. The three preforms had the same stitch pitch of 4 stitches per 25.4 mm, but different stitch row spacings. The stitch spacings were 6.35 mm, 12.7 mm,

and 25.4 mm. A fourth preform with a thicker core was resin injected. The foam core was 25.4 mm thick, and the stitch row spacing of the panel was 12.7 mm.

5.3.1 Case 1 – 12.7 mm foam core with 12.7 mm stitch row spacing

The first case modeled was the preform with the 12.7 mm thick foam core and the 12.7 mm stitch row spacing. The mesh for this case can be seen in Figure 5.3, and contains 6,588 elements and 11,276 nodes. The porosity for this panel was calculated to be 0.0841.

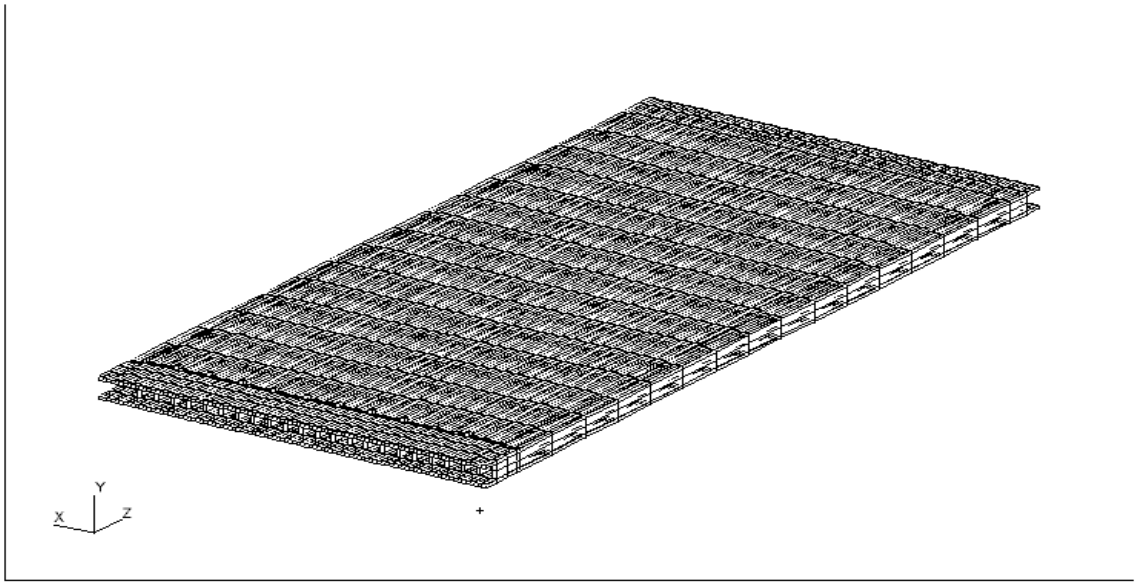

Figure 5.3 – Finite element mesh for the 12.7 mm thick foam core preform with 12.7 mm stitch row spacing.

Figures 5.4 through 5.11 show the progression of the flow front at the surface of the top face sheet of the preform. The flow front on the top surface is fairly uniform throughout the infiltration. Figure 5.12 shows the model predicted infiltration patterns for the surface of the top face sheet. The flow patterns in the upper face sheet have approximately the same shape as the measured flow patterns.

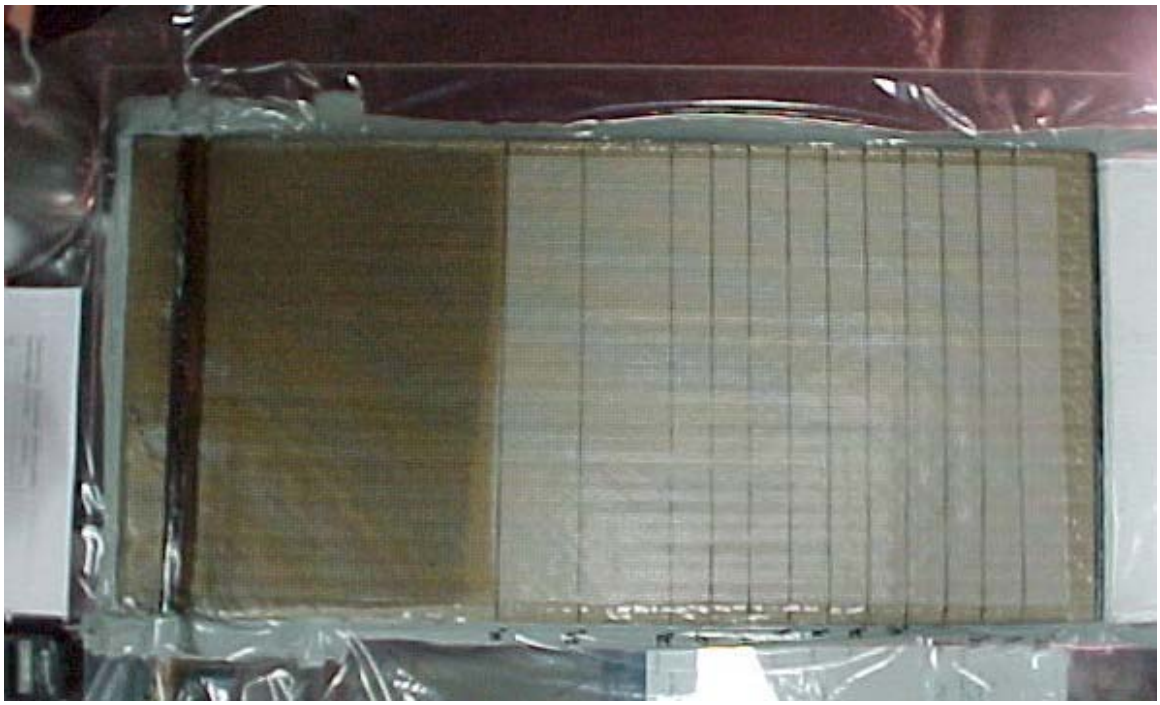

Figure 5.4 – 12.7 mm thick foam core preform with 12.7 mm stitch row spacing. Flow front is approximately 25.4 cm from injection edge.

Figure 5.5 – 12.7 mm thick foam core preform with 12.7 mm stitch row spacing. Flow front is approximately 30.5 cm from injection edge.

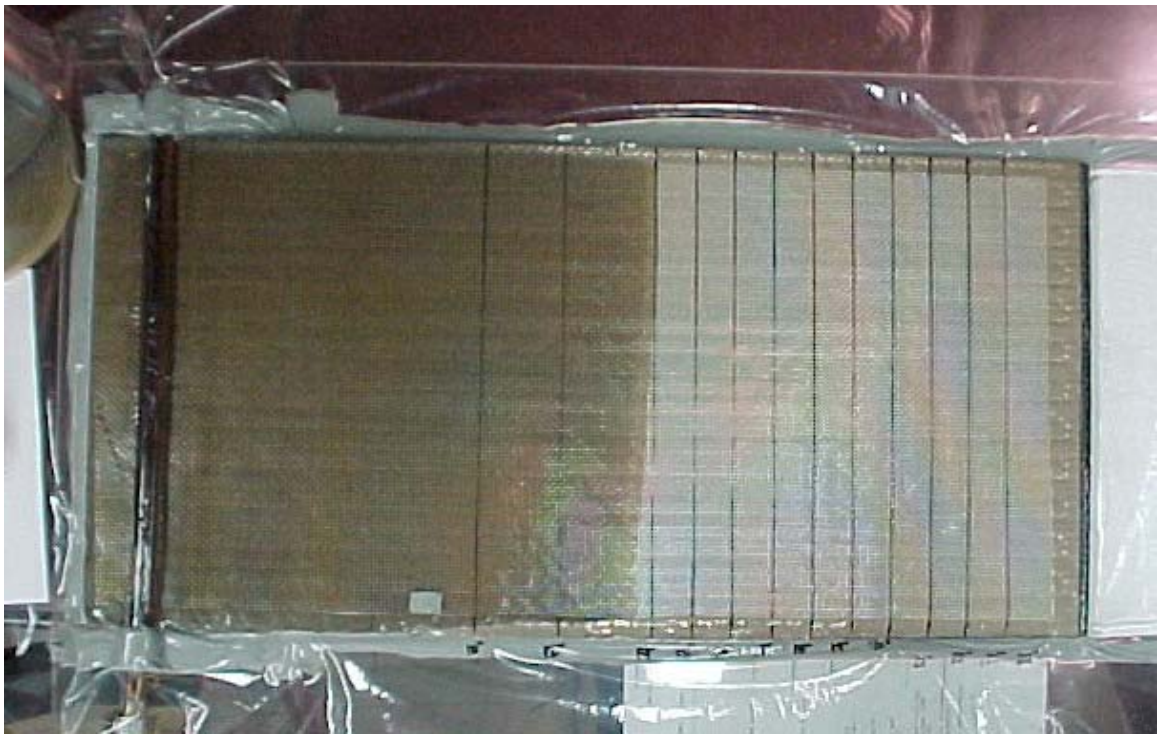

Figure 5.6 – 12.7 mm thick foam core preform with 12.7 mm stitch row spacing. Flow front is approximately 35.6 cm from injection edge.

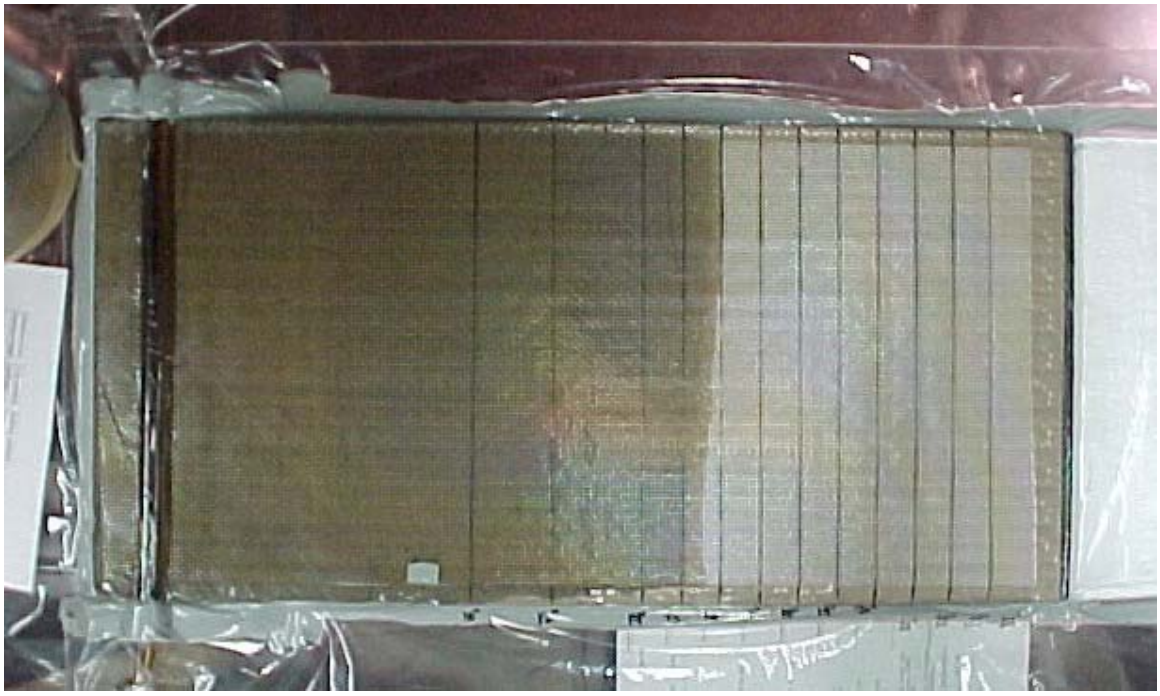

Figure 5.7 – 12.7 mm thick foam core preform with 12.7 mm stitch row spacing. Flow front is approximately 40.6 cm from injection edge.

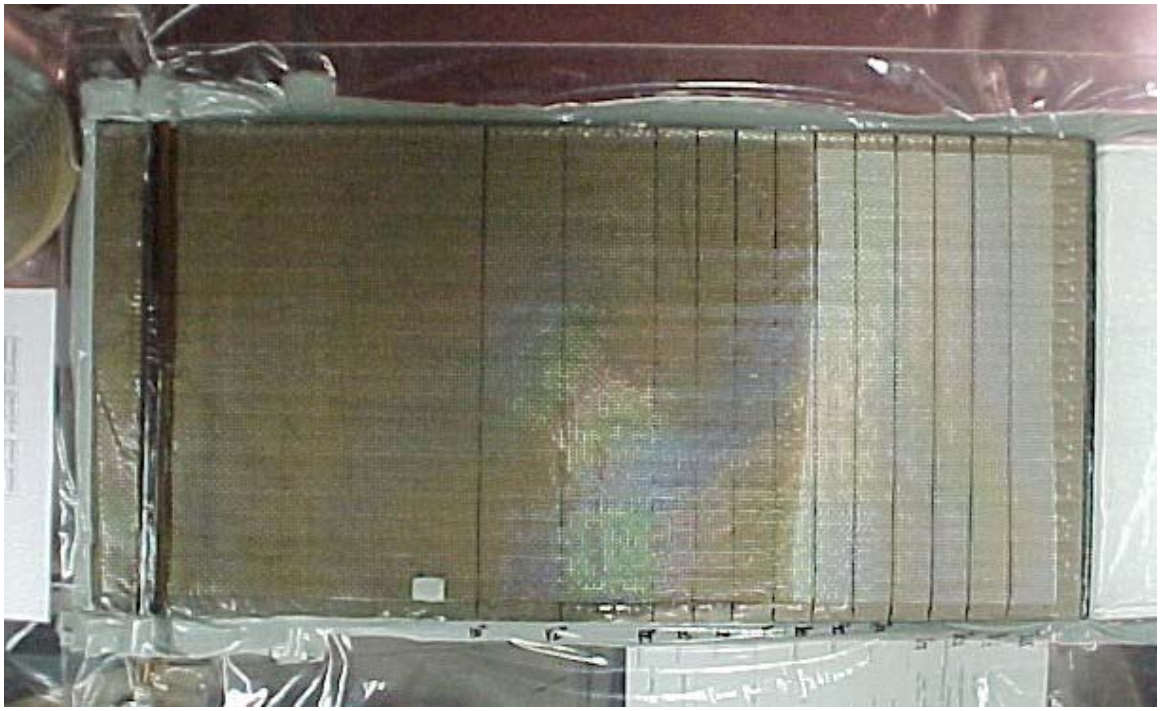

Figure 5.8 – 12.7 mm thick foam core preform with 12.7 mm stitch row spacing. Flow front is approximately 45.7 cm from injection edge.

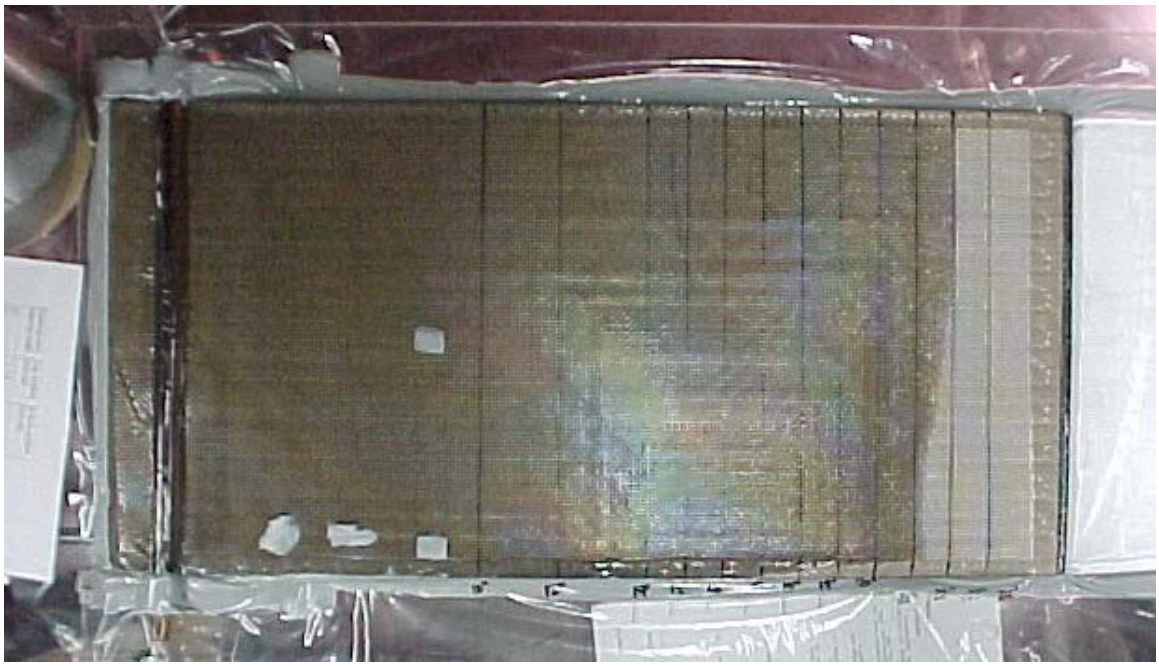

Figure 5.9 – 12.7 mm thick foam core preform with 12.7 mm stitch row spacing. Flow front is approximately 55.9 cm from injection edge.

Figure 5.10 – 12.7 mm thick foam core preform with 12.7 mm stitch row spacing. Flow front is approximately 61.0 cm from injection edge.

Figure 5.11 – 12.7 mm thick foam core preform with 12.7 mm stitch row spacing. The preform has been completely infiltrated.

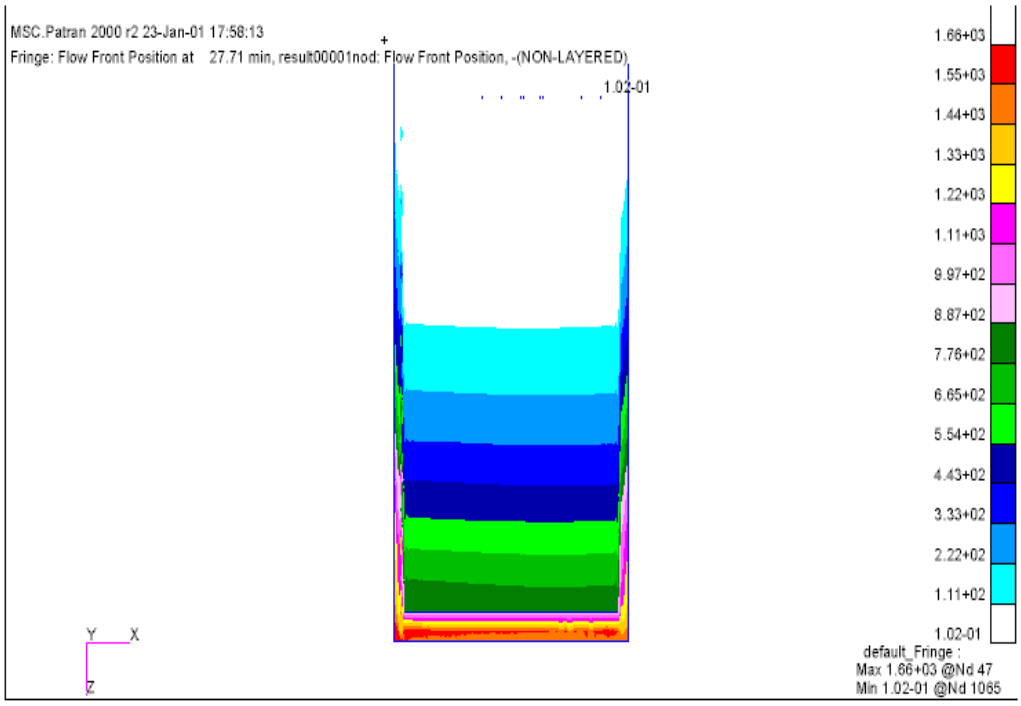

Figure 5.12 – 3DINFIL model predictions for flow in the 12.7 mm thick foam core preform with 12.7 mm stitch row spacing.

The total experimental infiltration time for this case was 26.4 minutes. This agreed well with the model prediction of 27.7 minutes. Figure 5.13 shows a graph of the measured and predicted flow front locations versus time for the top surface of the preform in the region of the high permeable distribution medium.

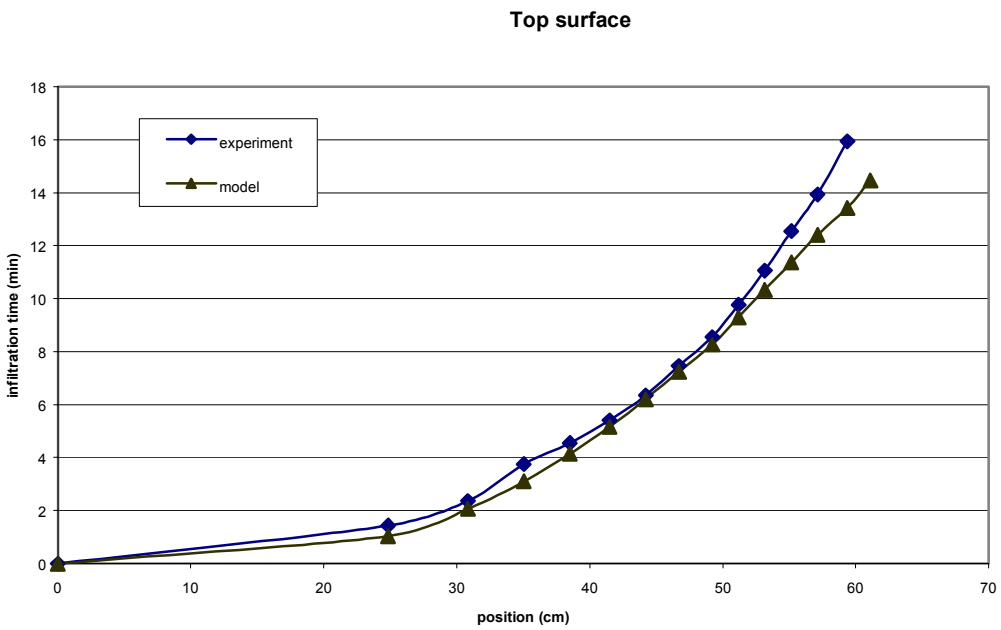

Figure 5.13 – Measured and calculated flow along the top surface of the 12.7 mm thick foam core preform with 12.7 mm stitch row spacing. The flow is in the region of the high permeable distribution medium.

The flow front at the bottom surface of the lower face sheet was less uniform than what was observed at the surface of the upper face sheet. The resin enters the lower face sheet through the stitching before areas in between the stitching are filled. Thus, there is some non-uniformity in the geometry of the flow front, which is predicted by the model. Figures 5.14 through 5.23 show the flow progression along the surface of the lower face sheet. Figure 5.24 shows the model predicted infiltration times at the surface of the lower face sheet.

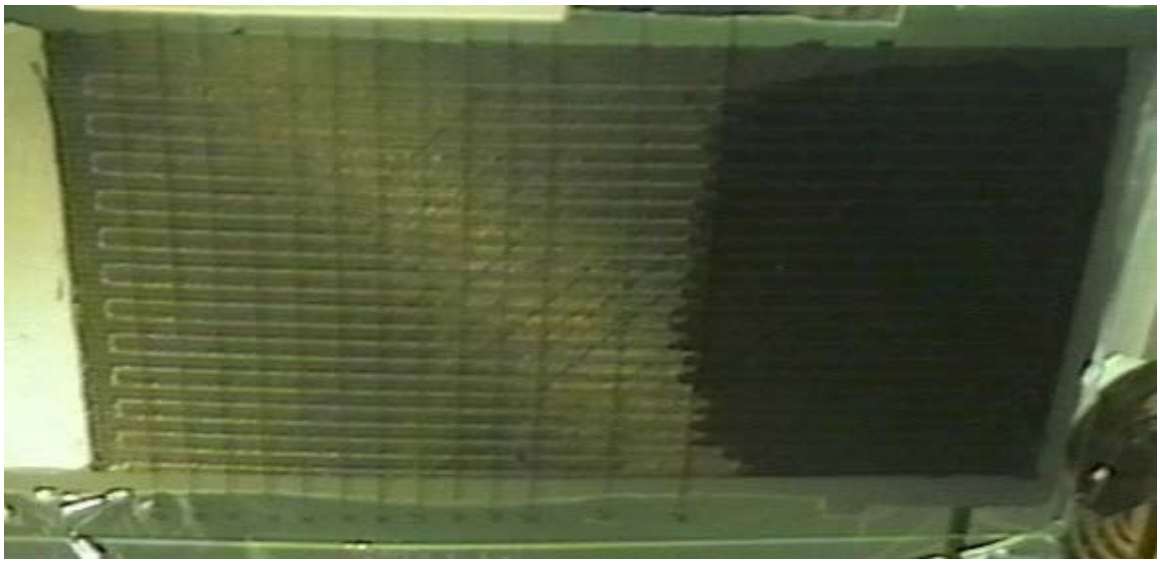

Figure 5.14 – Bottom surface of 12.7 mm thick foam core preform with 12.7 mm stitch row spacing. Flow front is approximately 25.4 cm from injection edge.

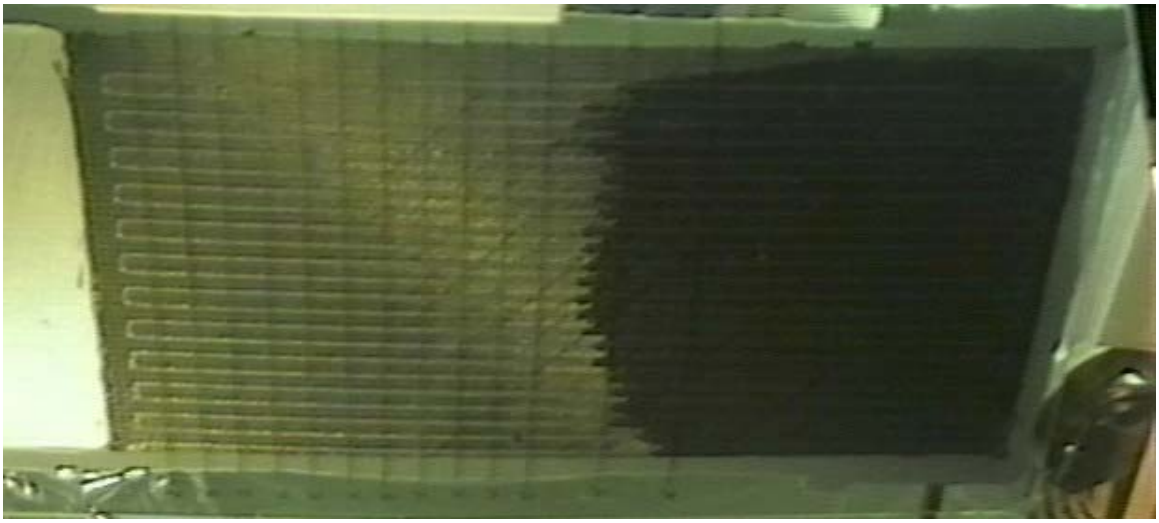

Figure 5.15 – Bottom surface of 12.7 mm thick foam core preform with 12.7 mm stitch row spacing. Flow front is approximately 30.5 cm from injection edge.

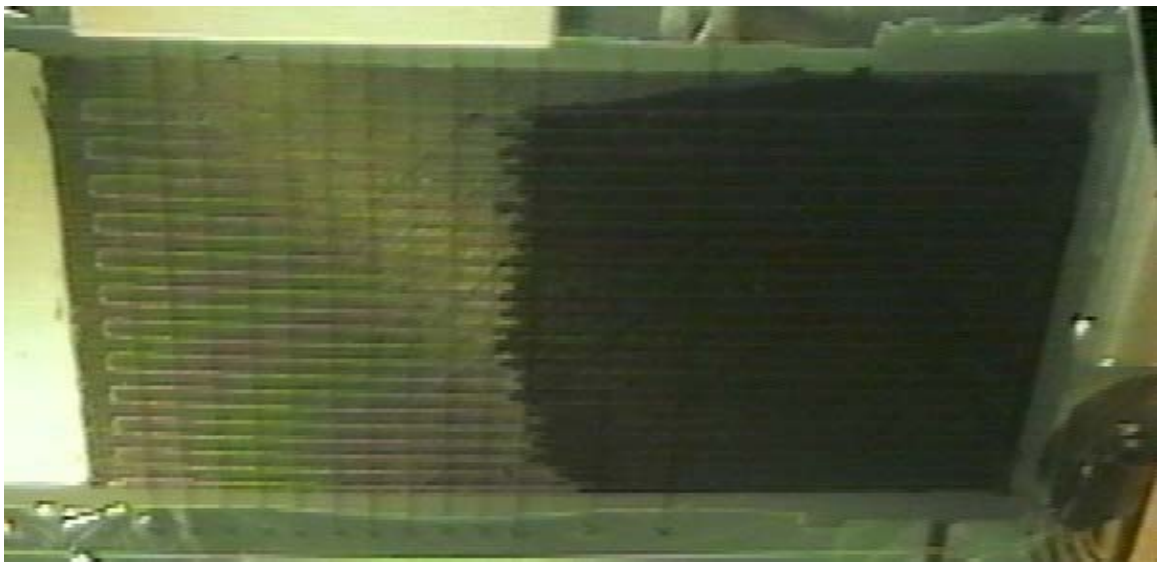

Figure 5.16 – Bottom surface of 12.7 mm thick foam core preform with 12.7 mm stitch row spacing. Flow front is approximately 35.6 cm from injection edge.

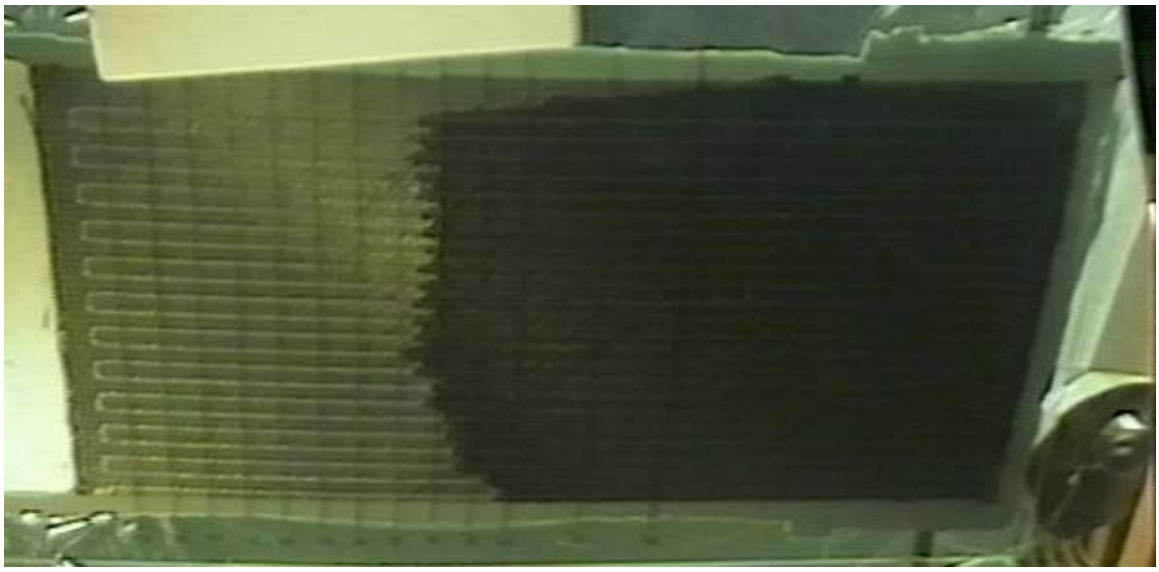

Figure 5.17 – Bottom surface of 12.7 mm thick foam core preform with 12.7 mm stitch row spacing. Flow front is approximately 40.6 cm from injection edge.

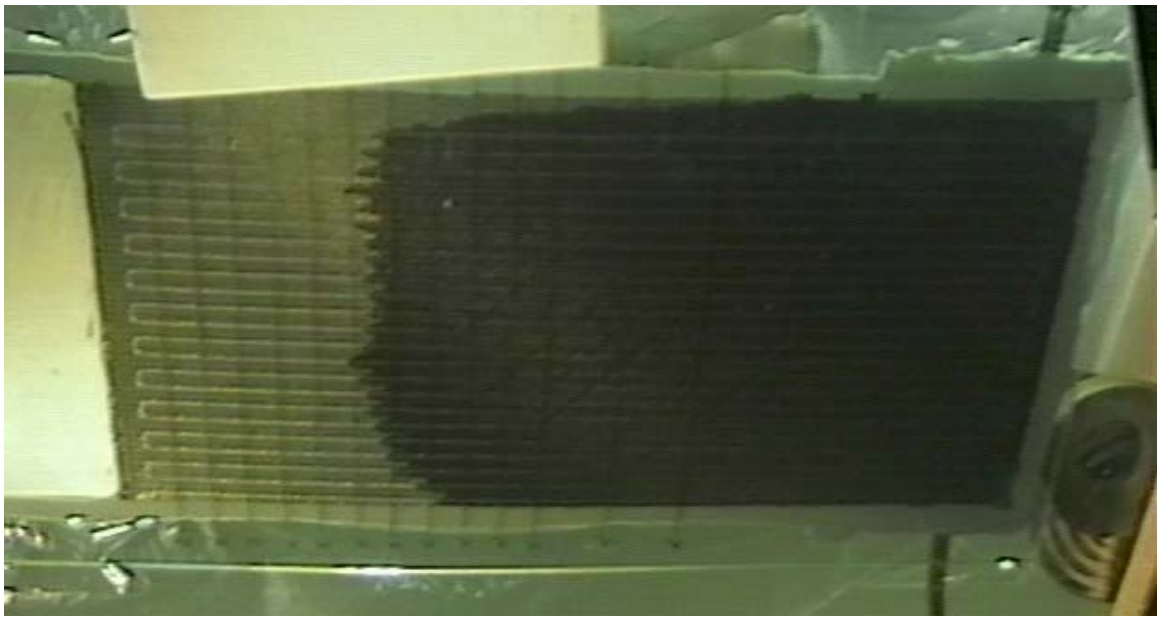

Figure 5.18 – Bottom surface of 12.7 mm thick foam core preform with 12.7 mm stitch row spacing. Flow front is approximately 45.7 cm from injection edge.

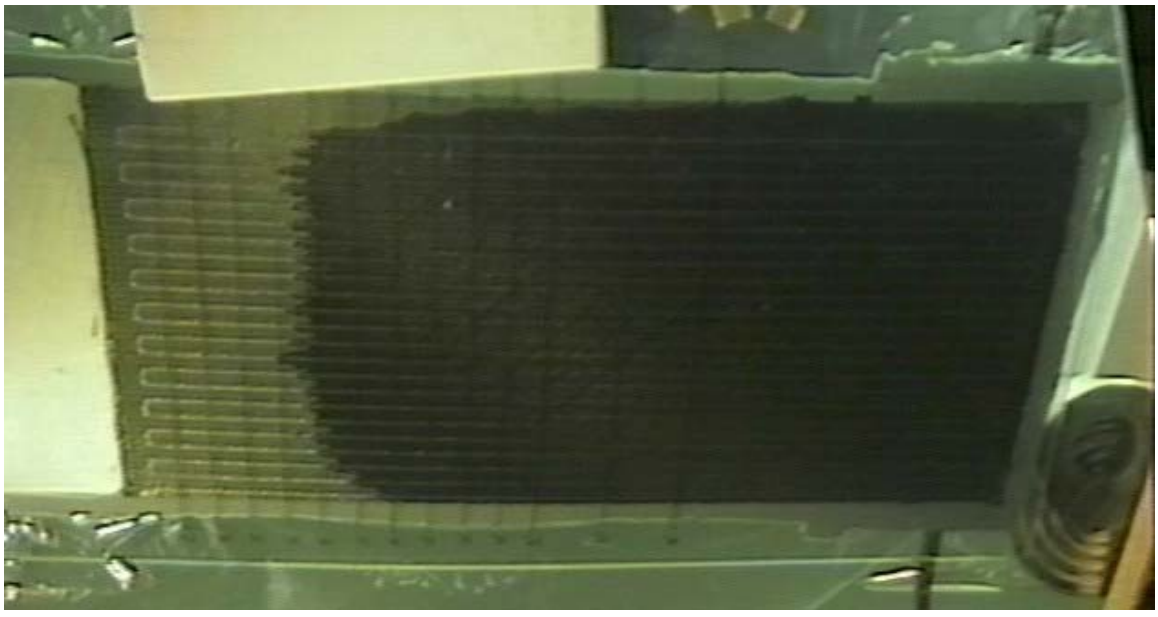

Figure 5.19 – Bottom surface of 12.7 mm thick foam core preform with 12.7 mm stitch row spacing. Flow front is approximately 50.8 cm from injection edge.

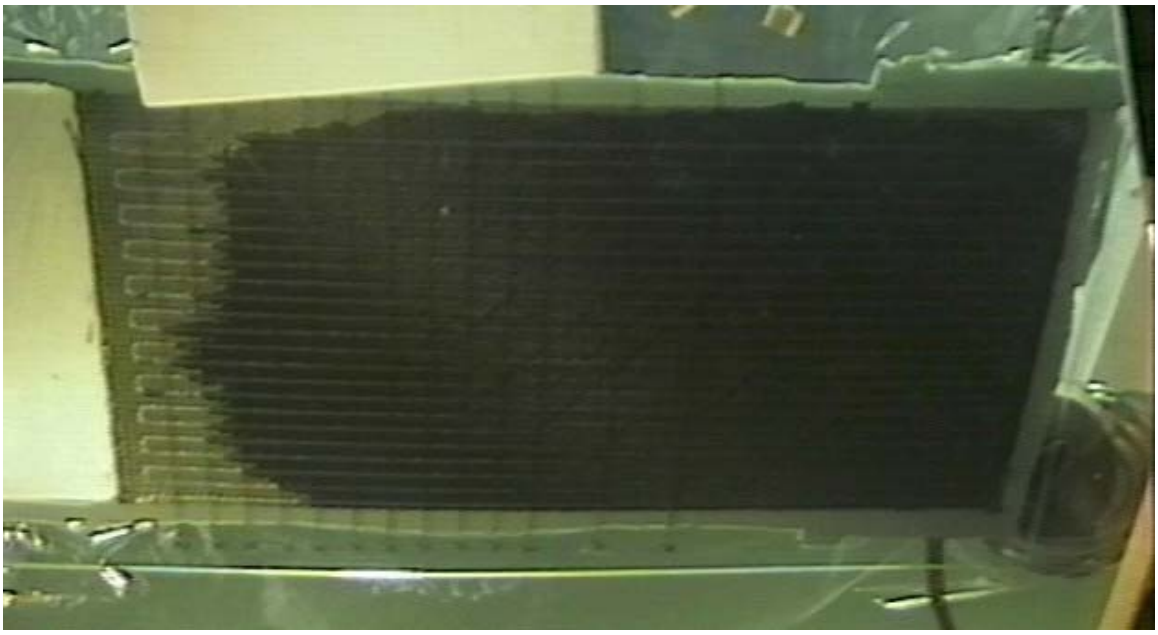

Figure 5.20 – Bottom surface of 12.7 mm thick foam core preform with 12.7 mm stitch row spacing. Flow front is approximately 55.9 cm from injection edge.

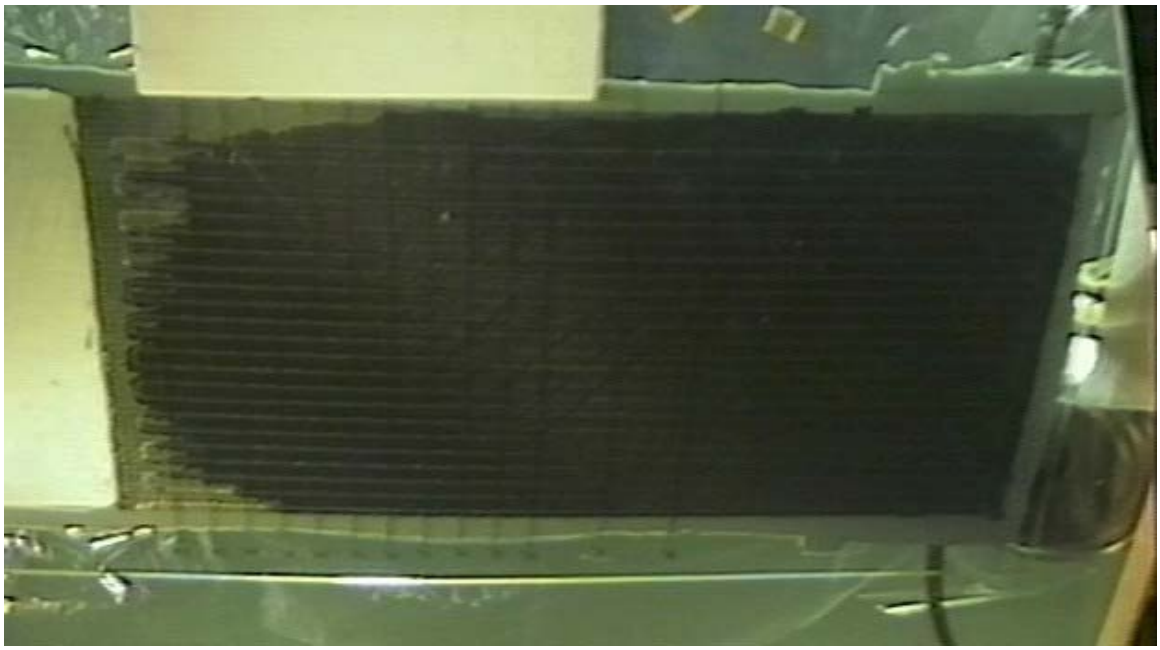

Figure 5.21 – Bottom surface of 12.7 mm thick foam core preform with 12.7 mm stitch row spacing. Flow front is approximately 61.0 cm from injection edge.

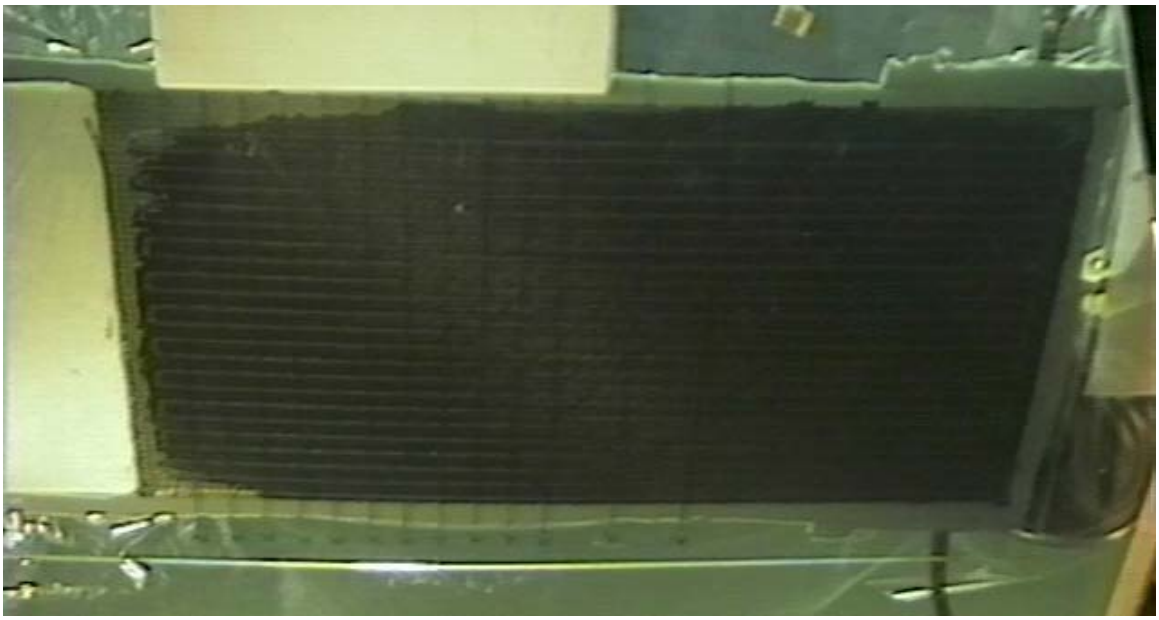

Figure 5.22 – Bottom surface of 12.7 mm thick foam core preform with 12.7 mm stitch row spacing. Flow front is approximately 63.5 cm from injection edge.

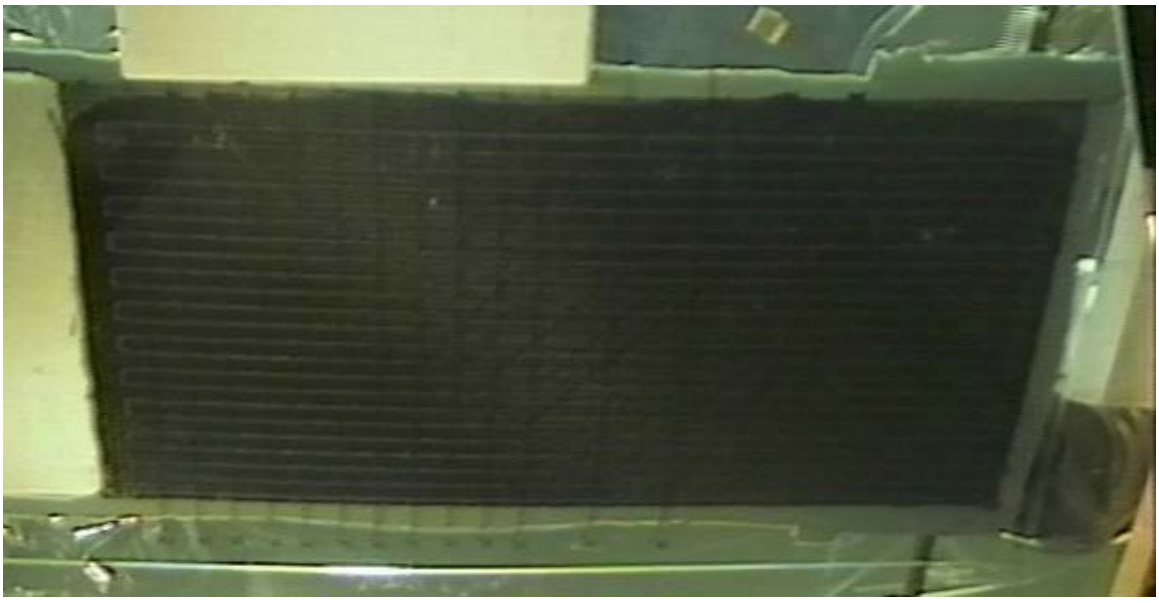

Figure 5.23 – Bottom surface of 12.7 mm thick foam core preform with 12.7 mm stitch row spacing. The preform has been completely infiltrated.

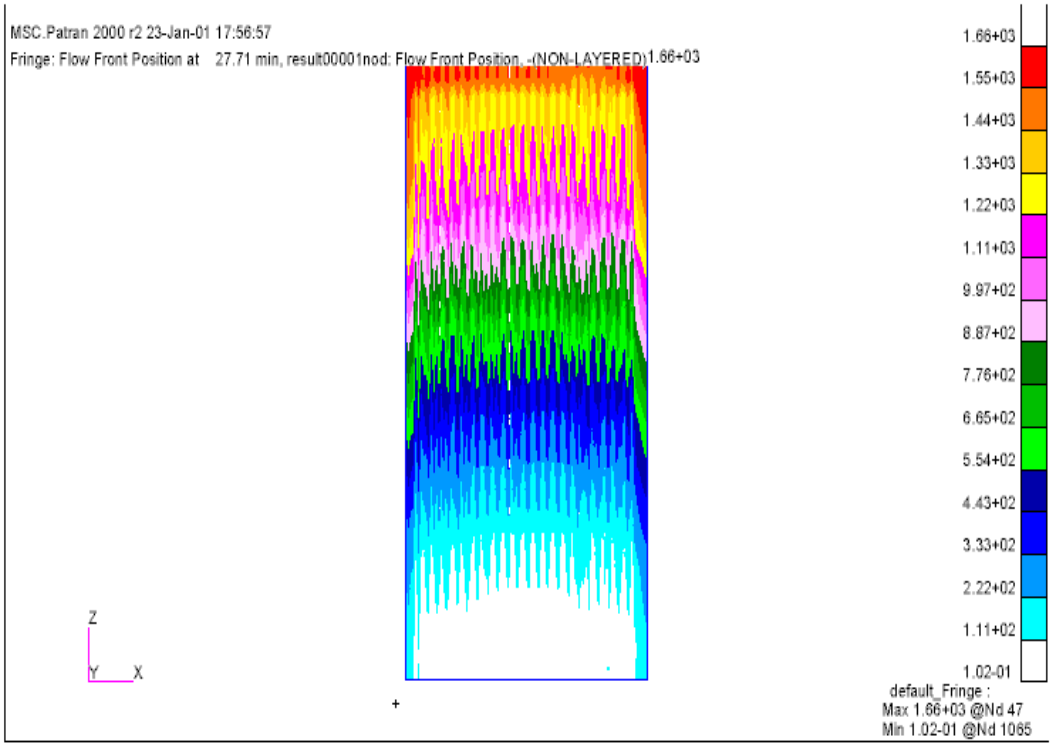

Figure 5.24 – Model prediction for the 12.7 mm thick foam core preform with 12.7 mm stitch row spacing. Note the non-uniform flow front as seen in the experimental verification.

Again, note that the flow front along the bottom surface is non-uniform, and thus accurate measurement of the flow front position is difficult. However, it should be noted that the model predicts flow along the stitches to lead flow in the bulk material, and this behavior is observed experimentally.

5.3.2 Case 2 – 12.7 mm foam core with 6.35 mm stitch row spacing

The second geometry considered was a 12.7 mm foam core with 6.35 mm stitch row spacing. The mesh for this case can be seen in Figure 5.25, and contains 7,666 elements and 12,592 nodes. The porosity for this panel was calculated to be 0.089.

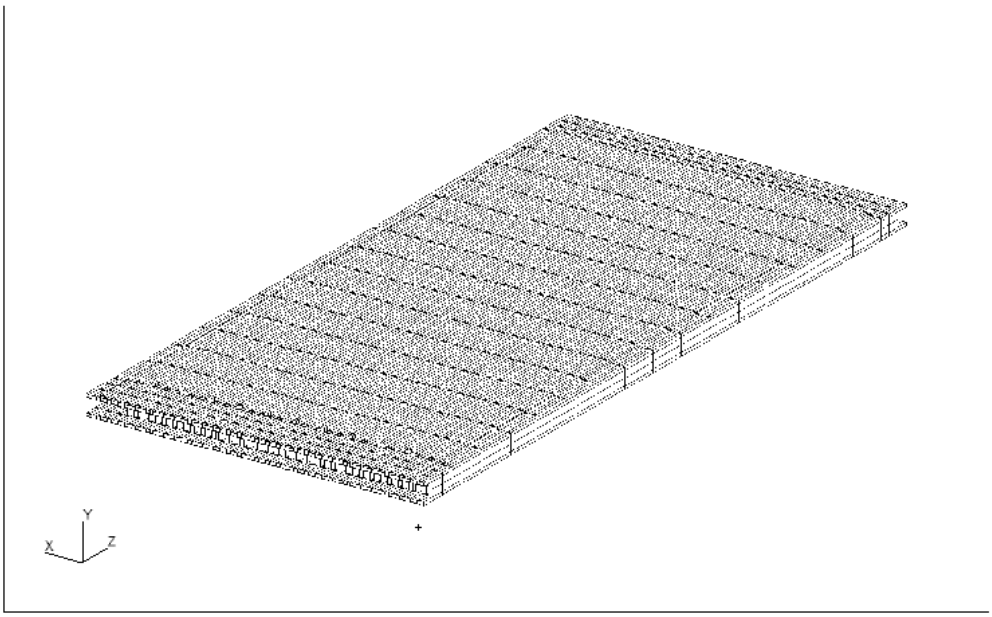

Figure 5.25 – Finite element mesh for the 12.7 mm thick foam core preform with 6.35 mm stitch row spacing.

The geometry of the flow front for this case was somewhat non-uniform on both the top and bottom surfaces due to the fact that the stitching of the preform was asymmetric. A strip approximately 38.1 mm wide on the edge of the preform was not stitched. This was taken into account in the modeling of the preform by reducing the number of porous strips. The model prediction for the top surface of the panel is shown in Figure 5.26. Again, the geometry of the flow front predicted by the model matched that of the

experiment. The flow front progression along the top surface of the panel for all cases was similar to that observed in the 12.7 mm stitch row spacing.

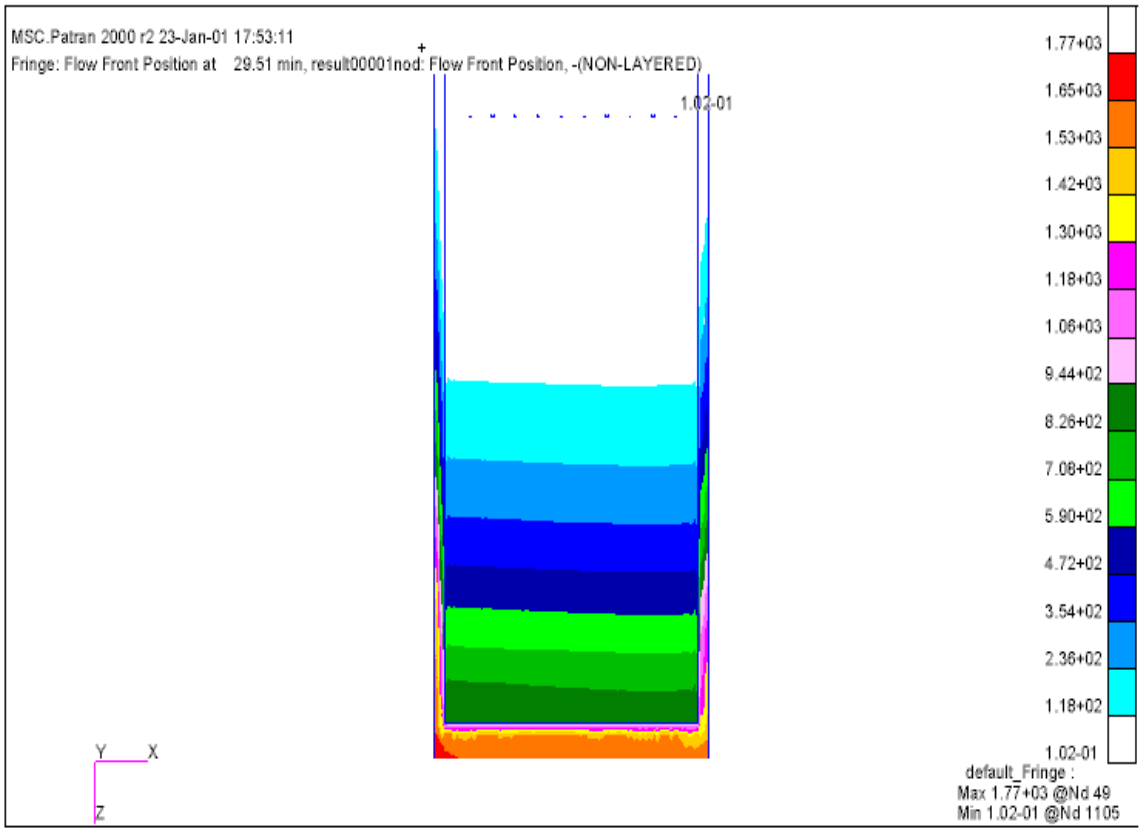

Figure 5.26 – 3DINFIL predictions for flow along the top surface of the 12.7 mm thick foam core preform with 6.35 mm stitch row spacing.

The total experimental infiltration time for this case was 29.8 minutes. This agreed well with the model prediction of 27.5 minutes. Figure 5.27 shows a graph of the experimental and model predicted flow front locations versus time for the top surface of the panel.

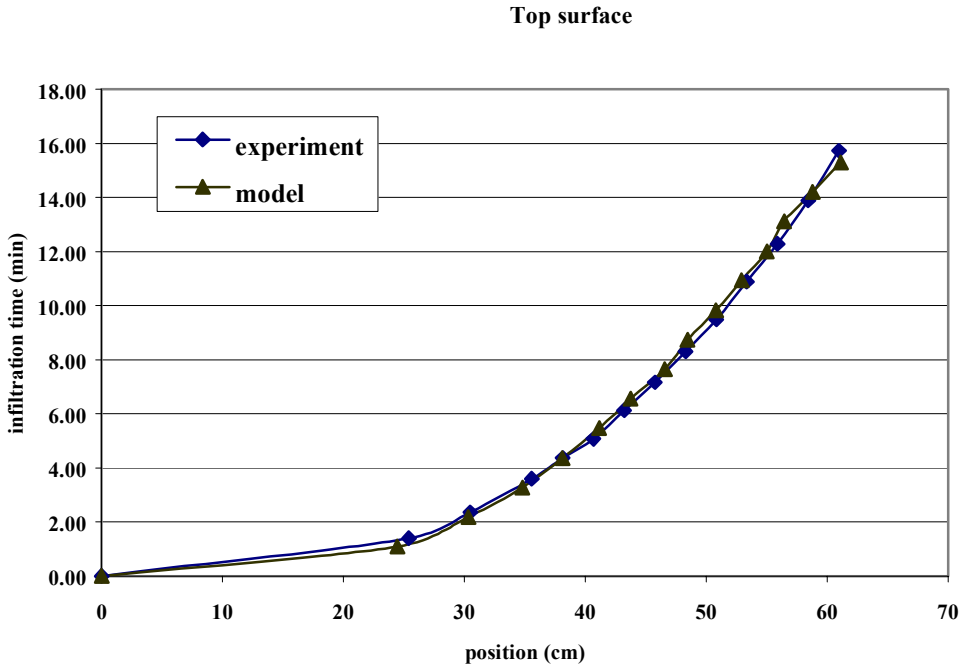

Figure 5.27 – Measured and calculated flow along the top surface of the 12.7 mm thick foam core preform with 6.35 mm stitch row spacing. The flow is in the region of the high permeable distribution medium.

The geometry of the flow front along the bottom surface was more uniform than the 12.7 mm stitch row spacing case due to the fact that the rows of stitches were closer together and there was less lag in the area between rows. Figures 5.28 through 5.34 show the flow front progression along the bottom surface of the panel. The model prediction for the bottom surface of the panel is shown in Figure 5.35. As shown in Figure 5.27, the agreement between the predicted and measured resin flow in the high permeable distribution medium was very good. The total infiltration time for the 12.7 mm thick panel with 6.35 mm stitch row spacing agreed within 8% of the total time. For this case, the model was able to predict both the flow front location and total infiltration times with good accuracy.

Figure 5.28 – Bottom surface of 12.7 mm thick foam core preform with 6.35 mm stitch row spacing. Flow front is approximately 25.4 cm from injection edge.

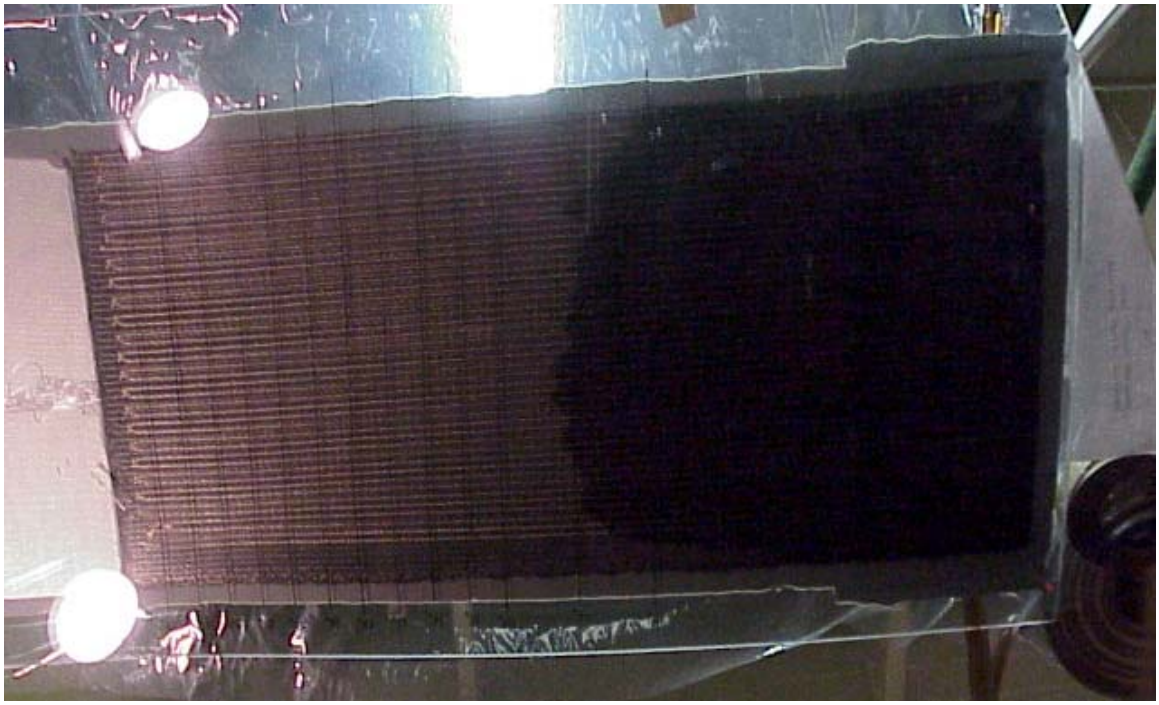

Figure 5.29 – Bottom surface of 12.7 mm thick foam core preform with 6.35 mm stitch row spacing. Flow front is approximately 30.5 cm from injection edge.

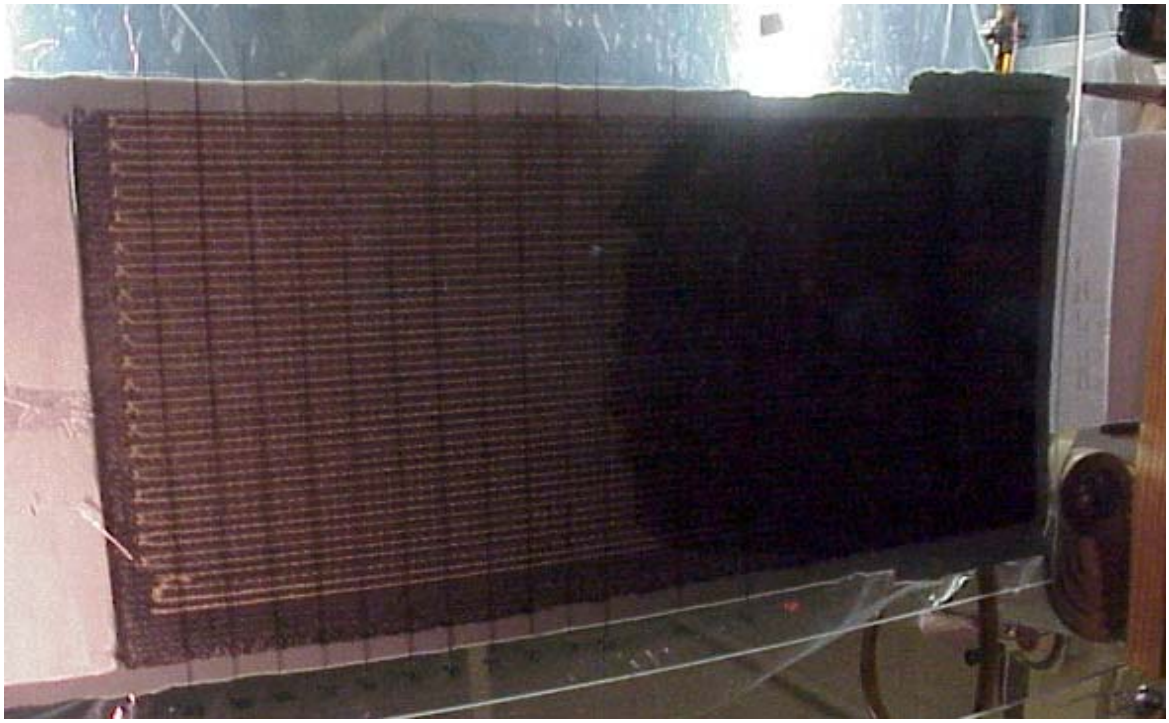

Figure 5.30 – Bottom surface of 12.7 mm thick foam core preform with 6.35 mm stitch row spacing. Flow front is approximately 35.6 cm from injection edge.

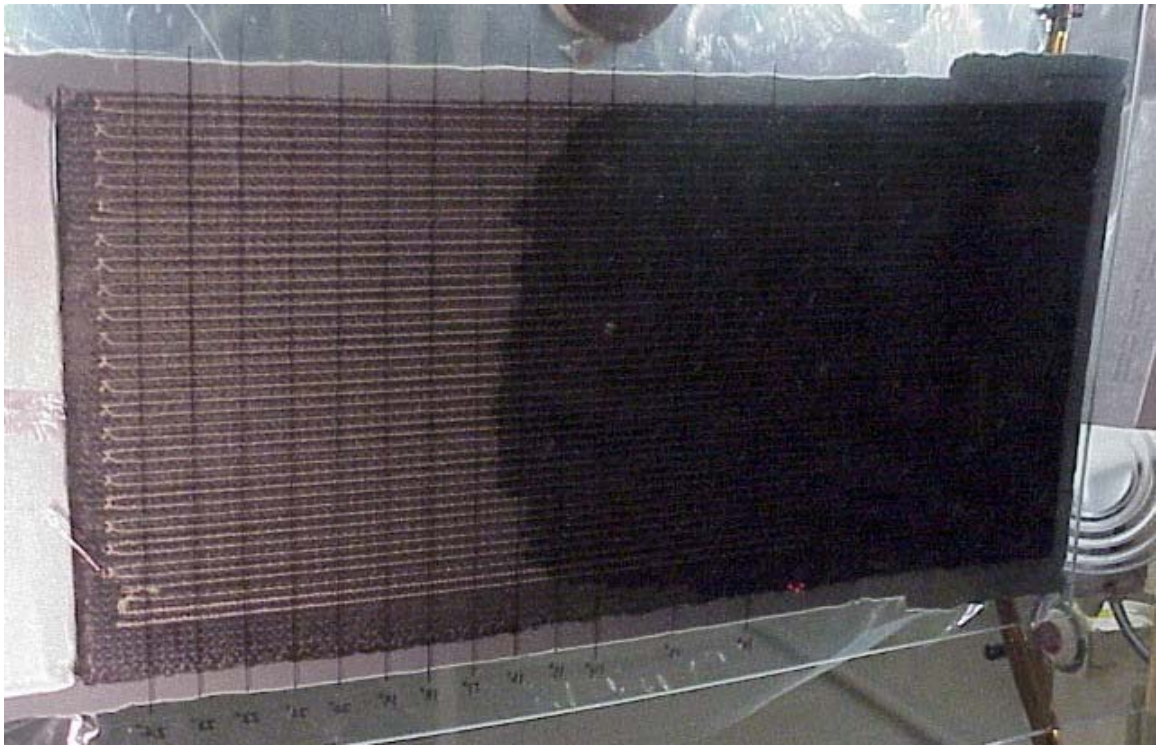

Figure 5.31 – Bottom surface of 12.7 mm thick foam core preform with 6.35 mm stitch row spacing. Flow front is approximately 40.6 cm from injection edge.

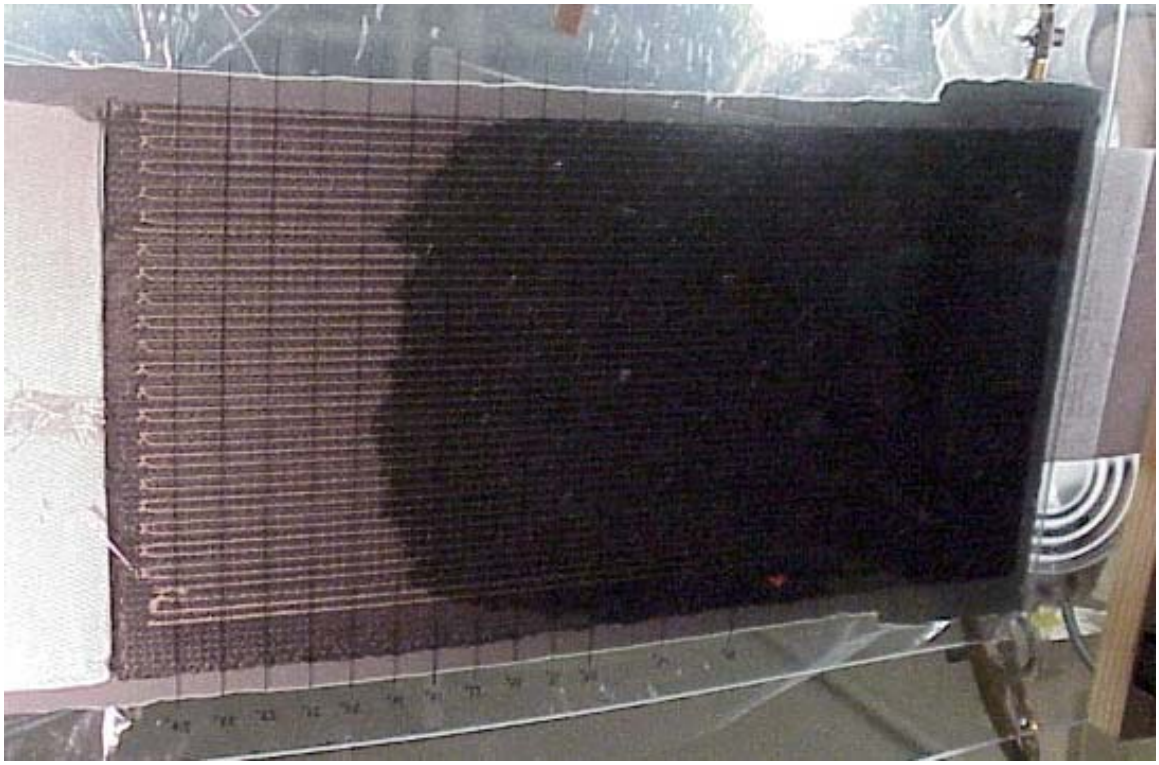

Figure 5.32 – Bottom surface of 12.7 mm thick foam core preform with 6.35 mm stitch row spacing. Flow front is approximately 48.3 cm from injection edge.

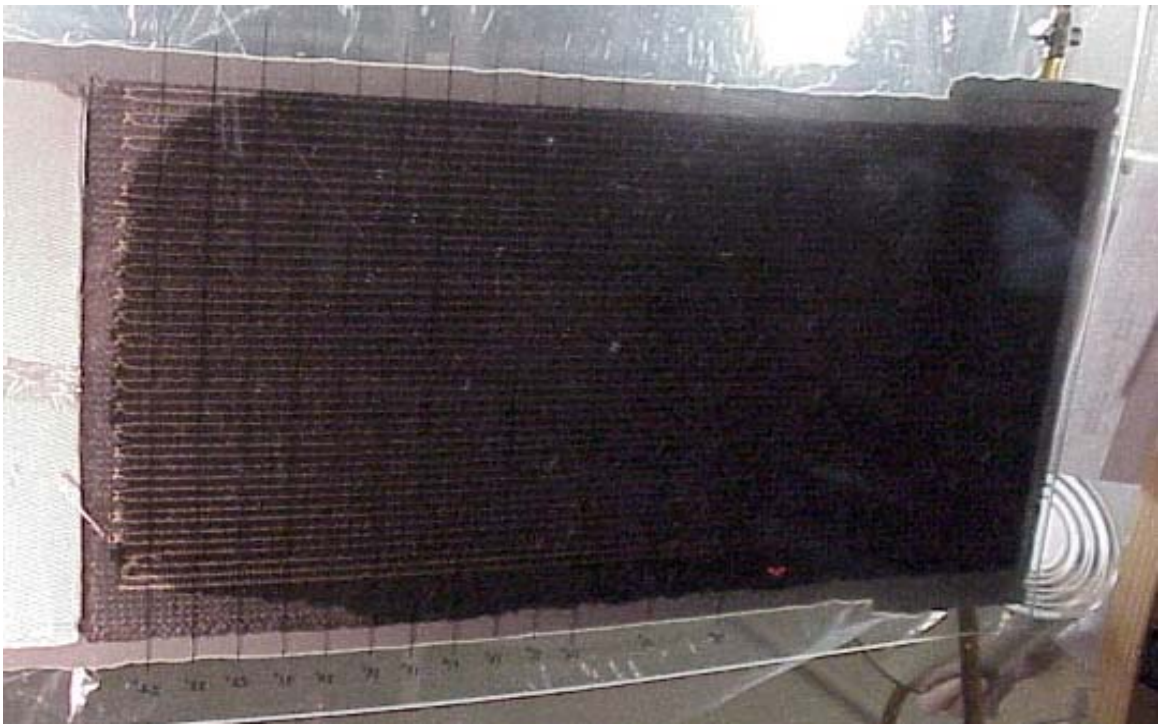

Figure 5.33 – Bottom surface of 12.7 mm thick foam core preform with 6.35 mm stitch row spacing. Flow front is approximately 61.0 cm from injection edge.

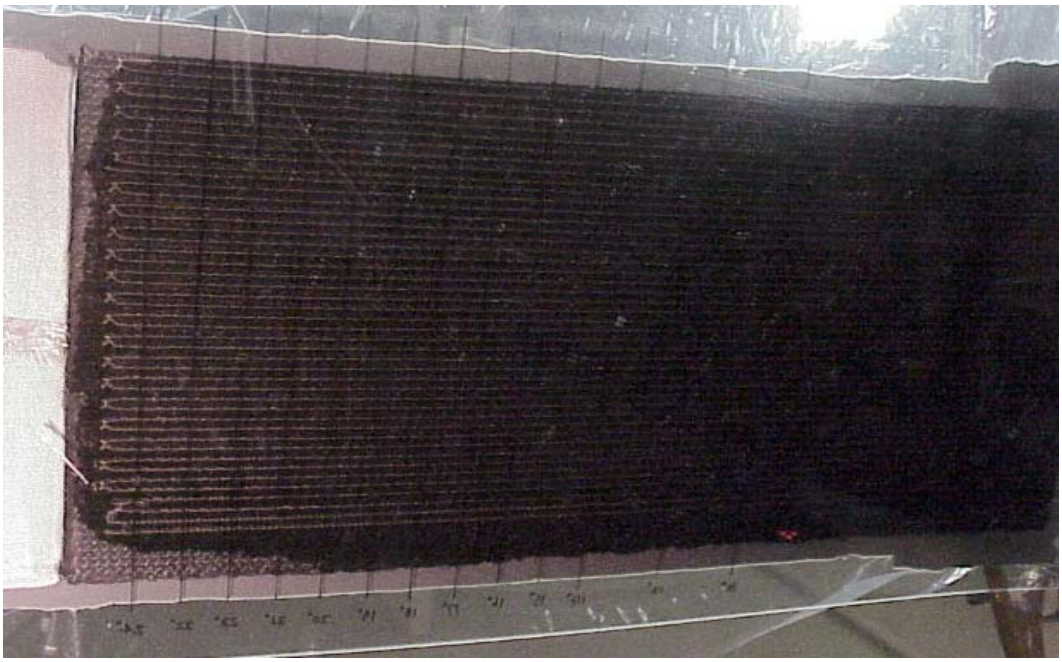

Figure 5.34 – Bottom surface of 12.7 mm thick foam core preform with 6.35 mm stitch row spacing. The infiltration of the preform is nearly complete.

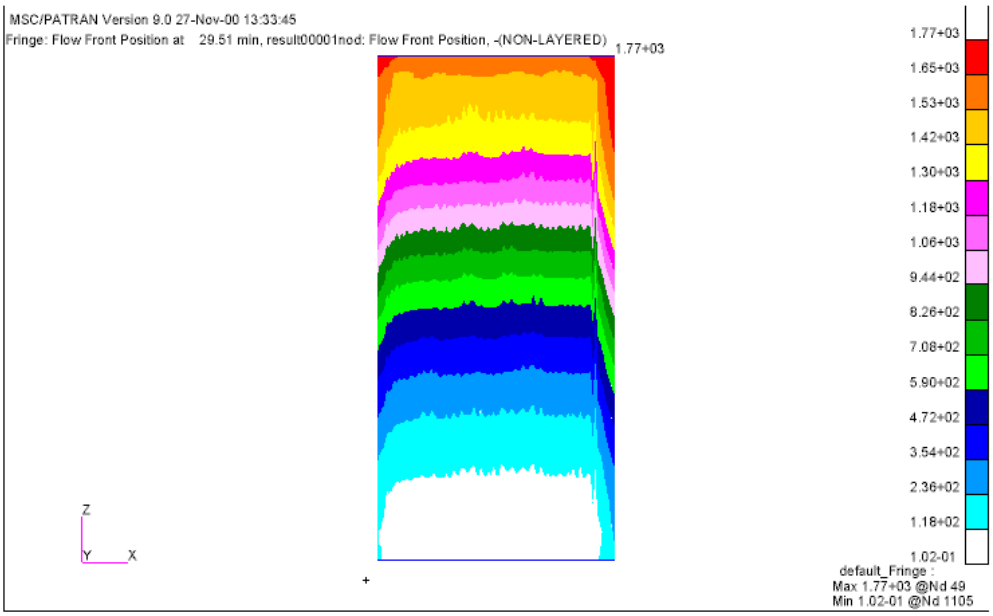

Figure 5.35 – 3DINFIL predictions for flow along the bottom surface of the 12.7 mm thick foam core preform with 6.35 mm stitch row spacing.

5.3.3 Case 3 – 12.7 mm foam core with 25.4 mm stitch row spacing

The third geometry considered was a 12.7 mm foam core preform with 25.4 mm stitch row spacing. The mesh for this case can be seen in Figure 5.36 and contains 6,170 elements with 10,836 nodes. The porosity for this panel was calculated to be 0.0894.

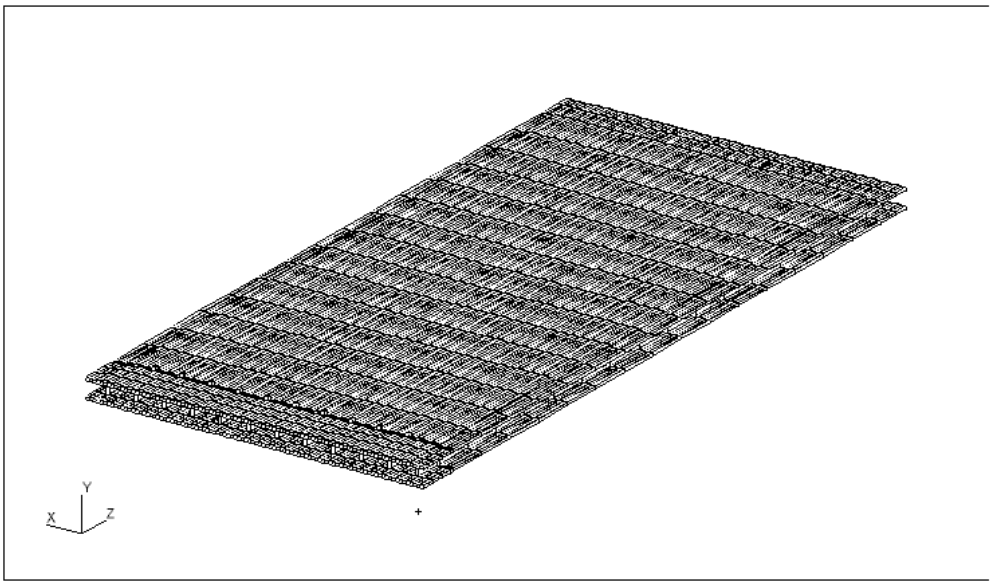

Figure 5.36 – Finite element mesh for the 12.7 mm thick foam core preform with 25.4 mm stitch row spacing.

The shape of the flow front along the top surface of the panel was similar to that observed experimentally in the 6.35 and 12.7 mm stitch row spacing panels. The model predicted flow front versus time at the surface of the upper face sheet preform is shown in Figure 5.37.

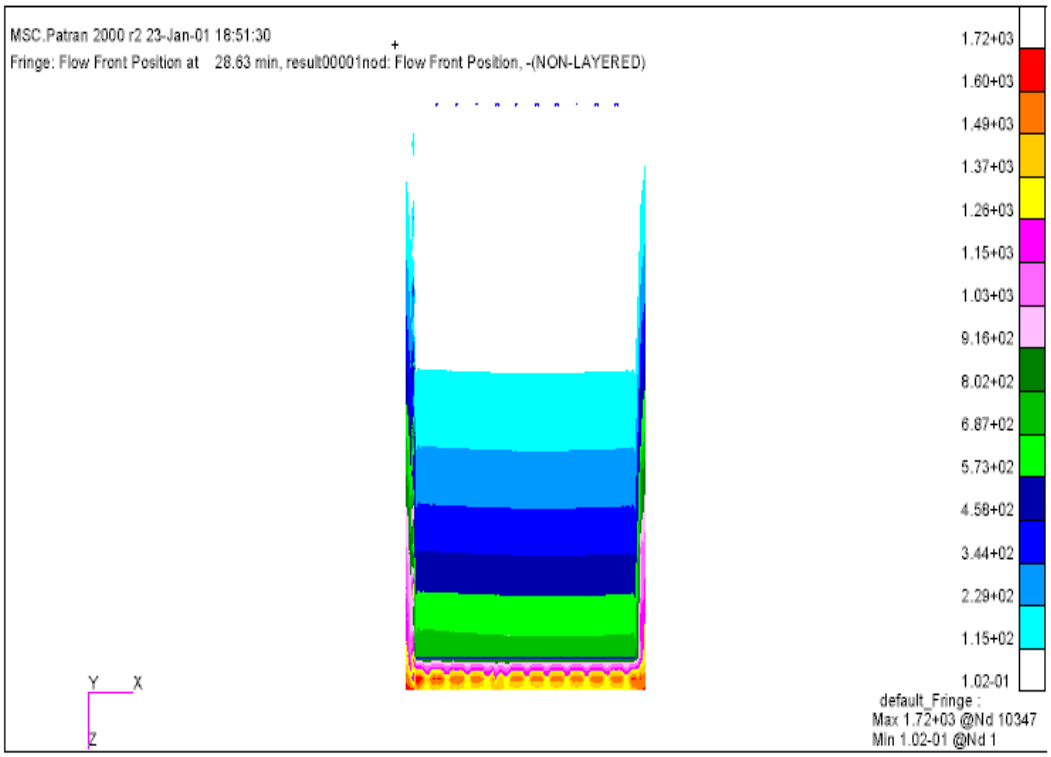

Figure 5.37 – 3DINFIL predictions for infiltration along the top surface of the 12.7 mm thick foam core preform with 25.4 mm stitch row spacing.

The resin infiltration patterns along the bottom surface of the preform was the least uniform, due to the increased spacing between rows. Figures 5.38 through 5.42 show the flow front progression along the bottom surface, while Figure 5.43 shows an enlarged view of how the resin flow along the rows of stitching leads the flow in the bulk of the face sheet material.

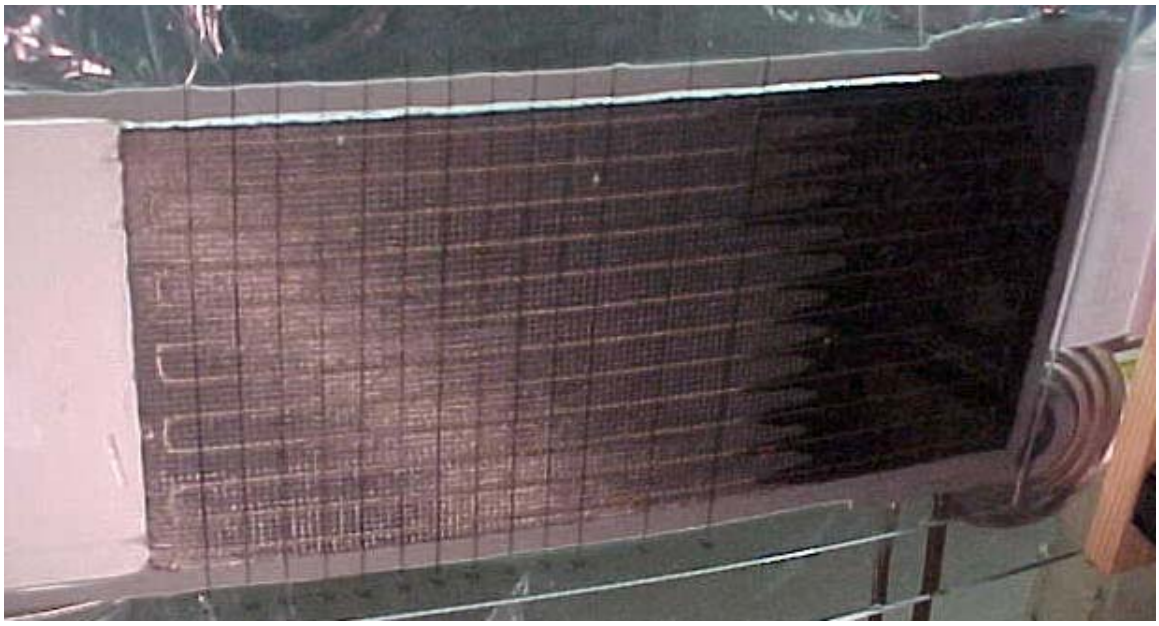

Figure 5.38 – Bottom surface of 12.7 mm thick foam core preform with 25.4 mm stitch row spacing. Flow front is approximately 20.3 cm from injection edge.

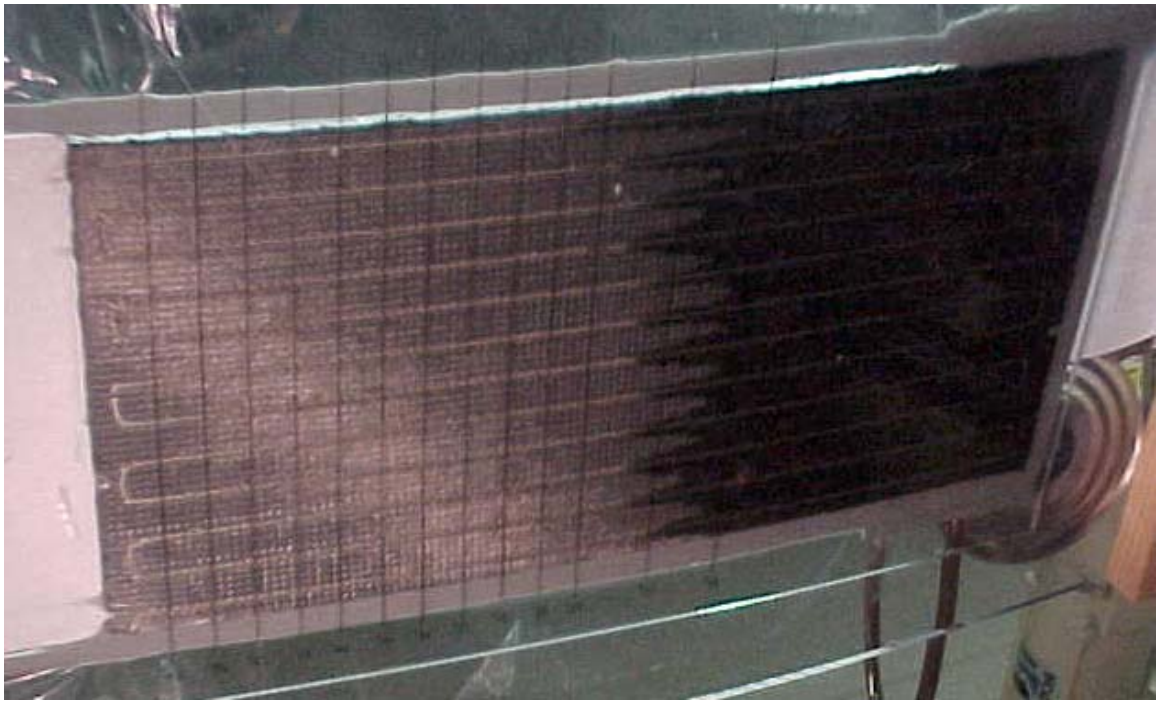

Figure 5.39 – Bottom surface of 12.7 mm thick foam core preform with 25.4 mm stitch row spacing. Flow front is approximately 28.0 cm from injection edge.

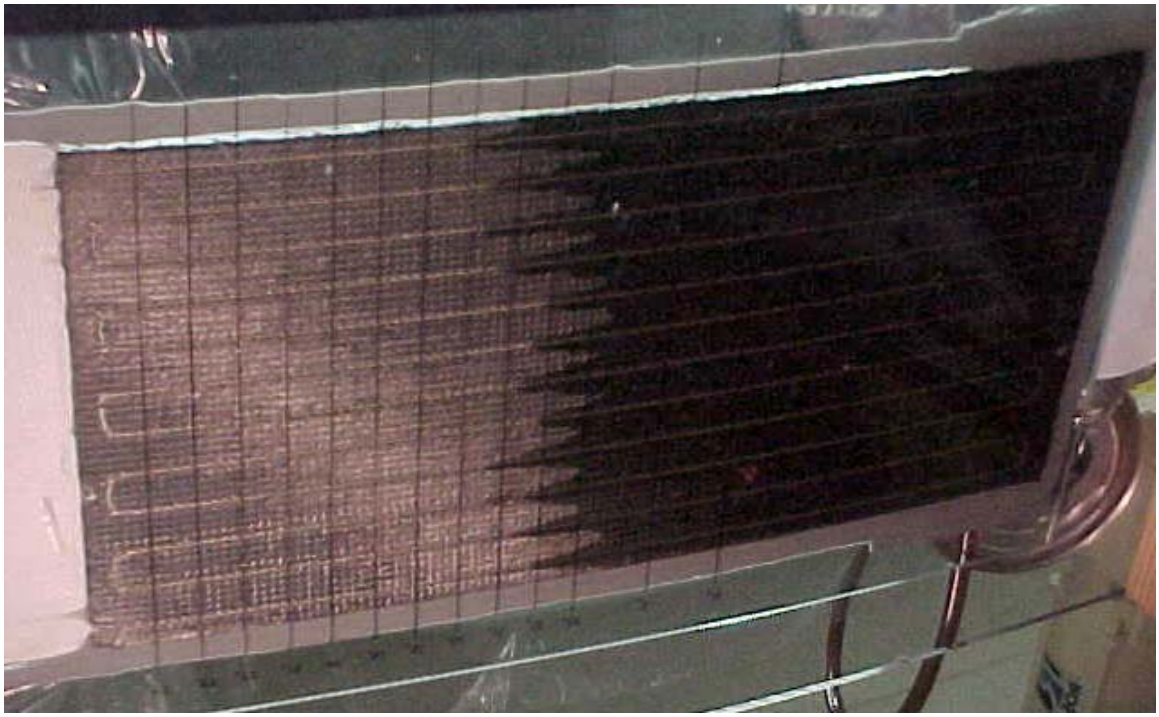

Figure 5.40 – Bottom surface of 12.7 mm thick foam core preform with 25.4 mm stitch row spacing. Flow front is approximately 35.6 cm from injection edge.

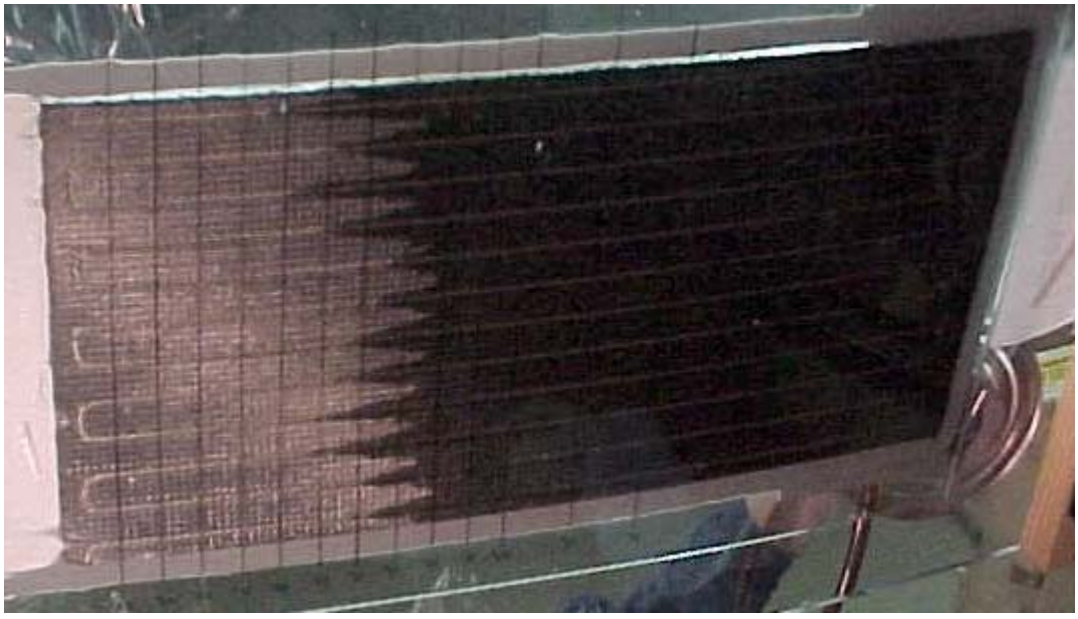

Figure 5.41 – Bottom surface of 12.7 mm thick foam core preform with 25.4 mm stitch row spacing. Flow front is approximately 40.6 cm from injection edge.

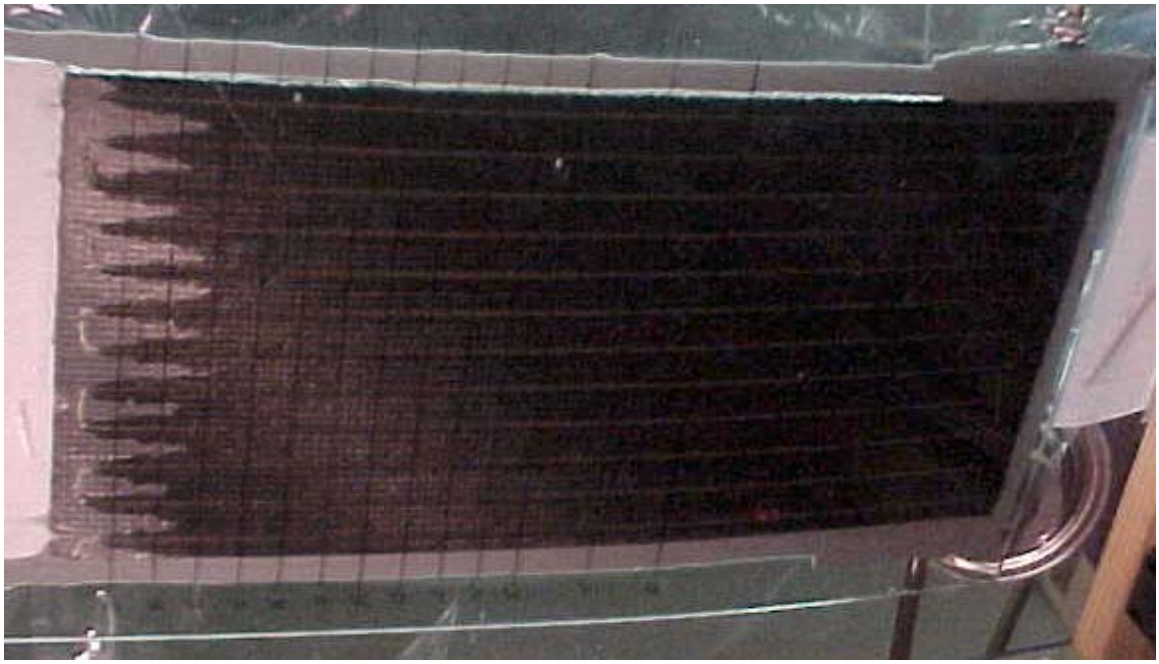

Figure 5.42 – Bottom surface of 12.7 mm thick foam core preform with 25.4 mm stitch row spacing. Flow front is approximately 58.4 cm from injection edge.

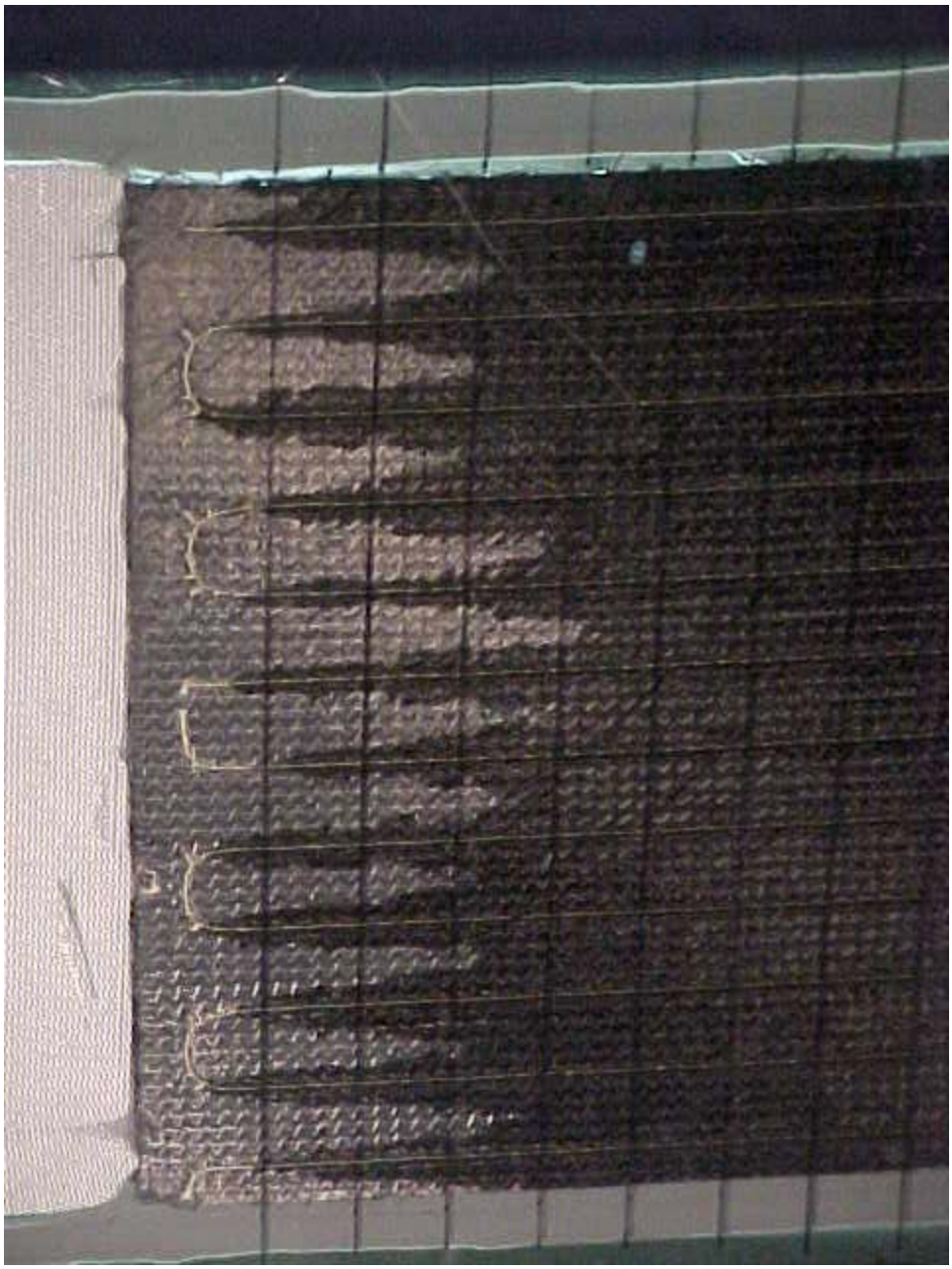

Figure 5.43 – Bottom surface of 12.7 mm thick foam core preform with 25.4 mm stitch row spacing. Note that the resin flow along the stitching precedes infiltration in the area between rows.

The total experimental infiltration time for this case was 23.5 minutes. The model overpredicts the total infiltration time for these conditions. The model results show a total infiltration time of 28.6 minutes. Agreement in the region of the high permeable

distribution medium was reasonable, as shown in Figure 5.44. However, the predictions along the bottom surface were slower than that observed in the experiment. The model output for flow along the bottom surface of the panel is shown in Figure 5.45. The total infiltration time for this case is less than for the 6.35 and 12.7 mm stitch row spacing due to the fact that the volume of resin in the panel is less, as there are less needle penetrations. However, the model prediction did not agree as well with the experimental data in the case. The model overpredicted total infiltration times by more than 20% for this case. Permeability of the preform is one factor that could have influenced this disagreement. Because of the larger space between the rows of stitching, more in-plane flow of the resin occurred between the rows. A more fully characterized preform permeability could reduce some of the model error.

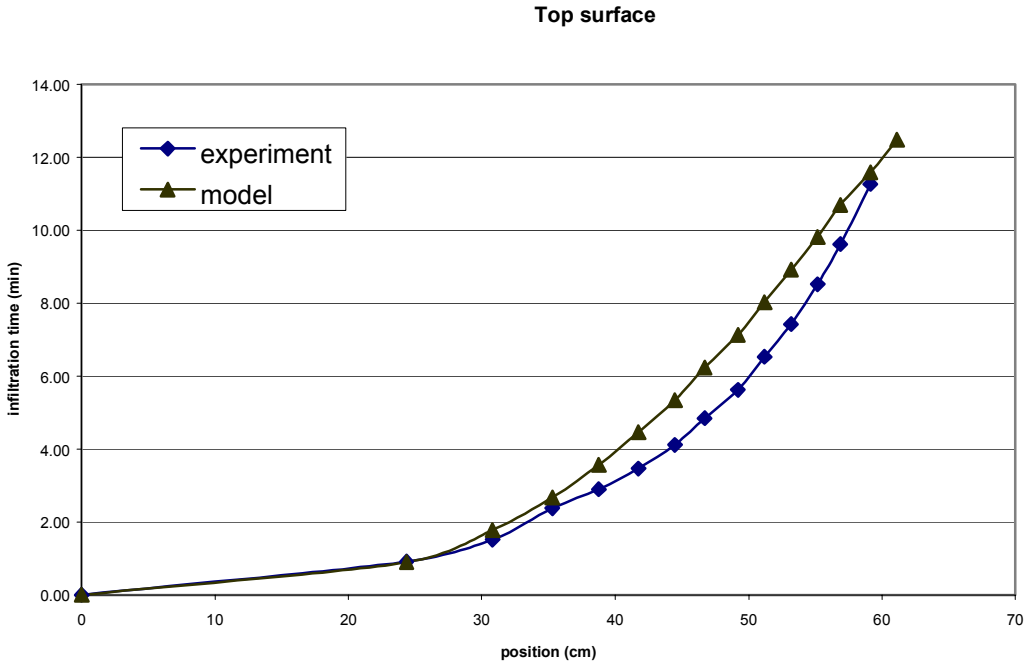

Figure 5.44 – Measured and calculated flow along the top surface of the 12.7 mm thick foam core preform with 25.4 mm stitch row spacing. The flow is in the region of the high permeable distribution medium.

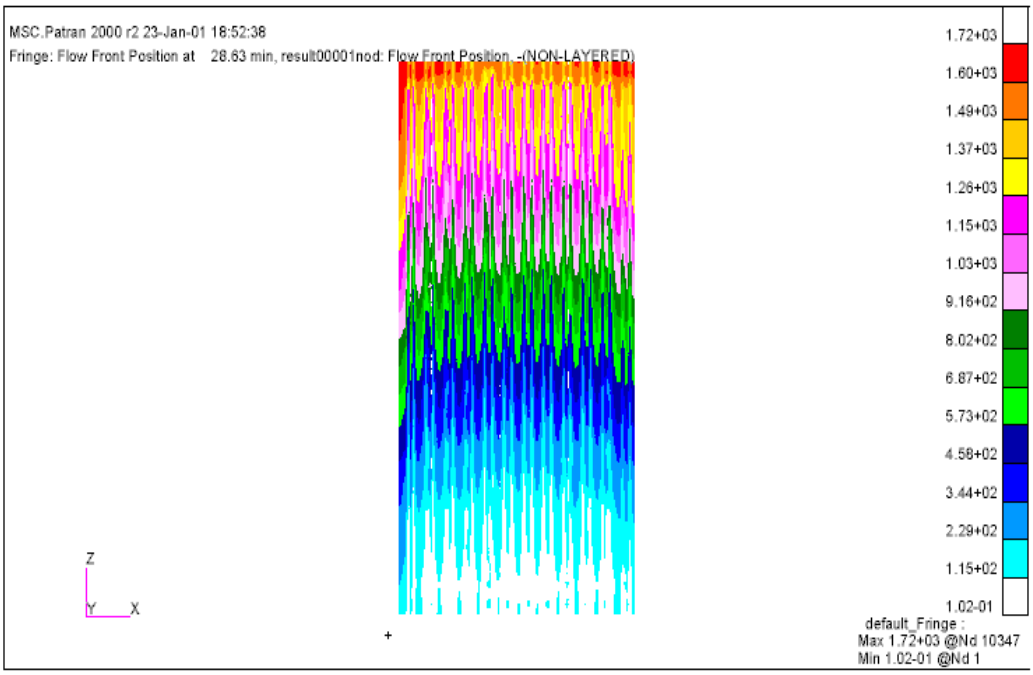

Figure 5.45 – 3DINFIL model predictions for resin flow along bottom surface of 12.7 mm thick foam core preform with 25.4 mm stitch row spacing.

5.3.4 Case 4 – 25.4 mm foam core with 12. 7 mm stitch row spacing

The fourth preform resin infiltrated used a 25.4 mm foam core with 12.7 mm stitch row spacing. The finite element mesh for this case is shown in Figure 5.46, and contains 15,856 elements with 27,085 nodes. The dimensions of this panel were slightly different than the other panels, thus the strip size of the mesh was 3.175 mm x 603.25 mm x 25.4mm, with a total of 25 strips modeled in the core. The porosity was calculated to be 0.0884.

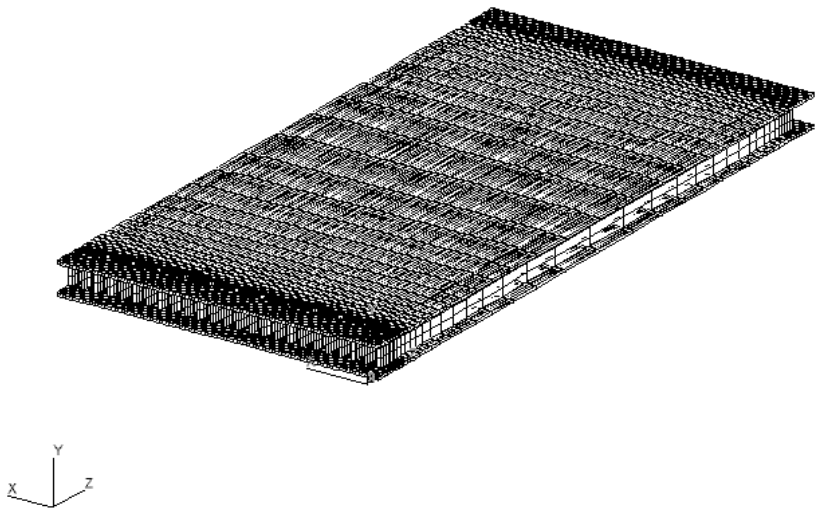

Figure 5.46 – Finite element mesh for the 25.4 mm thick foam core preform with 12.7 mm stitch row spacing.

Two panels were resin injected for this case and did not agree well with the model predictions. Though the predicted flow front geometry was consistent with the observed patterns, the model overpredicted the infiltration times. The experimental infiltration time for the first panel was 22.5 minutes, while the total infiltration time for the second panel was 22.6 minutes. However, the model predicted a total infiltration time of 33.6 minutes. Figure 5.47 shows the model predicted infiltration times for the surface of the top face sheet.

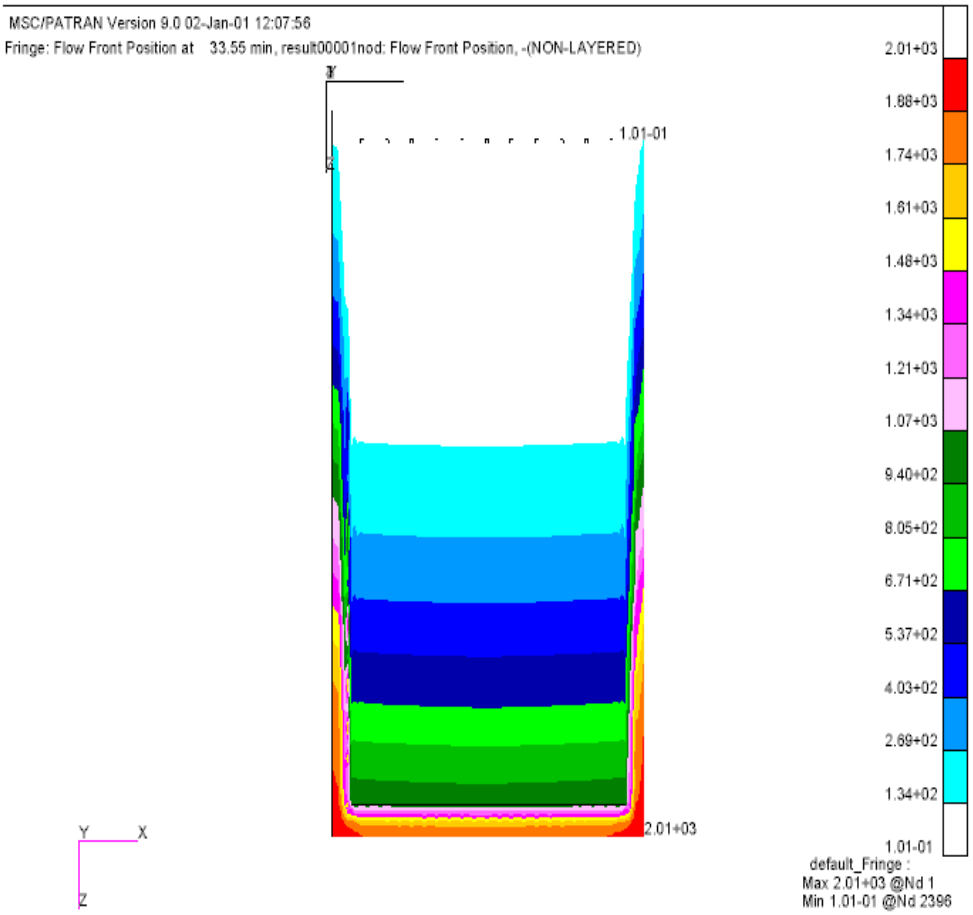

Figure 5.47 – 3DINFIL model predictions for flow along the top surface of the 25.4 mm thick foam core preform with 12.7 mm stitch row spacing.

Figure 5.48 shows a graph of the experimental and model predictions for flow front location versus time in the distribution medium of the top surface. The model overpredicts the measured infiltration time by more than 11 minutes. This represents a disagreement of over 50% between the predicted and measured values. The only variable which has changed between this case and the baseline 12.7 mm thick foam core with 12.7 mm thick stitch row spacing is the thickness of the foam core. The poor agreement indicates that the one-dimensional 'strip' mesh elements connecting the top and bottom face sheets are not adequate to describe the flow in the region between face sheets.

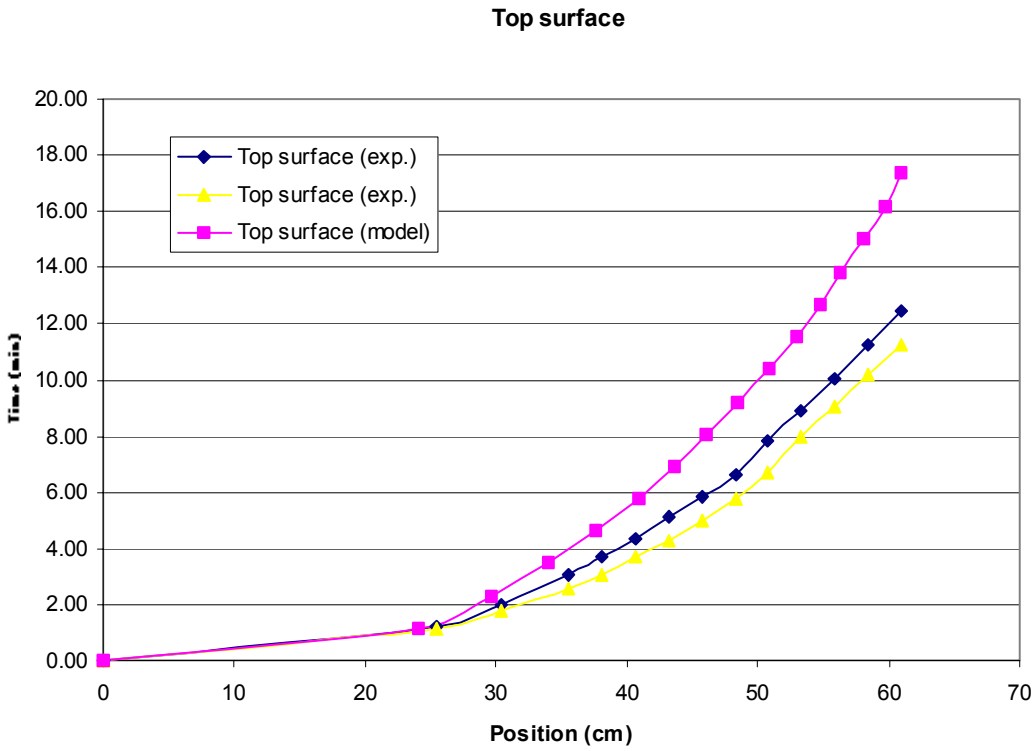

Figure 5.48 – Comparison between model predicted and measured flow front position along the top face sheet of the 25.4 mm thick foam core preform with 12.7 mm stitch row spacing. The flow is in the region of the high permeable distribution medium.

Figures 5.49 through 5.56 show the flow front progression along the bottom surface of the panel. The shape of the flow front was similar to the model prediction, which is shown in Figure 5.57. However, the total infiltration times did not match well between the model prediction and experimental infiltration.

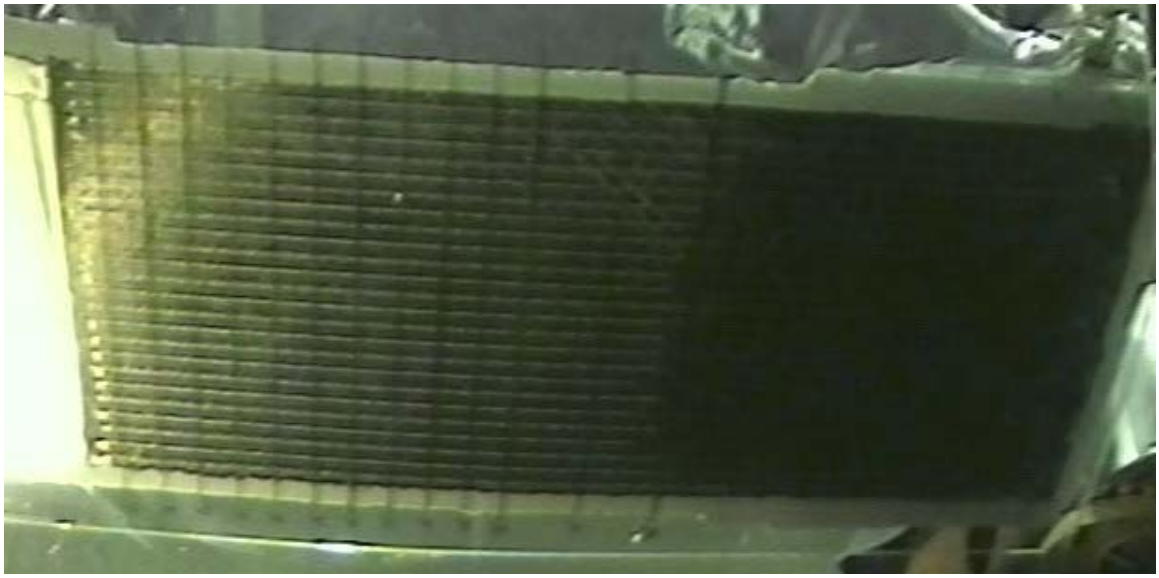

Figure 5.49 – Bottom surface of 25.4 mm thick foam core preform with 12.7 mm stitch row spacing. Flow front is approximately 25.4 cm from injection edge.

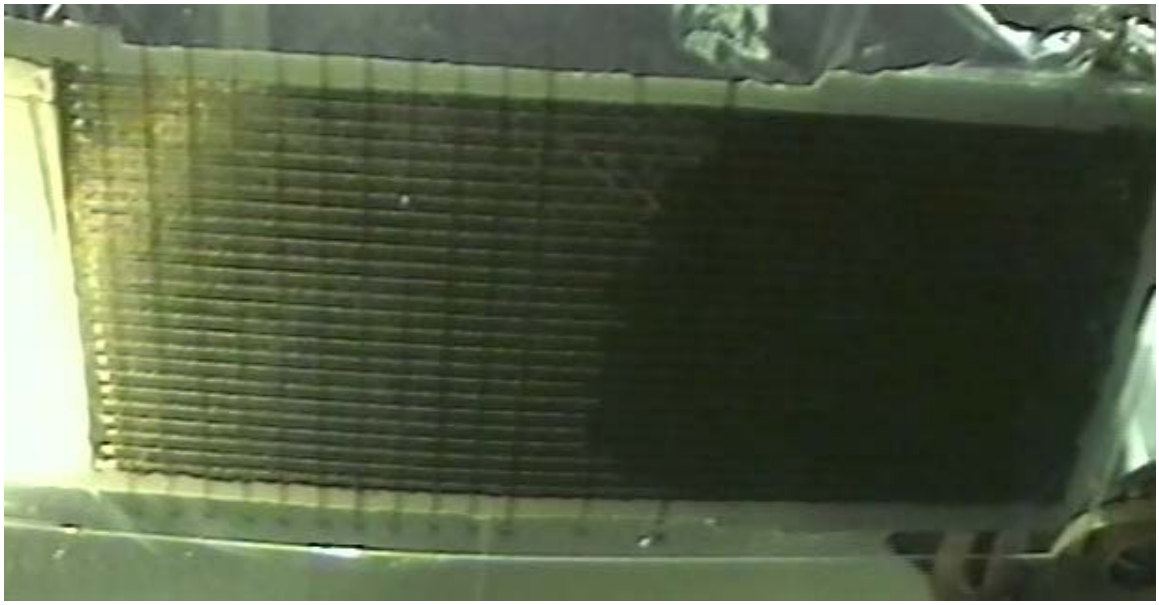

Figure 5.50 – Bottom surface of 25.4 mm thick foam core preform with 12.7 mm stitch row spacing. Flow front is approximately 30.5 cm from injection edge.

Figure 5.51 – Bottom surface of 25.4 mm thick foam core preform with 12.7 mm stitch row spacing. Flow front is approximately 35.6 cm from injection edge.

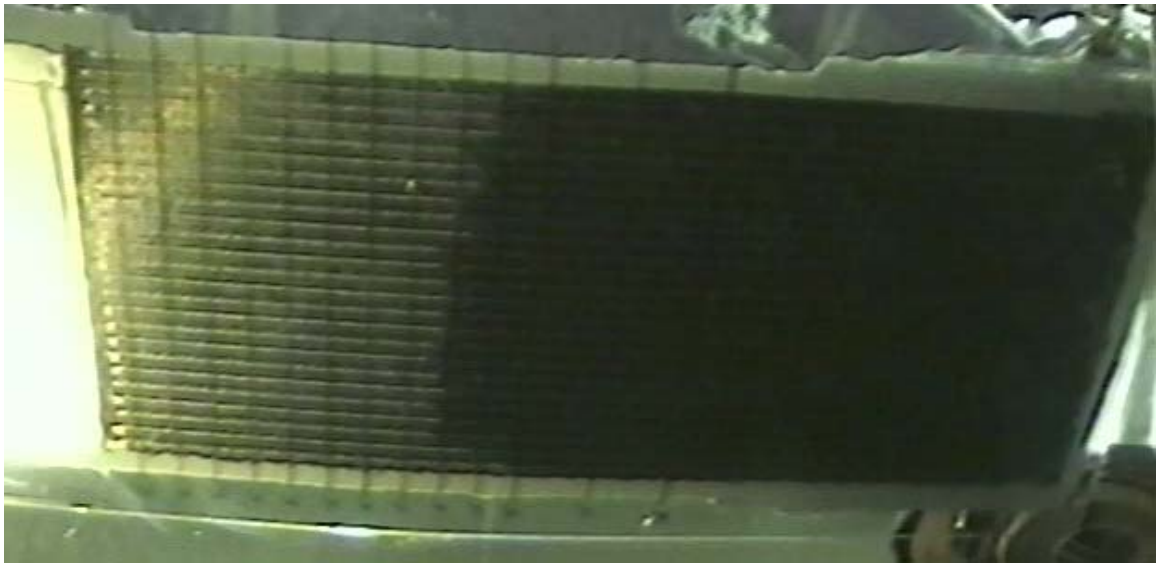

Figure 5.52 – Bottom surface of 25.4 mm thick foam core preform with 12.7 mm stitch row spacing. Flow front is approximately 40.6 cm from injection edge.

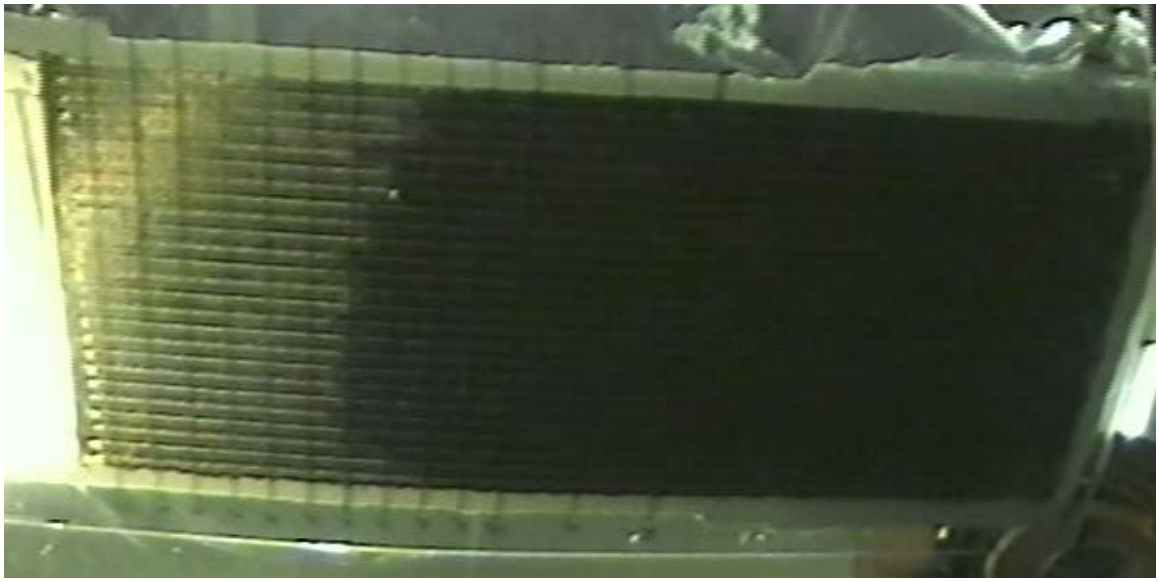

Figure 5.53 – Bottom surface of 25.4 mm thick foam core preform with 12.7 mm stitch row spacing. Flow front is approximately 45.7 cm from injection edge.

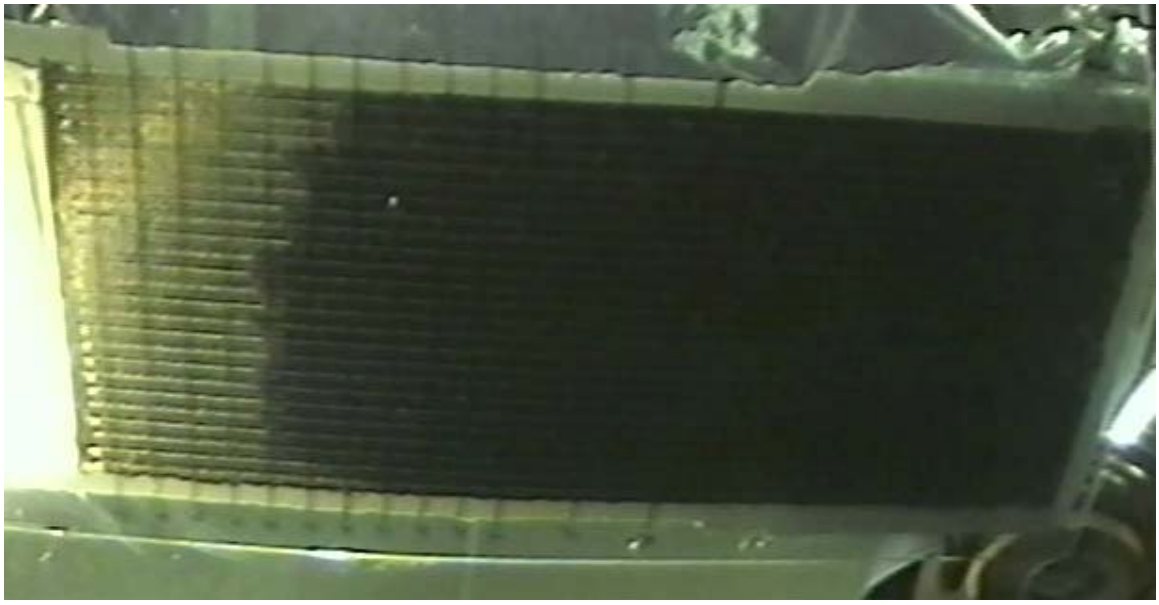

Figure 5.54 – Bottom surface of 25.4 mm thick foam core preform with 12.7 mm stitch row spacing. Flow front is approximately 50.8 cm from injection edge.

Figure 5.55 – Bottom surface of 25.4 mm thick foam core preform with 12.7 mm stitch row spacing. Flow front is approximately 55.9 cm from injection edge.

Figure 5.56 – Bottom surface of 25.4 mm thick foam core preform with 12.7 mm stitch row spacing. The preform is completely infiltrated.

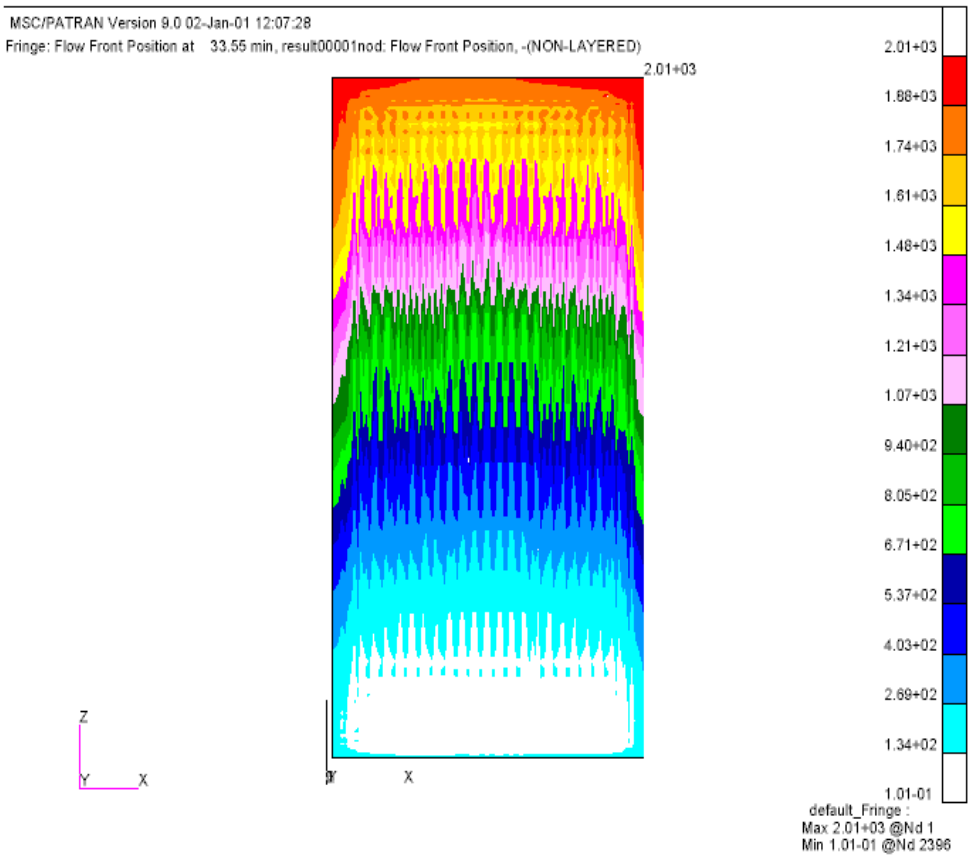

Figure 5.57 – 3DINFIL model predictions for flow along the bottom surface of the 25.4 mm thick foam core preform with 12.7 mm stitch row spacing.

5.4 Flow in transverse direction

Resin 'leaks' through the needle penetrations of the stitching to infiltrate the preform in the transverse direction. This effect can be observed experimentally, as flow along the bottom surface lags flow in the top face sheet. The resin path along the stitches from the upper face sheet to the lower face sheet can be seen in a cross-sectional view of the stitching in Figure 5.58.

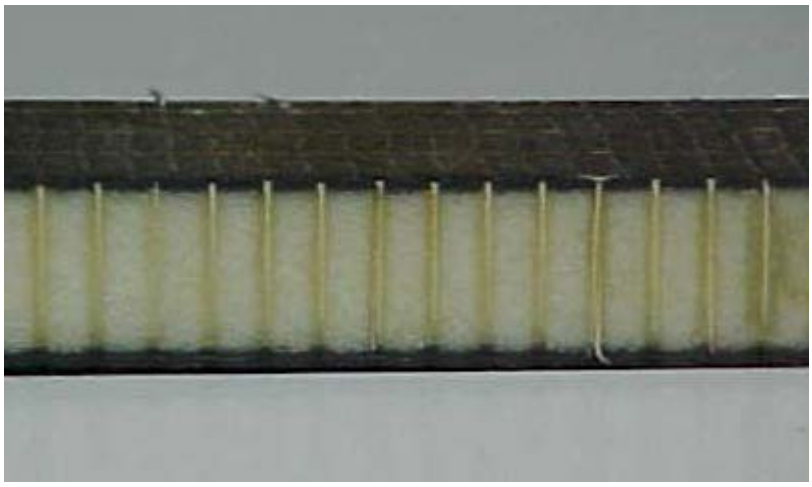

Figure 5.58 – Cross sectional view of stitching. Note resin flow from top face sheet to bottom face sheet along the stitching.

Chapter 6. Conclusions

Manufacturing procedures were developed to resin infiltrate both stitched and unstitched sandwich structures using vacuum assisted resin transfer molding. Viscosity profiles of Dow Derakane 510A-40 vinyl ester resin were gathered to determine the processing window at room temperature. Visual experiments were conducted to verify a three-dimensional finite element model of the infiltration of a stitched foam core composite panel. The flow front progression as a function of time was recorded and compared to experimentally predicted values. Total infiltration times were also compared between experimental observation and model predictions. Differential scanning calorimetry was used to determine the degree of cure of the resin.

6.1 Conclusions

Differential scanning calorimetry was used to evaluate the degree of cure of the room temperature Dow Derakane 510A-40 vinyl ester resin with 0.2% Cobalt Napthenate and 1.0% methyl ethyl ketone peroxide content. Samples tested at the completion of a 24 hour room temperature cure indicate that a post cure may be necessary to achieve a higher degree of cure. Room temperature viscosity profiles of the vinyl ester showed a reactive system with dynamic viscosity behavior during the processing window. The viscosity profiles helped determine the working pot life for the resin. With this information, manufacturing procedures were successfully developed to infiltrate both stitched and unstitched sandwich structures. Though the model verification was only performed on the stitched materials, results of the manufacturing trials showed that it was possible to resin infiltrate the unstitched structures using VARTM.

3DINFIL was used with varying degrees of success to model the process and predict the flow front geometry, position, and total infiltration times. For the baseline preform geometry which consists of a 12.7 mm thick foam core, 12.7 mm stitch row spacing and a pitch of 4 stitches per 25.4 mm, the model was able to predict the total infiltration time within 5% of what was observed experimentally. For the 12.7 mm thick foam core preform with 6.35 mm stitch row spacing, the predicted infiltration time was within 8%

of the experimentally observed infilatration time. However, the model overpredicted infiltration times for the 12.7 mm thick foam core preform with 25.4 mm stitch row spacing by more than 20%. For the preform with the 25.4 mm thick foam core panel, the model overpredicted the total infiltration time by more than 50%.

There are a variety of places where error could have been introduced into the model and the experimental verification. Experimental error can be attributed to the complex geometry of the flow front on the bottom surface of all the panels manufactured. This caused difficulty in accurately determining the flow front location at a given time. A second source of experimental error could have been caused by vacuum leaks in the layup. Though the vacuum capability of the pump has been verified, verification of vacuum during infiltration is not performed with a gage. Common autoclave manufacturing processes dictate a seal which holds full vacuum within 0.5 inch Hg over a 5 minute period. However, leaks during this process were only verified via inspection.

One possible source of error in the modeling is the constant viscosity assumption for the resin at room temperature injection. The rheological data show that the viscosity of the resin increases during the processing window. A second source of error can be attributed to the elements used to connect the top and bottom face sheets. A one-dimensional element was used in the mesh. This proved adequate for the 12.7 mm foam core, but when the thickness of the foam core increased to 25.4 mm, the total infiltration time was overpredicted by more than 50%. Another source of error is the permeability data available in the 3DINFIL materials database. Significant differences in the published permeability data and that of the Saertex material used in this study could exist due to the transverse stitching. Finally, the most accurate model would be one that modeled each needle perforation and reinforcing thread separately. However, this is not practical due to the size of the mesh that would be required and the small needle diameter and large number of stitches. The strip model has proven successful in describing the behavior of the infiltration for certain geometric conditions.

6.2 Recommendations for future work

It has been determined that stitching of a multiaxial warp knit material affects the permeability. Testing to determine the exact permeability of the face sheets or the entire stitched preform could greatly affect the model predictions and increase the agreement between model and experimental observation.

Resin flow models are also highly dependent on the kinetic and viscous behavior of the resin. 3DINFIL allows for kinetic and viscosity models to be input. The catalyst and promoter contents in the resin can affect both behaviors. Initial viscosity studies have shown that the constant viscosity assumption for the vinyl ester is inaccurate. Development of complete kinetic and viscosity models could change the model predictions.

Determining the effect of various processing variables on the total infiltration time would aide in selecting optimum manufacturing conditions. Possible variables include cycling the vacuum prior to injection to attempt to increase nestling effects and thus increase permeability and decrease injection time, and varying the amount of distribution medium used.

Mechanical property data of stitched preforms manufactured by VARTM would also be of value to determine the appropriate applications and design criteria of stitched sandwich structures.

References

1. Beckwith, S.W., Hyland, C.R., "Resin transfer molding: a decade of technology advances", *SAMPE Journal*, v. 34, n. 6, Nov-Dec 1998, p. 7-19.
2. Juska, T.D., Dexter, H.B., Seemann, W.H. III, "Pushing the limits of VARTM", International SAMPE Symposium and Exhibition, v. 43, n. 1, 1998, p. 33-43.
3. Lazarus, P., "Resin infusion of marine composites", International SAMPE Symposium and Exhibition (Proceedings), v. 41, n. 2, 1996, p. 1447-1458.
4. Nguyen, L.B., Juska, T.D., Mayes, J.S., "Evaluation of low cost manufacturing technologies for large scale composite ship structures", Collection of Technical Papers – AIAA/ASME/ASCE/AHS/ASC Structures, Structural Dynamics & Materials Conference, v. 2, 1997, p. 992-1001.
5. Ostberg, D.T., Dunfee, R.S., "Composite Armored Vehicle Advanced Technology Demonstrator", International SAMPE Symposium and Exhibition, v. 41, n. 2, 1996. p. 1459-1471.
6. Pike, T., McArthur, M., Schade, D., "Vacuum assisted resin transfer molding of a layered structural laminate for application on ground combat vehicles", Technology Transfer in a Global Community, International SAMPE Technical Conference, v. 28, 1996, p. 374-380.
7. Hosur, M.V., Vaidya, U.K., Jadhav, N., Jeelani, S., "Static and high strain rate compression testing of thick section S-2 glass/vinyl ester composites for integral armor application", Mechanical Behavior of Advanced Materials, American Society of Mechanical Engineers, Materials Division, MD-Vol. 84, p. 293-300.
8. Weinhold, P.D., Wozniak, J.J., "The application of SCRIMP VARTM fabrication technology to the compressed natural gas integrated storage system", *SAMPE Journal*, v. 34, n. 1, January/February 1998, p. 5-10.
9. Sheu, Ming-Fa., Lin, Yung-Kun., Chuang, Yu-Hwey., "The process development for composite electric buses body using resin transfer molding technique", International SAMPE Symposium and Exhibition, v. 45, n. 2, 2000. p. 2332-2343.
10. Kosmatka, J.B., Policelli, F.J., "The development of the DARPA/BIR composite Army bridge: phase I accomplishments", *Journal of Advanced Materials*, v. 31, n. 3, July 1999, p. 23-36.
11. Livesay, M.A., "UV-VARTM fabrication of low cost composite structures", International SAMPE Symposium and Exhibition, v. 44, n. 2, 1999, p. 1338-1344.
12. Vastava, R.B., et al., "An assessment of E-beam technologies for aircraft applications", International SAMPE Symposium and Exhibition, v. 43, n. 2, 1998, p. 1681-1690.
13. Heider, D., Eckel, D.A. II., Don, R.C., Fink, B.K., Gillespie, J.W. Jr., "Process monitoring during manufacturing of large-scale composite parts", Proceedings of the SPIE – the International Society for Optical Engineering., v. 3538, November 1998, p. 226-236.
14. Heider, D., Graf, A., Fink, B.K., Gillespie, J.W. Jr., "Feedback control of the vacuum assisted resin transfer molding (VARTM) process", Proceedings of the SPIE – the International Society for Optical Engineering., v. 3589, March 1999, p. 133-141.

15. Heider, D., Hofmann, C., Gillespie, J.W. Jr., "Automation and control of large-scale composite parts by VARTM processing", International SAMPE Symposium and Exhibition, v. 45, n. 2, 2000. p. 1567-1575.
16. Poe, C.C. Jr., Dexter, H.B., Raju, I.S., "Review of the NASA textile composites research", Journal of Aircraft, v. 36, n. 5, September – October 1999, 876-884.
17. English, L.K., "Honeycomb: million-year-old material of the future", *Materials Engineering*, v. 101, n.1, January 1985, p.29-33.
18. English, L.K., "Lighter weight and lower cost with foam-core composites", *Materials Engineering*, v.104, n. 9, September 1987, p.51-54.
19. McGowan, D.M., Ambur, D.R., "Structural response of composite sandwich panels impacted with and without compression loading", *Journal of Aircraft*, v. 36, n. 3, May-June 1999, p.596-602.
20. Ishai, O., Hiel, C., Luft, M., "Long-term hygrothermal effects on damage tolerance of hybrid composite sandwich panels', *Composites*, v. 26, n. 1, 1995, p.47-55.
21. Ishai, O., Hiel, C., "Damage tolerance of a composite sandwich with interleaved foam core", *Journal of Composites Technology & Research*, v. 14, n. 3, Fall 1992, p. 155-168.
22. Burchardt, C., "Fatigue in sandwich structures loaded in transverse shear", *Composite Structures*, v. 40, n. 1, 1998, p. 73-79.
23. King, M.J., Chen, J., "Fatigue of tapered sandwich structures", 31st International SAMPE Technical Conference, v. 31, 1999, p. 422-430.
24. Hodge, A.J., Kaul, R.K., McMahon, W.M., "Sandwich composite, syntactic foam core based, application for space structures", International SAMPE Symposium and Exhibition, v. 45, n. 2, 2000. p. 1567-1575.
25. Smith, S.A., Emmanwori, L.L., Sadler, R.L., Shivakumar, K.N., "Evaluation of composite sandwich panels fabricated using vacuum assisted resin transfer molding", International SAMPE Symposium and Exhibition, v. 45, n. 1, 2000. p. 981-989.
26. Stanley, L.E., Gharpure, S.S., Adams, D.O., "Mechanical property evaluation of stitched composite sandwich panels", International SAMPE Symposium and Exhibition, v. 45, n. 2, 2000. p. 1650-1661.
27. McGarva, L.D., Astrom, B.T., "Experimental investigation of compression moulding of glass/PA12-PMI foam core sandwich components", *Composites: Part A*, v. 30, 1999, p. 1171-1185.
28. Kwon, Y.W., Yoon, S.H., Sistare, P.J., "Compressive failure of carbon-foam sandwich composites with holes and/or partial delamination", *Composite Structures*, v. 38, n. 1-4, 1997, p.573-580.
29. Palmese, G.R., Andersen, O.A., Karbhari, V.M., "Effect of glass fiber sizing on the cure kinetics of vinyl-ester resins", *Composites: Part A*, v. 30, 1999, p.11-18.
30. Um, M.K., Daniel, I.M., "A New Kinetic Model for Degree of Cure and Viscosity in Liquid Molding Application", International SAMPE Symposium and Exhibition, v. 45, n. 2, 2000. p. 1598-1612.
31. Brill, R.P., McCullough, R.L., Palmese, G.R., "Effect of Resin Formulation and Reaction Temperature on the Curing Kinetics of Vinyl Ester Resins", Proceedings of the American Society for Composites, 1996, p. 576-583.

32. Li, L., Sun, X., Lee, L.J., "Low Temperature Cure of Vinyl Ester Resins", *Polymer Engineering and Science*, v. 39, n. 4, April 1999, p.646-661.
33. Ziaee, S., Palmese, G.R., "Effects of Temperature on Cure Kinetics and Mechanical Properties of Vinyl-Ester Resins*", Journal of Polymer Science: Part B: Polymer Physics*, v. 37, 1999, p. 725-744.
34. Dua, S., McCullough, R.L., Palmese, G.R., "Copolymerization Kinetics of Styrene/Vinyl-Ester Systems: Low Temperature Reactions", *Polymer Composites*, v. 20, n. 3, June 1999, p.379-391.
35. Hammami, A., Gebart, B.R., "Analysis of the Vacuum Infusion Molding Process", *Polymer Composites*, v. 21, n. 1, February 2000, p.28-40.
36. Sun, X., Li, S., Lee, L.J., "Mold filling analysis in vacuum-assisted resin transfer molding. Part I: SCRIMP based on a high-permeable medium", *Polymer Composites*, v. 19, n. 6, December 1998, p.808-817.
37. Ni, J., Li, S., Sun, X., Lee, L.J., "Mold Filling Analysis in Vacuum-Assisted Resin Transfer Molding. Part II: SCRIMP Based on Grooves", *Polymer Composites*, v. 19, n. 6, December 1998, p.818-829.
38. Sayre, J.R., "Vacuum-Assisted Resin Transfer Molding (VARTM) Model Development, Verification, and Process Analysis", PhD Dissertation, Virginia Polytechnic Institute and State University, 2000.
39. McNamara, C., McNamara, J.R., "Finite Element Modelling of a Tied Composite Sandwich Structure", *Key Engineering Materials*, v. 118-119, 1996, p.43-50.
40. van Vuure, A.W., Pflug, J., Ivens, J.A., Verpoest, I., "Modelling the core properties of composite panels based on woven sandwich-fabric preforms", *Composites Science and Technology*, v. 60, n. 8, 2000, p.1263-1276.
41. Nedanov, P., Advani, S.G., "Mold Filling Simulation of Sandwich Composite Structures Manufactured by Liquid Molding: A Parametric Study", *Journal of Sandwich Structures and Materials*, v. 2, April 2000, p. 117-130.
42. Yousefi, A., Lafleur, P.G., Gauvin, R., "Kinetic Studies of Thermoset Cure Reactions: A Review", *Polymer Composites*, v. 18, n. 2, April 1997, p. 157-168.
43. Product literature obtained from nfgsales.com
44. McRae, J.D., M.Sc. Thesis, Virginia Polytechnic Institute and State University, 1994.
45. Fingerson, J.c., M.Sc. Thesis, Virginia Polytechnic Institute and State University, 1995.
46. Caba, A.C., M.Sc. Thesis, Virginia Polytechnic Institute and State University, 1998.
47. Knott, T.J., M.Sc. Thesis, Virginia Polytechnic Institute and State University, 1994.

Vita

Rebecca Ann McGrane

Rebecca McGrane was born October 24, 1976. She graduated from Chandler High School in Chandler, AZ with an International Baccalaureate diploma as a National Merit Scholar in 1994. Rebecca pursued a degree in Mechanical Engineering from Texas A&M University and completed studies in May of 1999. While enrolled at Texas A&M, she spent two years working as an engineer in Houston, TX for Hydril Company. It was during this time that she developed in interest in polymer composites, while working on a NIST Advanced Technology Program to develop spoolable composite tubing for oilfield applications. This led to graduate studies at Virginia Polytechnic Institute and State University, where she pursued a master's degree in Engineering Mechanics, specializing in composite manufacturing. After the completion of her studies in March of 2001, she began work as a Senior Engineer in composite materials for General Dynamics Land Systems in Sterling Heights, MI, and currently resides in Royal Oak, MI.